
Update of background concentrations over Norway

Philipp Schneider, Dag Tønnesen and Bruce Denby



Scientific report

Contents

	Page
Summary	3
1 Introduction	5
2 Methodology	5
2.1 Data sources	6
2.1.1 ETC Data	6
2.1.2 AirBase Database	7
2.1.3 Topography	10
2.1.4 EMEP Model	10
2.2 Mapping methodology	11
2.3 Decomposition of station time series	12
2.4 Station representativity of time series anomalies	13
3 Results and Discussion	14
3.1 Maps of background concentrations	15
3.2 Annual Variability	20
3.3 Daily Variability	23
3.4 Matrices of temporal variability	26
3.5 Excel Prototype	28
3.6 Online version	30
3.7 Assessment of error sources and uncertainty	30
3.8 Station distribution and density	32
4 Possible improvements	33
5 Summary	34
6 Acknowledgements	35
7 References	35
Appendix A Annual variability at all stations for all four species	39
Appendix B Daily variability at all stations for all four species	49
Appendix C Matrix visualization of annual and daily variation at all stations	59

Summary

A methodology for creating a new dataset of estimated background concentrations of NO₂, O₃, PM₁₀, and PM_{2.5} that are representative of a typical year over Norway, was developed. The dataset has a spatial resolution of 10 km × 10 km and an hourly temporal resolution. The underlying methodology is based on two components: First, annual mean background concentrations are mapped from raw station data as well as auxiliary data using geostatistical techniques. Second, time series of average annual and daily variability are computed from hourly raw station data over all suitable stations in Norway. The variability is thereby expressed as a relative anomaly from each station's long-term mean in order to make the temporal variability representative for neighboring grid cells that have different annual mean concentrations. Each grid cell is subsequently assigned to a specific station using a nearest neighbor approach and the relative anomaly computed at that station is used to estimate the mean background concentration for a given location and point in time. The dataset is available as a NetCDF file, an Excel spreadsheet, and as an online application on the website www.luftkvalitet.info. The dataset significantly improves the amount of information available about background concentrations in Norway, both on a spatial as well as a temporal dimension, as the result overview in Figur A illustrates.

Whereas the previously used VLUFT method of 1993 only provided spatially constant data at the county level, the new method presented here provides spatially continuous data at a comparatively high spatial resolution. Furthermore, while the previous method only gave a range of values that were considered valid throughout the entire year, the new technique provides continuous time series for a typical year at hourly resolution at any location in Norway.

While the presented method provides reasonable estimates of background concentrations in a typical year, significant uncertainty exists due to very low station density within Norway. In order to improve continuous estimates of background concentrations it is highly recommended to increase the number of air quality stations within Norway, with a particular focus on the northern part of the country.

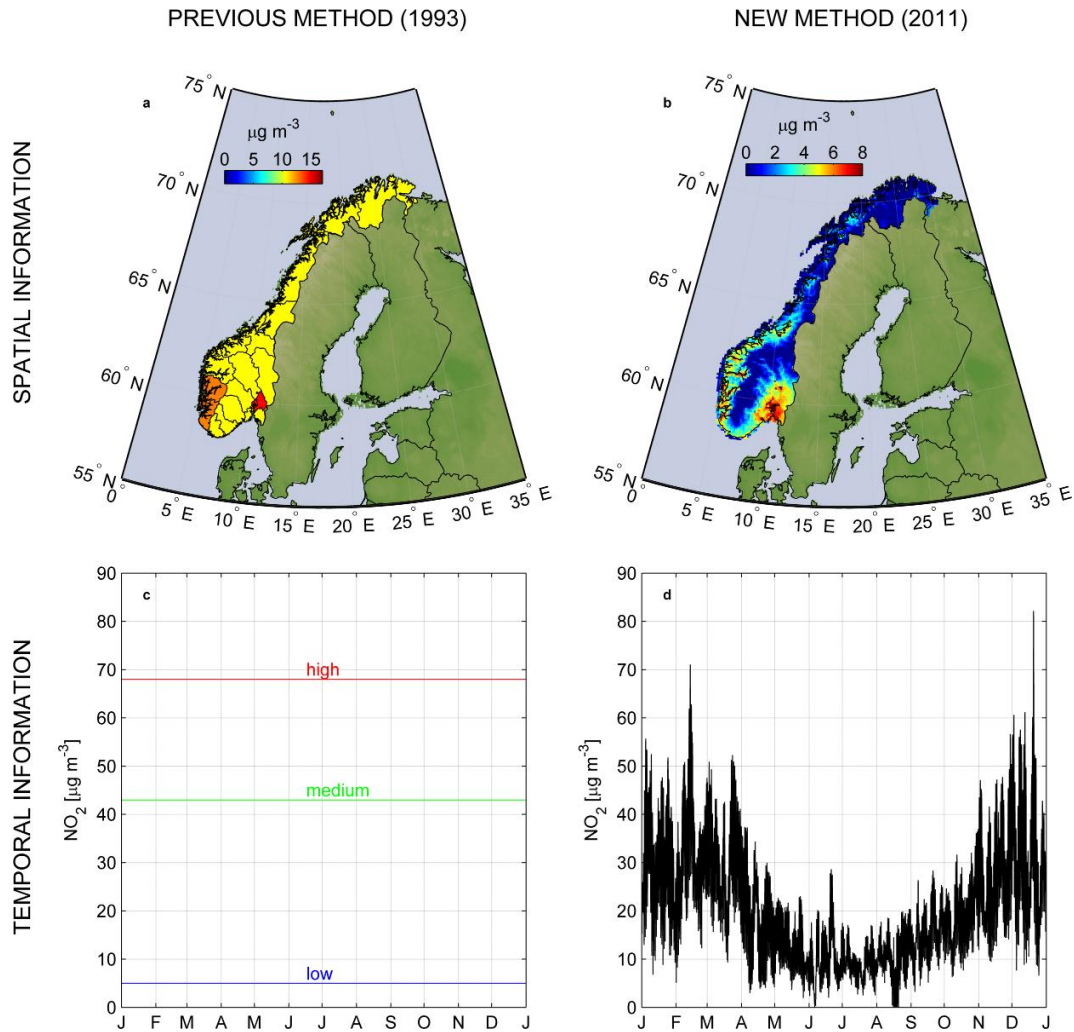


Figure A: Comparison of the information content about background concentrations obtained from the previous method and the method described in this report, shown for the example of NO₂. Panel a) shows 1993 VLUFT data for rural areas for the medium-level class, panel b) shows the annual mean background concentrations for 2008 derived using the method presented here, panel c) shows an example of temporal information available from VLUFT, here for Akershus county, and panel d) shows the temporal concentration information at Kjeller in Akershus county for a typical year as derived by the method presented here. Note that the values from VLUFT given in panel a) are "episodic high hourly concentrations" and are thus not directly comparable to the annual mean values shown in panel b).

Update of background concentrations over Norway

1 Introduction

For a variety of applications it is helpful to have estimates of several air quality-related variables such as NO_2 , O_3 , PM_{10} , and $\text{PM}_{2.5}$. Such applications include for example calculations of air quality, in particular with respect to contributions from emission sources such as roads, tunnels, or industrial plants. Furthermore there is demand for air quality calculations with respect to areal planning within the municipalities. Such applications are important for reducing the vulnerability of the population to the impacts of air pollution and for engaging in initiatives in order to ensure that the various existing criteria for appropriate air quality are met accordingly.

At the present time, a frequently used source for such information within Norway is the “Bakgrunnsatlas fra VLUFT” report which was developed in 1993. While a useful source of information on rough estimates of background concentrations, the information contained therein is nearly 20 years old and needs to be updated to reflect more recent data on background concentrations and new technical and scientific developments for estimating such values.

More specifically, in updating such a database on background concentrations over Norway it appears useful to include recent research on mapping Europe-wide mean annual concentrations of various species and to target the results and methods used within this work for estimating background concentrations for the major air quality-related indicators specifically over Norway. As the background concentrations for all the above mentioned species vary considerably over time, the information on spatial patterns obtained from such mapping can then be combined with data on temporal patterns at existing air quality stations to provide estimates of background concentrations not only at locations throughout Norway but also for a given date and time.

Therefore, the primary goal of the project was to deliver maps of annual mean background concentrations of NO_2 , O_3 , PM_{10} , and $\text{PM}_{2.5}$ over Norway for a given reference year. A further objective was to provide estimated values for a given day and time using annual and daily decomposition of time series at station measurements, while maintaining ease of use.

2 Methodology

The estimation of Norwegian background concentrations for NO_2 , O_3 , PM_{10} , and $\text{PM}_{2.5}$ is based on two components. The first component consists of maps of the average annual concentration for recent years that are derived from station observations in conjunction with spatially distributed auxiliary data using geostatistical techniques. However, since most of the species considered vary significantly with time, maps of annual averages alone are not sufficient. The second component of the methodology is therefore based on a quantitative

description of the average long-term temporal behavior of the observations at each station. Both components will be described in detail in the following sections.

2.1 Data sources

A variety of data sources were used within the framework of this project, both as primary and secondary sources of information. The properties of the main datasets used for this project are briefly summarized in the following sections.

2.1.1 ETC Data

Where possible, existing data sets generated by the European Topic Centre for Air and Climate Change (ETC/ACC) were used for the mapping component. The methodology underlying the mapping procedure has been refined over many years and the datasets have been extensively validated (Horálek et al., 2007, 2010; Denby et al., 2011). Such data was available for NO₂, PM₁₀, and PM_{2.5}, however not for O₃. The annual average map for O₃ over Norway was produced at NILU from raw datasets using a similar methodology (See section 2.2).

The mapping methodology used by the ETC/ACC is described in detail in various reports, such as Horálek et al. (2007), Horálek et al. (2010), and Denby et al. (2011), and therefore will only be summarized here briefly. The approach uses a combination of a linear regression model which is then followed by the kriging of the resulting residuals, a process also known as residual kriging (Goovaerts, 1997). Separate maps are created for urban and rural areas which are later combined using specific merging rules based on population density. For each species and mapping type, a varying number of spatially exhaustive auxiliary variables are used which guide the interpolation process in areas of low station density. The type and number of auxiliary variables used within the mapping procedure is dependent on their respective impact to an improved fit of the regression model. For example, the interpolation of PM₁₀ in rural areas used output from the EMEP model (see section 2.1.4), a digital elevation model for information on altitude, data on wind speed, and data on solar radiation. On the other hand, for PM₁₀ mapping in urban areas the used auxiliary variables consisted solely of the output from the EMEP model. For more detail on the auxiliary variables used for the mapping of NO₂, PM₁₀, and PM_{2.5} see the reports provided by Horálek et al. (2007), Horálek et al. (2010) and Denby et al. (2011).

Once the multiple linear regression against the appropriate auxiliary variables is accomplished, residuals are acquired at each location where station data is available. These residuals are subsequently interpolated using ordinary kriging (Cressie, 1993; Goovaerts, 1997; Wackernagel, 2003). This interpolation process is based on variogram analysis, according to which the spatial autocorrelation of the data is fitted using a (often spherical) variogram model. Kriging weights are obtained as a result of this process and the optimal prediction of residual concentration is made at each 10 km × 10 km grid cell. Subsequently, a final map of estimated concentrations is obtained by adding the gridded result from the linear regression and from the kriging of the residuals.

In addition to the linear regression and ordinary kriging techniques resulting in estimated concentration maps for rural and urban areas, the ETC/ACC

methodology further uses a fairly sophisticated merging procedure for combining the separately interpolated maps of urban and rural areas. The technique is based on the population density for each grid cell and assign the interpolated value from the rural map if the population density is less than a given threshold α_1 and assigns the interpolated urban value for all cells exceeding a population density of α_2 . In case the population density is greater than α_1 but less than α_2 , a joint rural/urban value is computed using a weighting function and assigned to the respective grid cell. Once all the grid cells are assigned their appropriate concentration values based on their respective population density, a final concentration map of the parameter in question is obtained.

As the production of maps on NO_2 , PM_{10} , and $\text{PM}_{2.5}$ is summarized here and described in detail in the mentioned references, the remainder of the methodology focuses primarily on the technique for creating the map of annual O_3 concentration for the reference year 2008, which was not produced by the ETC/ACC.

2.1.2 AirBase Database

Raw data from air quality stations was used for both spatial mapping using residual kriging as well as for temporal decomposition of the time series. All station data was obtained from the *European Air quality dataBase*, AirBase (<http://acm.eionet.europa.eu/databases/airbase/>). However, different datasets were acquired for each component. For the geostatistical analysis and the mapping of O_3 , annual mean O_3 concentrations were acquired for all European background stations in order to achieve a large enough sample size for variogram modeling and regression analysis. For the temporal characterization, only data for Norwegian stations were acquired for all four species, however this was done for the entire available record and at an hourly temporal resolution.

Table 1 lists all background air quality stations located in Norway for which data was retrieved from the AirBase database. Traffic and industrial stations were not used because of their limited spatial representativeness. Therefore, only background stations (urban, suburban, and rural) were considered. The geographical context is shown in Figure 1 which shows the location of all available background air quality stations in Norway with suitably long time series for each component.

In addition, Table 2 gives an overview of station type and the components measured at each station with suitably long time series, as well as the respective long-term means for each component. Note that only a small number of stations provides suitable time series for NO_2 and only one stations provides data for $\text{PM}_{2.5}$. Swedish and Finnish stations were not used here but could provide valuable additional information in future work.

Table 1: Overview of Norwegian background air quality stations that were used for temporal characterization. All station data was acquired from AirBase. Note that not all stations provide data for all air quality indicators and that stations not listed here were not considered due to short time series or other reasons.

Station ID	Station Name	City	Lat. [deg]	Long. [deg]	Elevation [m]
NO0075A	Barnehagen	LILLEHAMMER	61.121	10.467	210
NO0001R	Birkenes		58.383	8.250	190
NO0081A	Bærum		59.952	9.645	80
NO0070A	Grimmerhaugen	AALESUND	62.472	6.166	21
NO0077A	Gruben	MO I RANA	66.310	14.194	10
NO0062A	Haukenes		59.200	9.400	25
NO0056R	Hurdal		60.367	11.067	300
NO0045R	Jeløya		59.433	10.600	5
NO0055R	Karasjok		69.467	25.217	333
NO0039R	Kårvatn		62.783	8.883	210
NO0016A	Nedre Storgate	DRAMMEN	59.746	10.207	20
NO0041R	Osen		61.250	11.783	440
NO0043R	Prestebakke		59.000	11.533	160
NO0015A	Rådhuset	BERGEN	60.395	5.327	5
NO0052R	Sandve		59.200	5.200	40
NO0072A	Skøyen	OSLO	59.920	10.733	10
NO0073A	Sofienbergparken	OSLO	59.356	10.766	25
NO0063A	Stener Heyerdahl	KRISTIANSAND	58.090	7.586	12
NO0015R	Tustervatn		65.833	13.917	439
NO0065A	Våland	STAVANGER	58.961	5.731	33
NO0080A	Øyekast		59.133	9.645	40

Table 2: Overview of station type and components measured at each station as well as their respective long-term mean. All means are given in units of $\mu\text{g m}^{-3}$. When no annual mean is indicated the data either did not have sufficiently long time series for computing annual and daily means or the component was not measured at that station.

Station ID	Station Name	Type	NO ₂	O ₃	PM ₁₀	PM _{2.5}
NO0075A	Barnehaugen	urban	19.2	-	19.0	8.8
NO0001R	Birkenes	rural	-	55.2	-	-
NO0081A	Bærum	urban	-	39.0	-	-
NO0070A	Grimmerhaugen	urban	-	-	13.1	-
NO0077A	Gruben	suburban	-	-	17.4	-
NO0062A	Haukenes	suburban	5.6	54.8	-	-
NO0056R	Hurdal	rural	-	54.6	-	-
NO0045R	Jeløya	rural	-	56.1	-	-
NO0055R	Karasjok	rural	-	65.7	-	-
NO0039R	Kårvatn	rural	-	58.6	-	-
NO0016A	Nedre Storgate	urban	-	-	19.9	-
NO0041R	Osen	rural	-	55.8	-	-
NO0043R	Prestebakke	rural	-	58.5	-	-
NO0015A	Rådhuset	urban	34.7	-	17.9	-
NO0052R	Sandve	rural	-	66.2	-	-
NO0072A	Skøyen	urban	-	-	21.8	-
NO0073A	Sofienbergparken	urban	-	-	22.0	-
NO0063A	Stener Heyerdahl	urban	-	-	22.1	-
NO0015R	Tustervatn	rural	-	70.0	-	-
NO0065A	Våland	urban	16.7	-	15.8	-
NO0080A	Øyekast	urban	14.5	-	17.1	-

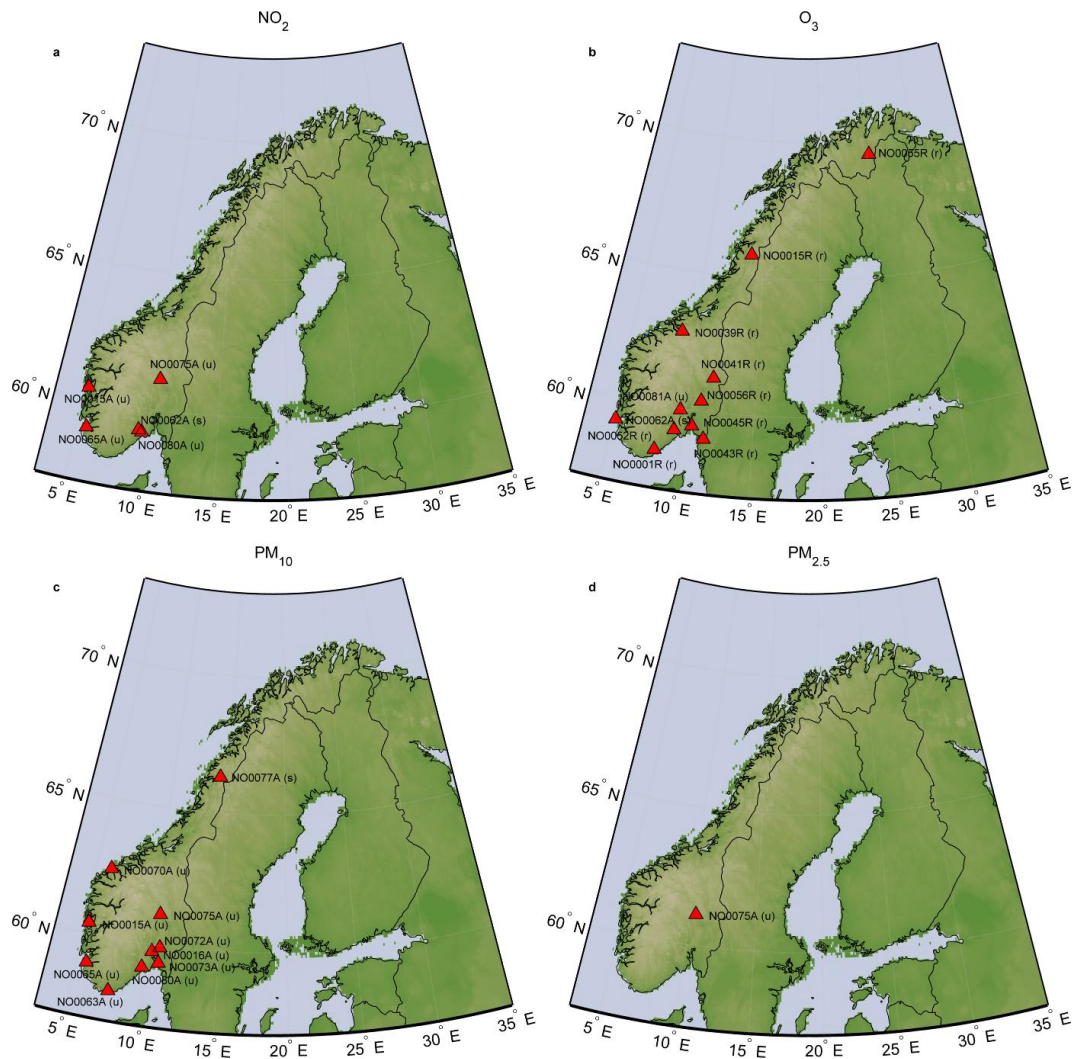


Figure 1: Location of the Norwegian background air quality stations whose data was used in this project for purposes of spatial mapping and temporal decomposition for a) NO₂, b) O₃, c) PM₁₀, and d) PM_{2.5}. The station type is indicated in the label as (u) for urban, (s) for suburban, and (r) for rural. Note that only stations with sufficiently long time series are shown.

2.1.3 Topography

Elevation is one of the most important auxiliary variables used throughout the mapping process. It is used for all four species. Spatially distributed data on topography over Norway was acquired for this project from the global 1-km digital elevation model GTOPO30, which is available at 30 arcsecond resolution (approximately 1 km) (EROS Data Center, 1996; Gesch et al., 1999). The data was resampled to the final grid resolution of 10 km × 10 km using cubic convolution.

2.1.4 EMEP Model

As the density of air quality stations over Norway is very sparse, it is particularly important to guide the interpolation process of the station data using appropriate auxiliary variables. The output of a chemical transport model is helpful for this

purpose as it can provide physically realistic estimates of concentrations, albeit at a relatively coarse spatial resolution. For this project, modeled Europe-wide concentrations were obtained from the Unified EMEP (European Monitoring and Evaluation Programme, (Fagerli et al., 2011)) model (Simpson et al., 2003). The Unified EMEP model is an Eulerian chemical transport model that has been developed at the EMEP/MSC-W (Meteorological Synthesizing Centre West of EMEP) and has been extensively validated (Fagerli et al., 2003). Emissions used for the model are described in Vestreng et al. (2007). The modeled annual average concentrations were acquired as a grid with a 50×50 km horizontal spatial resolution. They were resampled to the final grid resolution used here of $10 \text{ km} \times 10 \text{ km}$ through cubic convolution.

2.2 Mapping methodology

The background maps are created using residual kriging with auxiliary variables. Kriging is an interpolation technique that makes use of a model of spatial autocorrelation (usually in the form of a variogram model) to infer optimal estimates of a variable at a given set of locations (Isaaks and Srivastava, 1989; Cressie, 1993; Goovaerts, 1997; Wackernagel, 2003).

The mapping procedure applied in this study is based on the previous work by Horálek et al. (2007), Horálek et al. (2010), and Denby et al. (2011) and involves a linear regression analysis against multiple auxiliary variables in conjunction with kriging of the residuals. It should be noted that the cited work incorporates a procedure for separately mapping urban and rural areas and then combining the interpolated maps using a fairly sophisticated merging technique. This part of the algorithm was not implemented in the O_3 mapping procedure due to the scarcity of stations in Norway.

The concentration $\hat{Z}(s_0)$ is mapped at a given location s_0 using the model

$$\hat{Z}(s_0) = c + a_1 X_1(s_0) + a_2 X_2(s_0) + \dots + a_n X_n(s_0) + \eta(s_0) \quad (1)$$

where c , a_1 , a_2 ... a_n are parameters of the multiple linear regression and $X_1(s_0)$... $X_n(s_0)$ are the values of the auxiliary variables used at location s_0 . Finally, $\eta(s_0)$ represents the results of the ordinary kriging of the residuals at location s_0 .

The first step in the process was therefore to establish a linear relationship between the variable in question and the auxiliary variables at each station. Although the geographic region of interest here was Norway, this task was performed throughout all background stations in Europe available within AirBase in order to obtain a more representative relationship. This was done here for O_3 only but the same method was applied by the ETC/ACC for mapping the other components. Multiple linear regression was used. In the case of O_3 , elevation and EMEP model results were used as auxiliary variables. These and other auxiliary variables were also used by the ETC/ACC for mapping the other species.

Kriging makes use of a model describing the spatial autocorrelation. Most often, the semivariogram $\gamma(h)$ at a certain lag distance h is used to describe this. Different types of models are then fitted to the empirical semivariogram, with a

spherical model probably being the most common. Figure 2 shows an example of the empirical semivariogram and the fitted spherical model used for residual kriging of O_3 over Europe.

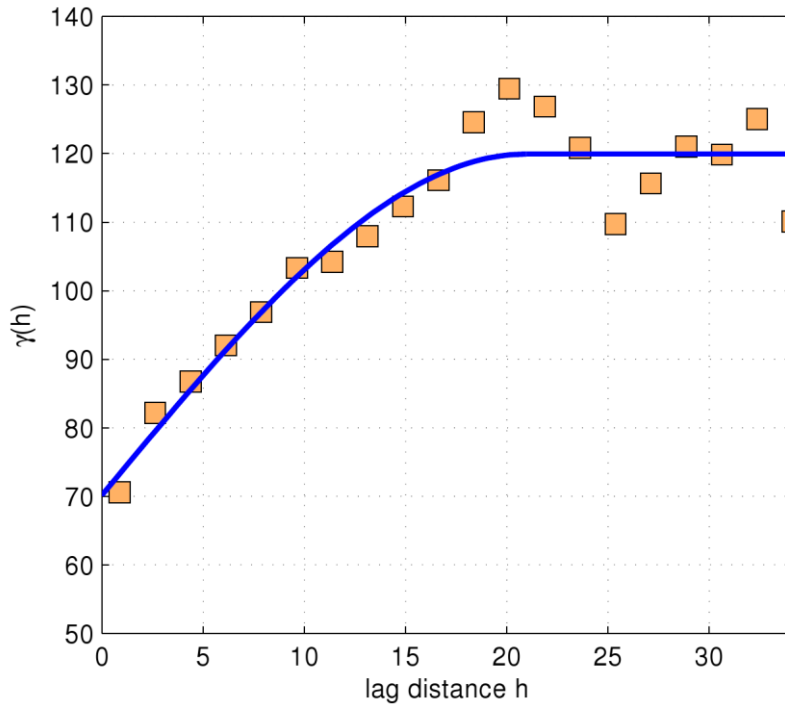


Figure 2: The empirical semivariogram for O_3 residuals after multiple linear regression and the fitted spherical model.

For kriging of O_3 residuals, a model was fitted to the empirical semivariogram with a nugget effect of $70.2 \mu\text{g m}^{-3}$ and a spherical model of range $a_0 = 21.0$ degrees and sill $c_0 = 49.7 \mu\text{g m}^{-3}$ such that the semivariance $\hat{\gamma}(h)$ at lag h is given

as

$$\hat{\gamma}(h) = \begin{cases} 49.7 \cdot \left[\frac{3}{2} \frac{h}{21.0} - \frac{1}{2} \left(\frac{h}{21.0} \right)^3 \right] & \text{for } h \leq a_0 \\ 49.7 & \text{for } h > a_0 \end{cases} \quad (2)$$

The fitted semivariogram model is then used in the kriging process to determine appropriate weighting factors for each data point. More detailed information about the kriging process can be found in the literature, e.g. in Isaaks and Srivastava (1989), Cressie (1993), or Goovaerts (1997).

The kriged residuals are then added to the results from the multiple linear regression as indicated in Equation 1 and through this process the final maps shown in Figures 4 through 7 are obtained.

2.3 Decomposition of station time series

While the maps of annual mean background concentration are helpful for identifying spatial patterns, the actual concentrations at each location vary significantly throughout the year as well as throughout the day. It is thus

necessary to combine the maps of annual mean background concentration with information on cyclical temporal variability at varying frequencies for each species. This information can be obtained by means of temporal decomposition of reasonably long time series at air quality stations.

This was accomplished within the framework of this project by averaging several years of hourly measurements on an annual as well as on a daily basis. The resulting time series for a typical year and a typical day were further smoothed to ensure that the observations are representative of cyclical temporal patterns and do not just reflect short-term variability. The representative annual and daily time series are subsequently converted from absolute concentrations given in $\mu\text{g m}^{-3}$ to anomalies from the long-term mean at the station given in percent. This ensures the applicability of the temporal information for neighboring areas with differing annual mean background concentrations.

Due to the often short time series available at each station and the associated small sample size, random noise which is not representative of the overall long-term temporal variability is abundant in the time series and needs to be removed before using the relative anomalies for estimating concentrations at other locations. Such a task can for example be performed by using a moving average filter as is shown in Figures 15 through 22. However, for practical purposes this smoothing was performed here in the operational application by applying a two-dimensional low-pass filter on an hour-by-hour anomaly matrix for an average year. This results in a simultaneous smoothing of both the annual and daily average time series. The effect can be seen for all species and stations in subfigures c) and d) of Figures 31 through 58. It should be noted that the application of the filter was performed while the matrix was augmented by itself on all four sides in order to avoid erroneous edge effects caused by the filter.

The smoothed relative anomalies can then be applied to neighboring locations with different absolute annual mean concentrations (see Section 2.4 and Figure 3), and as such the average concentration can be estimated for a certain location given a certain day of the year and a time of day. The end result is then a simple offline or online application that can give an estimate of mean concentration of a certain species after the user provides a location (given as a latitude and longitude pair) and day and time.

2.4 Station representativity of time series anomalies

In order to apply relative anomalies calculated at air quality stations on a nationwide scale it is necessary to decide for all grid cells in the country which air quality station and thus which temporal pattern it is best represented by. For this purpose a fairly simple method was chosen that assigns a station to a grid cell based on the distance between them. In other words, each grid cell is assigned to the geographically closest station. Figure 3 provides an overview of the way in which the gridcells were assigned to the available stations with sufficiently long time series for each analyzed species. Clearly, more sophisticated approaches could be used here (and would be necessary if the final goal was computing entire maps for each point in time), however we found that for providing reasonable estimates of time series a simple *nearest neighbor* approach is sufficient. Further work could expand upon this approach for example using a weighting scheme for

the stations or an approach using expert knowledge for determining the area of influence for each station.

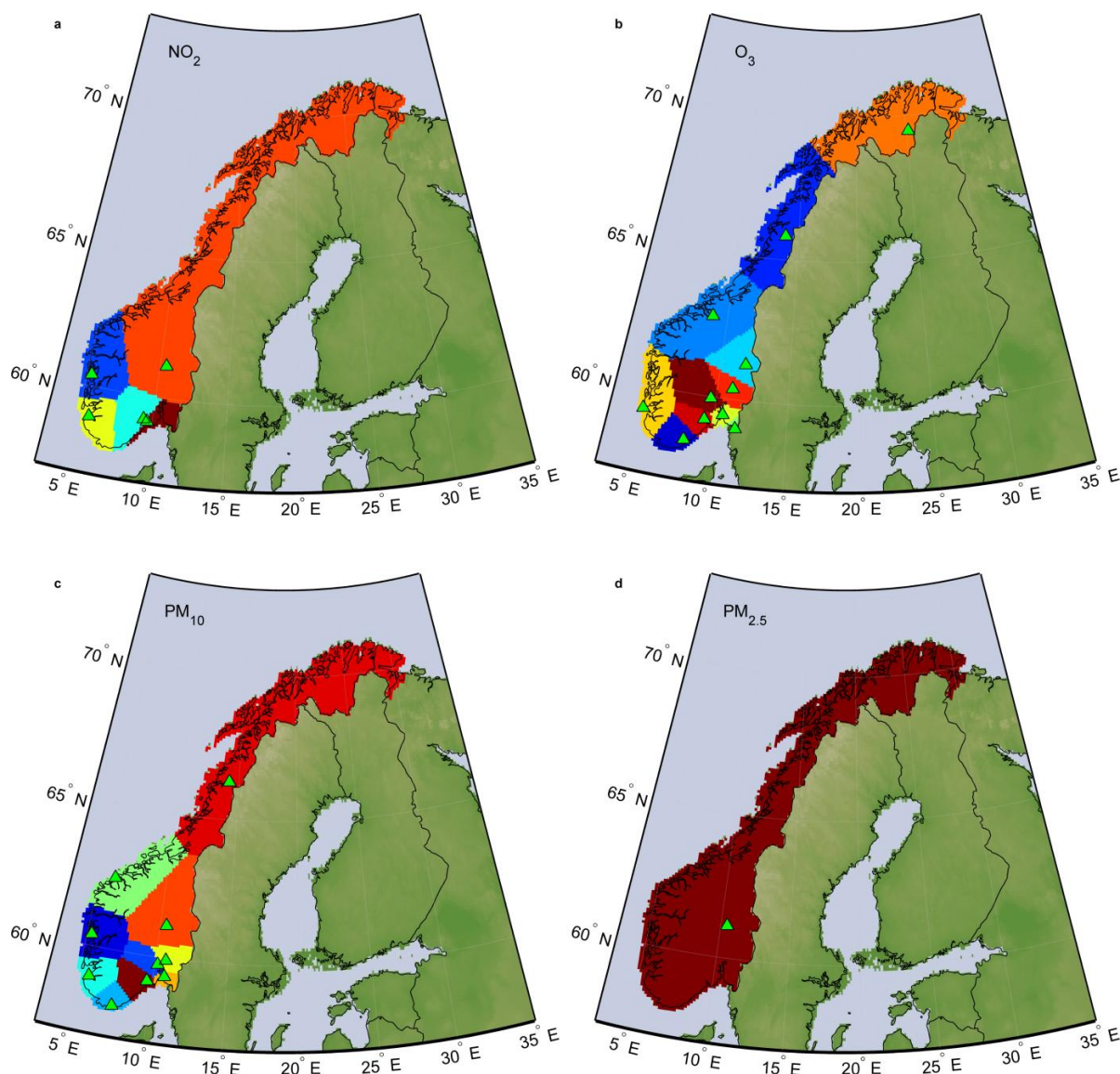


Figure 3: Maps depicting the representivity of air quality stations with sufficiently long time series for temporal averaging (4 years minimum with less than 60 days of missing data per year). The maps shown are for a) Nitrogen Dioxide, b) Ozone, c) PM_{10} , and d) $\text{PM}_{2.5}$. All gridcells shown in the same color are using the same information on temporal anomalies from the closest station. The green triangles mark the available stations for each species.

3 Results and Discussion

As mentioned previously, the methodology for this study consists of two major components. Firstly, spatial patterns in concentrations for all four species were derived from raw station data and various auxiliary dataset using geostatistical methods. Secondly, temporal patterns were derived from station observations for estimating the annual and daily cycles at each location. Here we first describe the

resulting maps of annual mean background concentrations, show some examples of annual and daily variability at selected stations and present a simple visualization for estimating the mean anomaly for a given hour and day at any station. Finally, we briefly demonstrate offline and online tools that were developed for easily obtaining approximate quantitative estimates of the background concentration of the four species at any location in Norway for any given day and time in a year. Note that only a small set of representative figures can be shown in the results section. For a complete set of figures of results for all species and stations please see the Appendix.

3.1 Maps of background concentrations

The spatial patterns in annual mean concentrations were derived by means of geostatistical techniques using raw data from air quality station and auxiliary variables such as model output, elevation etc. ETC/ACC data for NO₂ was only available for 2007. However, 2008 was chosen as a reference year for the remaining three species since existing data from the ETC/ACC was available for that year for PM₁₀ and PM_{2.5}. The map for O₃ was consequently computed using 2008 data as well. We assume that interannual variability in annual mean concentrations is reasonably small and that the years 2007/2008 can be seen as approximately representative of the current annual mean background concentrations.

Figure 4 shows the 2007 annual mean background concentration of NO₂ over Norway. As would be expected the area of highest mean NO₂ concentrations can be found over the greater Oslo area where population density and thus road traffic and other emissions are highest. Estimated mean annual NO₂ concentrations in the city of Oslo reach values of up to 22 $\mu\text{g m}^{-3}$, whereas the greater Oslo area still sees concentrations around 6–7 $\mu\text{g m}^{-3}$. Mean annual concentrations are estimated to be moderately high throughout most of Western and Southern Norway with values around 3–5 $\mu\text{g m}^{-3}$ and hotspots with values over 10 $\mu\text{g m}^{-3}$ over the cities of Kristiansand, Stavanger and Bergen. The situation is similar in Trøndelag with mean values around 4 $\mu\text{g m}^{-3}$ and a hotspot over Trondheim. The rest of the country, the mountainous inland areas of southern Norway as well as most parts of Northern Norway, shows generally very low mean annual concentrations of less than 1 $\mu\text{g m}^{-3}$. None of the grid cells exceed the legally allowed annual mean limit of 40 $\mu\text{g m}^{-3}$. However, several grid cells exceed an annual mean NO₂ concentration of 20 $\mu\text{g m}^{-3}$, namely the greater Oslo area, Kristiansand, and Bergen. It should be noted that the spatial resolution of the grid cells with 10 km × 10 km is relatively coarse for any type of urban-scale analysis. Although several urban areas are likely to have annual mean values exceeding the 40 $\mu\text{g m}^{-3}$ threshold, they do not appear in the maps since the affected areas are relatively small and the sub-pixel heterogeneity is significant, such that the average value over the grid cell's entire 100 km² area is relatively low and does not reflect such localized sub-gridcell hotspots.

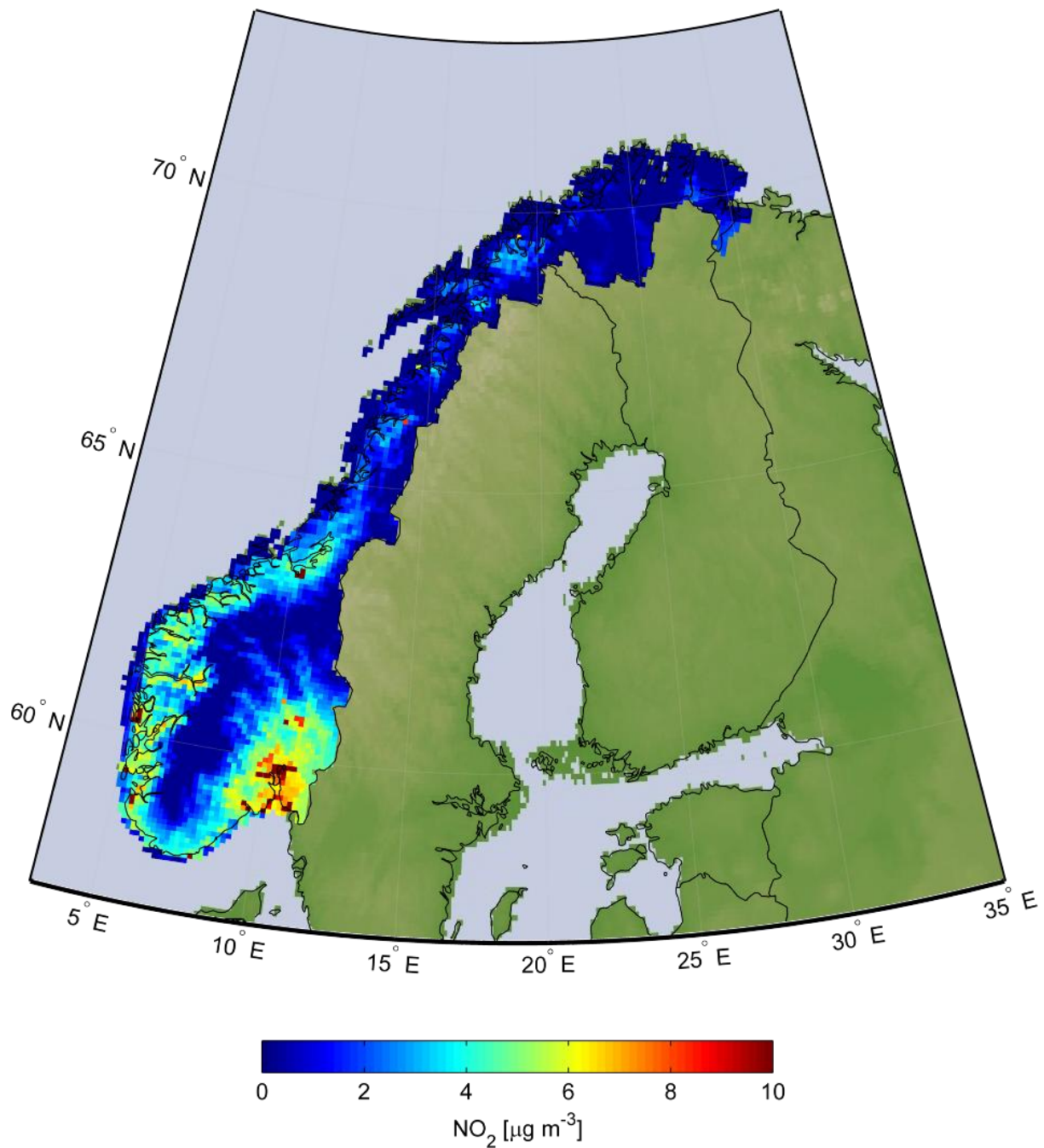


Figure 4: Map of annual mean NO₂ concentration for 2007 over Norway. The spatial resolution of the grid is approximately 10 km × 10 km. The map is based on data provided by the European Topic Centre on Air and Climate Change implementing a methodology described in Horálek et al. (2010).

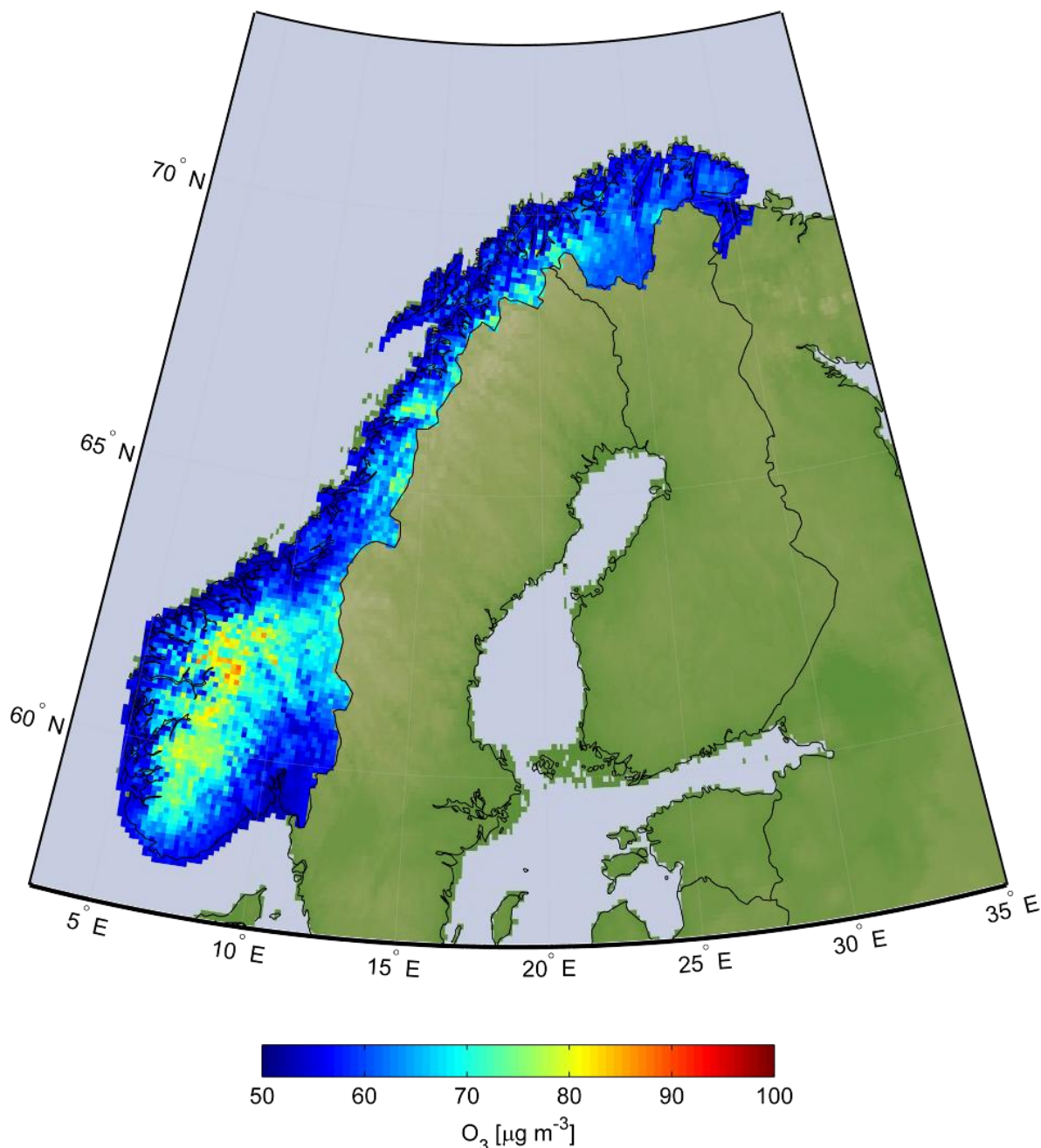


Figure 5: Map of annual mean O₃ concentration for 2008 over Norway. The spatial resolution of the grid is approximately 10 km × 10 km. The map was computed based on geostatistical techniques using raw station data and auxiliary variables.

Figure 5 shows the 2008 mean annual background concentrations of O₃ for Norway. In Southern Norway, the concentrations are mostly between 50 µg m⁻³ and 60 µg m⁻³ in the coastal areas and reach higher values of 70 µg m⁻³ to 90 µg m⁻³ in mountainous inland areas. In the northern half of the country mostly low values of 50–60 µg m⁻³ can be found although some areas with high concentrations of around 70–75 µg m⁻³ can be observed in some inland areas near the border to Sweden. It should be noted that this map is strongly dependent on altitude, as a digital elevation model was one of the primary auxiliary variables for the interpolation process.

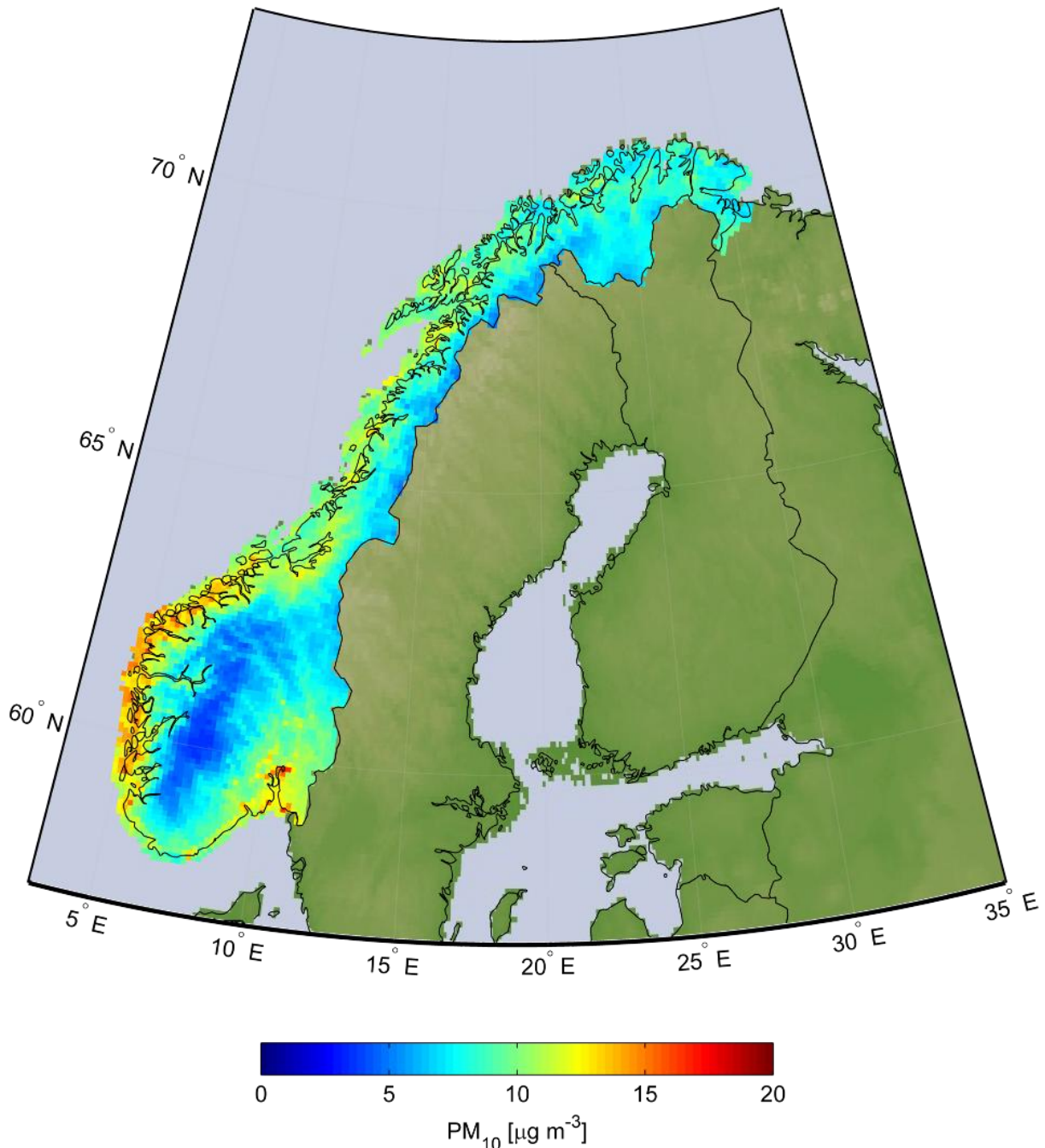


Figure 6: Map of annual mean PM_{10} concentration for 2008 over Norway. The spatial resolution of the grid is approximately $10 \text{ km} \times 10 \text{ km}$. The map is based on data provided by the European Topic Centre on Air and Climate Change implementing a methodology described in Horálek et al. (2010).

Figure 6 shows the 2008 average values of PM_{10} for Norway. The hotspots with the highest concentrations can be found in the city of Oslo where annual mean values over $20 \mu\text{g m}^{-3}$ are indicated. The greater Oslo area shows annual mean concentrations of around $11\text{--}13 \mu\text{g m}^{-3}$. Whereas the mountainous inland areas in the southern half of Norway appear to have quite low annual mean concentrations between $0 \mu\text{g m}^{-3}$ and $5 \mu\text{g m}^{-3}$, the situation is quite different along the coastlines.

The southern coast of Norway consistently shows concentrations of 10–12 $\mu\text{g m}^{-3}$ and the coastline in the western part of the country even reaches relatively high values between 12 $\mu\text{g m}^{-3}$ and 15 $\mu\text{g m}^{-3}$, presumably due to sea salt effects that are likely introduced by the EMEP model which was used as an auxiliary variable in the interpolation process. The northern half of the country has mostly lower concentrations between 5 $\mu\text{g m}^{-3}$ in the inland areas and 10–12 $\mu\text{g m}^{-3}$ in coastal areas.

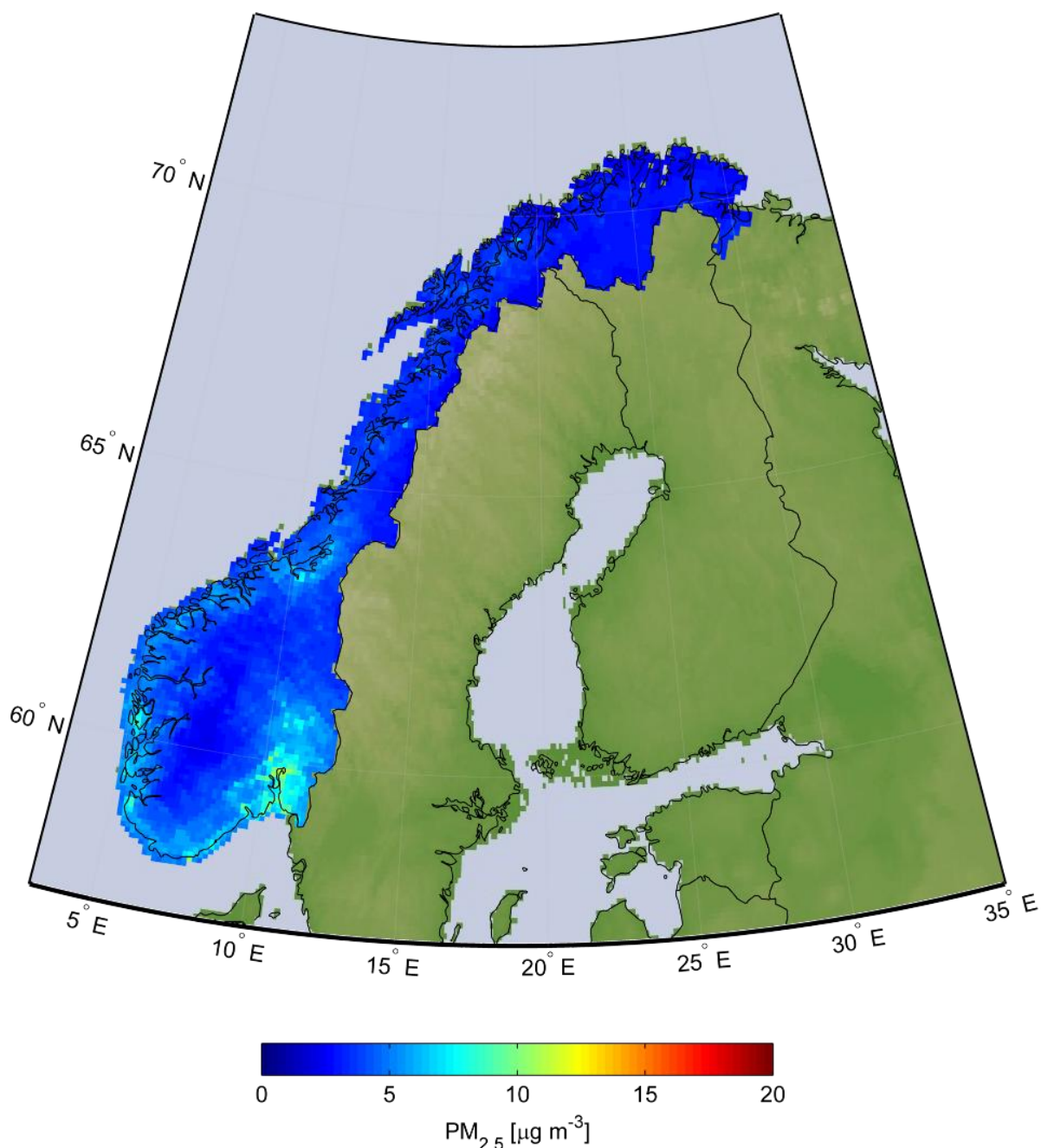


Figure 7: Map of annual mean $\text{PM}_{2.5}$ concentration for 2008 over Norway. The spatial resolution of the grid is approximately $10 \text{ km} \times 10 \text{ km}$. The map is based on data provided by the European Topic Centre on Air and Climate Change implementing a methodology developed by Denby et al. (2011).

Figure 7 shows a map of estimated 2008 mean annual concentrations of PM_{2.5} for Norway. The highest values of around 12–13 $\mu\text{g m}^{-3}$ can be found over the city of Oslo, whereas the greater Oslo area still shows concentrations between 7 $\mu\text{g m}^{-3}$ and 10 $\mu\text{g m}^{-3}$. The rest of the country exhibits very low mean annual PM_{2.5} concentrations of less than 5 $\mu\text{g m}^{-3}$, with the exception of several hotspots over the main urban areas of Kristiansand, Stavanger, Bergen, and Trondheim, where annual mean values of 8–10 $\mu\text{g m}^{-3}$ are indicated.

It should be noted that the maps shown in Figures 4 through 7 should be interpreted with care. While the underlying methodology involving geostatistics and multiple linear regression of auxiliary variables is quite robust and can deliver good results, the fact remains that it is an interpolation technique and as such prone to potentially significant errors. As with any spatial interpolation technique, the method's performance is proportional to the amount of input data. Since the number of usable air quality stations in Norway is quite limited (in fact, Scandinavia has one of the lowest station densities in all of Europe), the multiple linear regression with auxiliary variables plays a very important role and is actually close to the only source of information in areas that are far from the nearest applicable air quality station.

Besides adding further observation sites to increase station density, the quality of the maps could therefore be significantly improved by making use of more detailed or more accurate auxiliary variables. This could be accomplished, for example, by making use of higher-resolution model output, such as the 10 km \times 10 km regional reanalysis developed within the framework of the Monitoring Atmospheric Composition and Climate (MACC) project (Rouïl et al., 2011a,b) or the use of satellite-derived NO₂ observations as provided by sensors such as the SCanning Imaging Absorption spectroMeter for Atmospheric CartographY (SCIAMACHY) (Bovensmann et al., 1999; Gottwald et al., 2006), the Ozone Monitoring Instrument (OMI) (Levelt et al., 2006), or the Global Ozone Monitoring Experiment-2 (GOME-2) (Munro et al., 2006).

3.2 Annual Variability

The temporal patterns of concentrations express themselves in both annual and daily variability. The characteristic temporal behavior at each station was obtained by averaging long time series based on daily or hourly sampling intervals.

Annual variability was thus computed for each day of the year by averaging all such days occurring in the time series, while ensuring that only stations that can provide a minimum of 4 years of data were considered. This number was found to be a good compromise between obtaining a relatively representative mean value for each day, while at the same time ensuring that a reasonably large number of stations throughout Norway could be used.

The temporal anomaly A_t at time t in percent was computed as

$$A_t = \frac{x_t - \bar{X}}{\bar{X}} \cdot 100 \quad (3)$$

where x_t is the observed concentration at time t and X is the long-term mean concentration computed over all observations in the time series.

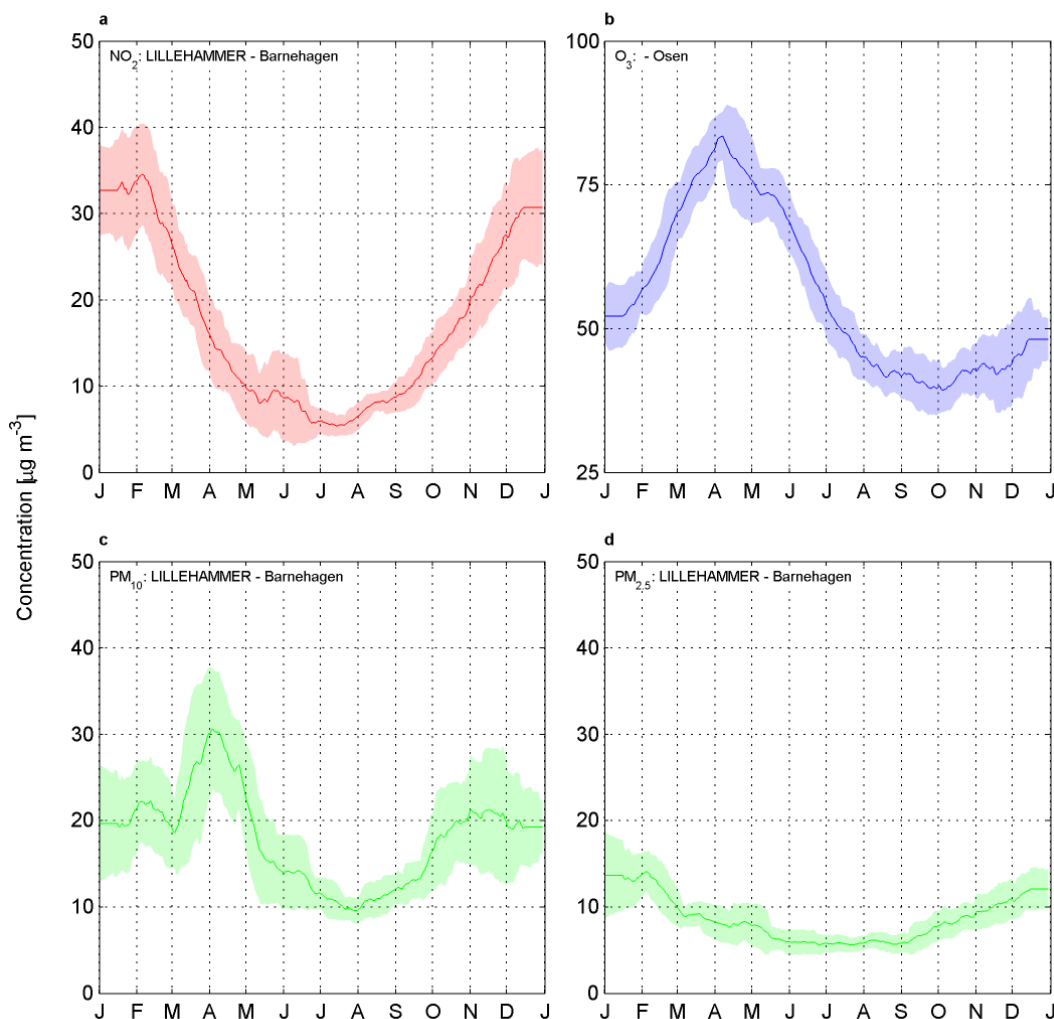


Figure 8: Examples of long-term average annual variability of a) NO_2 , b) O_3 , c) PM_{10} , and d) $\text{PM}_{2.5}$ in the Lillehammer area, given as absolute values of concentration. The solid line shows the 1-month moving average, whereas the shaded area represents the 1-month moving standard deviation. NO_2 , PM_{10} , and $\text{PM}_{2.5}$ are shown for the station NO0075A Lillehammer Barnebage. Note that no measurements of O_3 are available at this station, therefore the plot for O_3 shows the annual variability at the closest available O_3 station, NO0041R Osen. The constant values at the beginning and end of the year are artifacts due to the moving average filter.

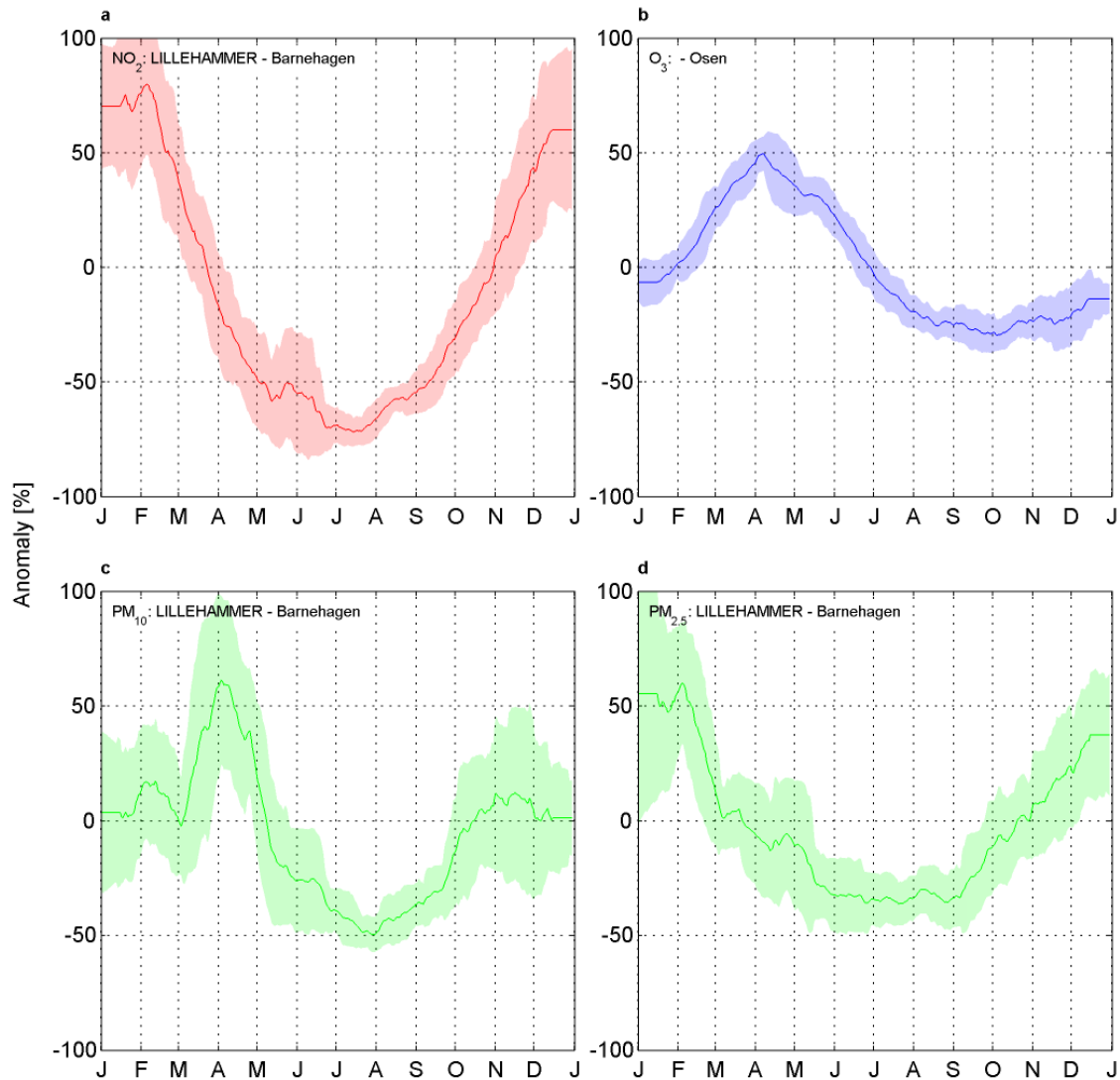


Figure 9: As Figure 8 but given as relative anomalies from the long-term mean concentration.

Figure 8 shows examples of observed average annual variability at one station, namely NO0075A Lillehammer Barnehaugen (with exception of O₃ which is shown for the closest neighboring station which measures O₃ concentrations). The Lillehammer station was selected as it was the only station in Norway that provides sufficiently long time series of at least three of the four species. Corresponding anomalies from the long-term mean were computed using Equation 3 and are shown in Figure 9.

All four species show distinct patterns throughout the year. NO₂ has a very clear and symmetrical annual cycle, reaching its maximum in the winter months between December and February when it exhibits values of 35 $\mu\text{g m}^{-3}$ or an anomaly of 65%. The concentrations then drop off rapidly throughout the spring until they reach their annual minimum of around 6–7 $\mu\text{g m}^{-3}$ in the month of July and August, which corresponds to an anomaly of approximately -70%. The concentrations then rise throughout the autumn to reach their winter maximum.

The O₃ concentrations start out early in the year slightly above 50 µg m⁻³ and increase rapidly until they reach their annual maximum at 80 µg m⁻³ or an anomaly of about 50%. They subsequently exhibit a gradual decrease over the summer months until they reach their annual minimum of 40 µg m⁻³ or -30% in October.

The concentrations of PM₁₀ hover around 20 µg m⁻³ (0–10%) in the first three months of the year before they rapidly increase to a brief annual maximum of 30 µg m⁻³ or 60% in April, which is likely due to road dust re-suspension. Throughout the summer months the PM₁₀ concentrations lie between 10 µg m⁻³ and 15 µg m⁻³ (or between -40% and -50%) until they reach the fairly constant winter values of 20 µg m⁻³ again in October and November.

The concentrations for PM_{2.5} also show a clear annual cycle with the maximum of about 15 µg m⁻³ or 50% occurring in the months of January and February. The concentrations are significantly lower in the summer months and reach only values of 6–7 µg m⁻³ (or -40%).

It should be noted that the annual cycles given here for the example of the *NO0075A Lillehammer Barnehaugen* station are not necessarily representative of all other stations. While some well-known general patterns exist throughout most stations (e.g. higher NO₂ concentrations in the winter months than in summer, or the spring peak in O₃ concentrations), other more local or short-term patterns vary significantly with region and station type. The reader is thus referred to Appendix A for more detailed information on seasonal patterns throughout the country.

Time series of mean annual variability given as the anomaly from the long-term mean and as depicted in Figure 9 are very helpful tools in scaling annual mean concentration at other locations and in estimating concentrations throughout the year. The complete set of figures depicting annual variability for all four species and all stations is provided in Appendix A.

3.3 Daily Variability

Daily variability is just as important as annual variability. The anomaly of the daily variability was computed in the same way as the anomaly of the annual variability following Equation 3. Figure 10 shows example plots of daily variability in the Lillehammer area. In addition, Figure 11 depicts the corresponding plots as anomalies.

The daily cycle of NO₂ reaches a minimum of 9 µg m⁻³ or -60% at 4:00 in the morning, subsequently increases rapidly during the morning rush hour to a local maximum of 25 µg m⁻³ (30%) at 8:00. The NO₂ concentrations then drop off slightly during the day before they reach the overall maximum of 27 µg m⁻³ (or an anomaly of 40%) during the evening rush hour at 18:00. The average daily cycle of O₃ at the *NO0041R Osen* station is much less complex. It approximately resembles a sinusoidal wave with a minimum of 45 µg m⁻³ at 4:00 in the morning and a maximum of 67 µg m⁻³ at 14:00.

The concentrations of PM₁₀ follow a mean daily cycle quite similar to that of NO₂. A minimum of just below 10 µg m⁻³ occurs at 4:00 in the morning, followed by a

rapid increase towards the first local maximum of $23 \mu\text{g m}^{-3}$ at 8:00. The second local maximum occurs again during the evening, reaching $27 \mu\text{g m}^{-3}$ at 19:00 and is caused also by woodburning.

Finally, $\text{PM}_{2.5}$ exhibits a slightly different daily cycle in that its temporal features are not as succinct. The first local maximum of the day with a value of $9 \mu\text{g m}^{-3}$ is reached after the main morning rush hour at 10:00 in the morning. As for PM_{10} the main maximum of $12 \mu\text{g m}^{-3}$ is reached at 19:00 and is caused by woodburning. The lowest values again occur at 3:00 and 4:00 in the morning and reach as low as $6 \mu\text{g m}^{-3}$.

It should be noted that the daily cycles given here for the example of the *Lillehammer Barnehaugen* are not necessarily representative of all other stations. While some well-known general patterns exist throughout most stations (e.g. relatively high NO_2 concentrations during the morning and evening rush hours, the afternoon peak of O_3 concentrations, or the evening peak of PM_{10}), other more local or short-term patterns vary significantly with region and station type. The reader is thus referred to Appendix B, which includes the complete set of figures depicting daily variability for all four species and all stations, for more detailed information on typical daily cycles throughout the country.

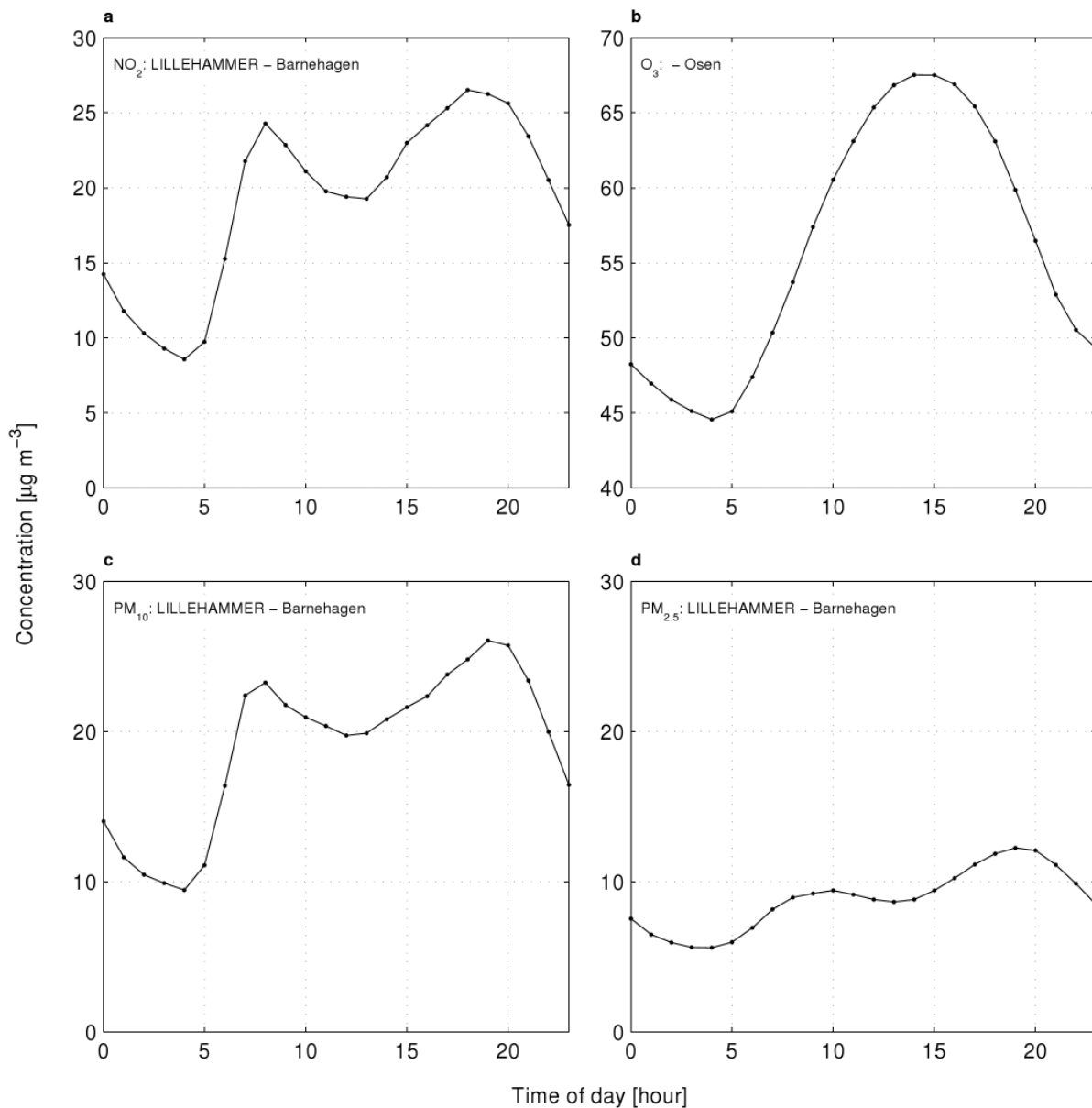


Figure 10: Examples of long-term average daily variability of a) NO_2 , b) O_3 , c) PM_{10} , and d) $\text{PM}_{2.5}$ in the Lillehammer area. NO_2 , PM_{10} , and $\text{PM}_{2.5}$ are shown for the station NO0075A Lillehammer Barnebage, given as absolute values of concentration. Note that no measurements of O_3 are available at this station, therefore the plot for O_3 shows the annual variability at the closest available O_3 station, NO0041R Osen.

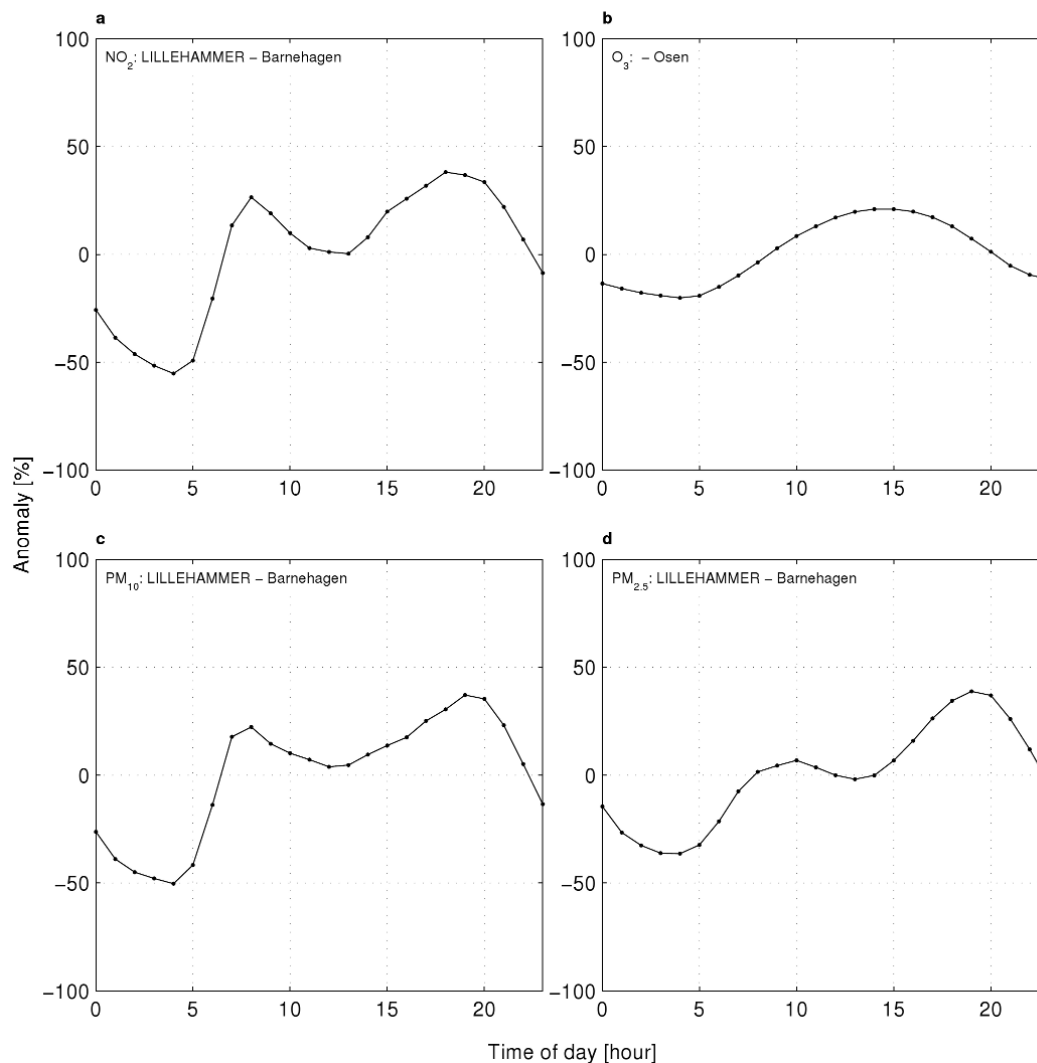


Figure 11: As Figure 10 but given as relative anomalies from the long-term mean concentration.

3.4 Matrices of temporal variability

While plots showing anomalies of annual and daily variability as for example in Figures 9 and 11 as well as in Appendices A and B are useful in their own right, for computational reasons it is advantageous to work with anomalies that combine the deviation from the long-term mean value for each individual hour of the year.

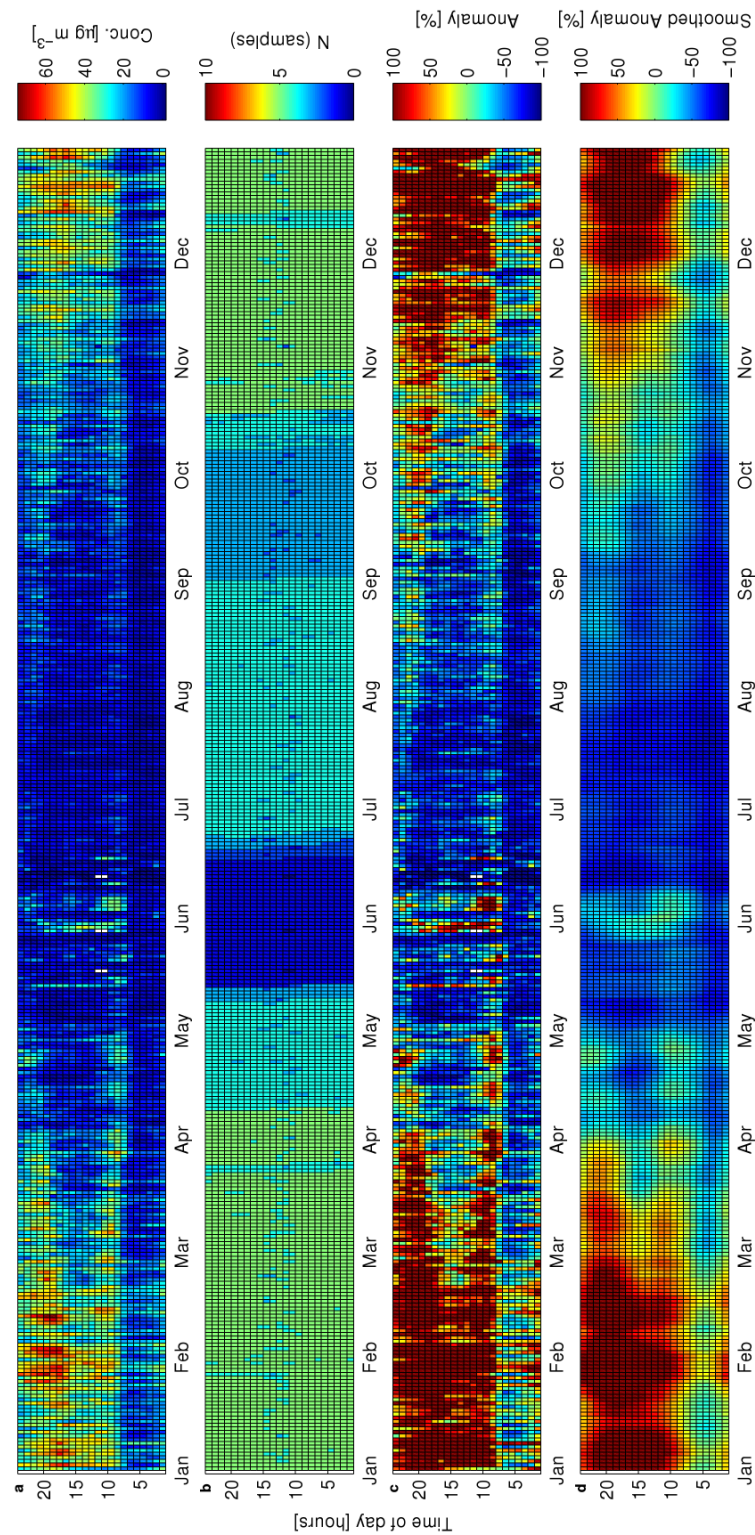


Figure 12: NO₂ at station NO0075A Barnehaven: Annual matrices of hourly averages computed over entire available time series, shown as a) Observations, b) number of years with available data, c) the anomaly computed from the long-term mean, and d) the anomaly from the long-term mean smoothed using a low-pass filter.

Figure 12 shows an example of a matrix plot illustrating both annual and daily variability, in this case for NO₂ at the *NO0075A Lillehammer Barnehaugen* station. The matrix of observations in Figure 12a was obtained by finding all existing samples in the time series that correspond to each of the 8760 hours in the year, and then averaging the concentrations reported over all the corresponding samples such that an average hourly value for all hours of each day of the year was obtained.

As the figure shows both the annual and daily variability as the same time it is very valuable for studying how the daily cycle of NO₂ changes throughout the year. In this case we can clearly see not only that the highest concentrations at this location occur in late January and early February but also that their absolute maxima occur in the hours between 15:00 and 20:00.

Often the time series of observations at air quality stations in Norway are not particularly long it is important to keep in mind the number of samples during the averaging process in order to ensure that a valid mean is computed. Figure 12b shows the number of samples (which is equivalent to the number of years of available data in this case) that was used to compute each hourly average in Figure 12a. In this example the number of samples is about 5 between November and April but drops to 4 throughout the summer months and even reaches 3 in June. The averages obtained during those times of low sample size are therefore less reliable and more prone to small-scale temporal variability which is not representative of the long-term average behavior. It should be noted that stations exceeding a number of 60 days per year for which the sample size was less than 4, were not considered in the analysis.

Figure 12c then shows the observed concentrations of NO₂ expressed as an anomaly, i.e. the percentage above or below the long-term mean. It can be seen that the values throughout the winter months are generally above 50% during the day with many days exceeding 100%. Finally, Figure 12d depicts the same anomaly as shown in 12c but after smoothing the matrix using a low-pass filter in order to eliminate spurious variability not representative of the long-term average variability. This is the type of matrix that was used to estimate concentrations at any time at any day of the year for any location within the station's representativity area (see Section 2.4).

The complete set of figures depicting matrix plots for all four species and all stations is provided in Appendix C for reference.

3.5 Excel Prototype

A simple prototype tool was developed in Microsoft Excel to provide easy access to the data. It consists of four spreadsheets, one for each considered species. Figure 13 shows an example of the user interface for estimating background NO₂ concentrations. Each spreadsheet contains several tabs for data and calculations, however the user only deals with the spreadsheet labeled "MainForm". Here, the user enters the coordinates of the location of interest in latitude and longitude given as decimal degrees. The user further enters information on the requested day of year and the hour of day and the output cell immediately is updated with the estimated concentration for the selected species. Note that the input values are not

tested for their validity, i.e. the user will not get an error message if a wrong datatype or a value outside the valid range is entered. The valid range for each input value is provided next to the input fields.

Behind the scenes, the requested coordinates are then compared to the coordinates of all available grid cells over Norway and the spatially closest one is selected. Together with the input on day of year and hour of day, this information is then used to access the corresponding concentration value in a pre-computed look-up table. This value is then displayed in the output field. Due to the limitation of Excel's ability to handle large datasets, the spreadsheets representing the four species had to be saved in separate files due to the size of the underlying look-up tables (200–300 MB per file).

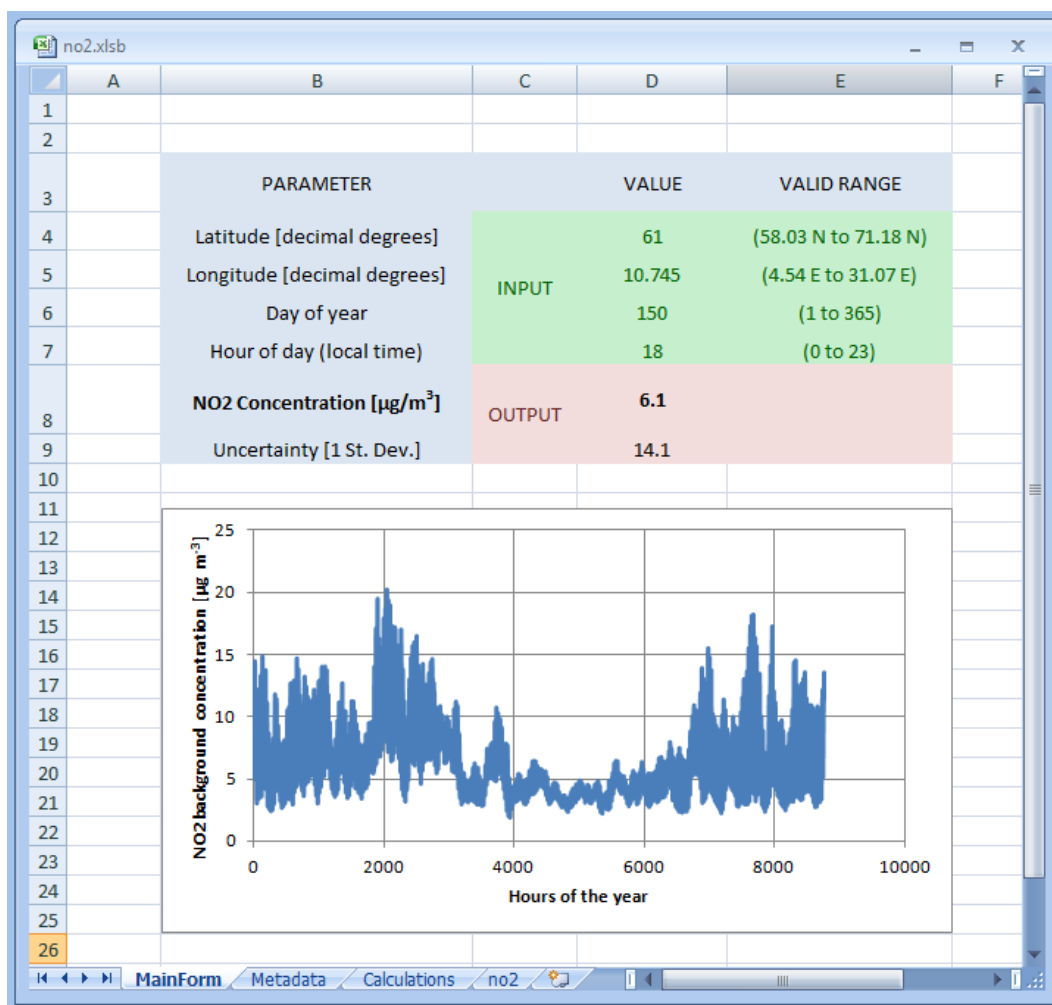


Figure 13: Screenshot of a simple Excel user interface for obtaining estimates of background concentrations for a given day of year and hour of day at any location in Norway, here shown for NO_2 . Time series of background concentration at hourly resolution can also be plotted.

The Excel prototype also contains a simple estimate of uncertainty. This estimate was obtained by combining the kriging uncertainty with an estimate of the hourly uncertainty due to temporal variability, which was obtained by validation against station data that were not used in the analysis. Note that the given uncertainties

are only very approximate estimates and it is highly recommended to perform a more detailed validation and uncertainty analysis in future work.

3.6 Online version

An online version of the dataset will be made accessible on the website www.luftkvalitet.info. In addition to displaying maps of annual mean values, it will enable the user to select a location in Norway and to acquire numeric values of concentrations for specific days and times or time series of concentrations at that location. Furthermore, the Excel-based version of the dataset as well as the same data in NetCDF file format will be made available online.

3.7 Assessment of error sources and uncertainty

The methodology for estimating Norwegian background concentrations developed within the scope of this project is prone to several sources of error that are associated with some of the simplifying assumptions listed in the following.

First, one of the most fundamental assumptions made as a part of this work is that concentrations of NO_2 , O_3 , PM_{10} , and $\text{PM}_{2.5}$ are strongly autocorrelated in both space and time. In the spatial domain this assumption is of course used within the applied geostatistical techniques in that a model of autocorrelation such as the semivariogram model is used (see Section 2.2). The autocorrelation in the temporal domain is analyzed and considered by using hourly observations at air quality stations.

A second major assumption is that background concentrations can be estimated at a reasonably high accuracy by using geostatistically derived maps of mean annual concentrations in conjunction with average relative daily and annual anomalies computed from time series at air quality stations. Geostatistical methods have been shown to be “optimal” in the sense of minimizing the error of the predicted values (Isaaks and Srivastava, 1989; Cressie, 1993; Goovaerts, 1997; Wackernagel, 2003), however even the most sophisticated interpolation techniques will produce highly uncertain predictions in the absence of observations. As such, the kriged predictions at locations that are quite distant from existing stations, e.g. in the mountainous inland areas of Norway, can be associated with substantial uncertainties, despite the fact that multiple linear regression with auxiliary datasets was used to partially overcome this problem. Figure 14 shows the spatial patterns of uncertainty associated with the residual kriging process for O_3 over Norway. It is obvious from this figure that the lowest uncertainties can be found in areas with relatively high station density (at least compared to the rest of Scandinavia) such as in southeastern Norway, whereas the highest uncertainties are located in the Lofoten and the very northeast of Norway along the border to Russia. When considering mapping the entire country of Norway it would thus be most helpful if additional O_3 stations were located in the area of Narvik or Tromsø as well as in the area of Kirkenes or the Varanger Peninsula. It would further be helpful for mapping purposes to have additional stations in the area between Bergen and Ålesund, as well as in the mountainous inland region in the area of Sognefjord or Jotunheimen. The latter stations should be able to reduce the mapping uncertainty for the entire southern half of the

country to approximately the same levels that are found in the greater Oslo area (see also Figure 3b).

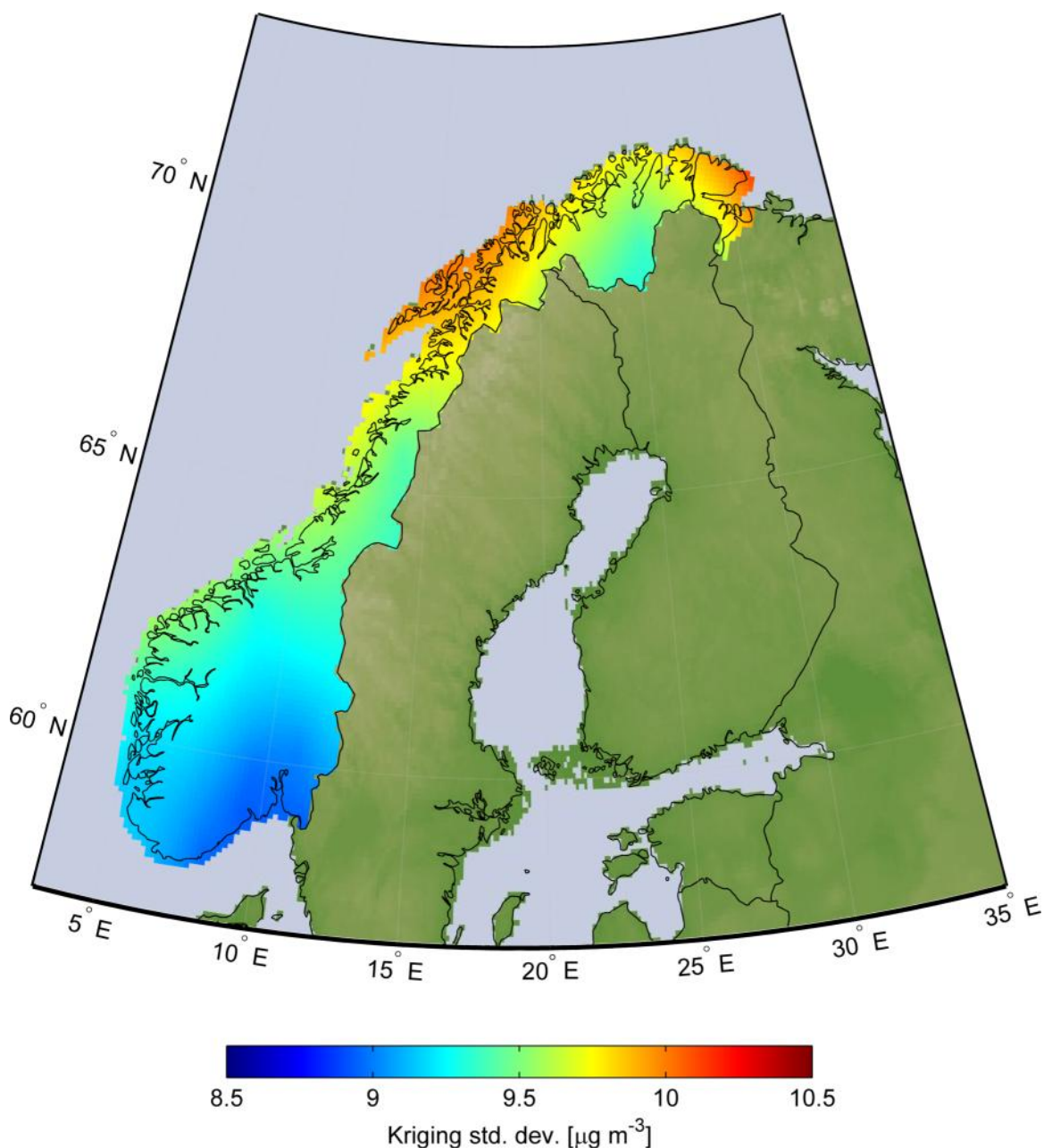


Figure 14: Uncertainty resulting from the geostatistical processing for O_3 , shown as the standard deviation. Note that this map only shows the uncertainty associated with the procedure of kriging the residuals and does not take into account additional uncertainty resulting the multiple linear regression of auxiliary variables or other sources of error.

It is important to stress that the uncertainty map provided in Figure 14 does not indicate the uncertainty of the final estimate of O_3 as seen in Figure 4. Instead it only shows the uncertainty that stems from the process of ordinary kriging of the residuals of the linear regression. Uncertainty due to multiple linear regression or other error sources is not considered. It should also be noted that the given

uncertainty is computed based on a variogram derived over all of Europe which is likely to provide uncertainty estimates for Norway that are biased low.

Third, it should be noted that only background concentrations for one year (2007 for NO₂ and 2008 for all other species) were considered and used as data for a reference year. While it is reasonable to assume that the interannual variability in annual means is small and that the spatial patterns of the concentrations are somewhat constant, the use of this background concentration in years whose annual mean values differ substantially from those observed in 2008 will obviously lead to significant errors. It would be therefore helpful to average the annual means over several years to eliminate spurious artefacts and spatial variability that is not consistent with the long-term average background concentrations.

As a fourth and final point, it should be noted that the use of the low-pass filter for smoothing the matrices of temporal variability can in some cases increase the uncertainty associated with the predictions. While useful for eliminating spurious short-term variability that is not representative of the long-term average variability, the smoothing of the temporal variability matrix as shown in Figure 12 and Appendix C using a low-pass filter can also accidentally remove wanted detail in the signal, such as the sharp onset of the daily NO₂ increase during the morning rush hour. More research will be necessary to determine the most appropriate smoothing techniques for each species considered. However, smoothing the temporal variability matrix is only necessary because for most stations and species the available time series are relatively short and thus the computed hourly averages are prone to large uncertainties. The importance of smoothing will decrease with a growing length of the time series as the averaging over significantly longer time series will serve the same purpose and will inherently provide smoother results.

In general, it should be noted that no comprehensive validation has been performed with respect to the final values obtained from both the geostatistical mapping and the temporal analysis. While the background map data obtained from ETC/ACC has been extensively validated, the values given for individual hours of the year as provided by the Excel prototype and the online version of the dataset are associated with significant uncertainties due to several simplifying assumptions and a variety of error sources in the applied methodology. It is thus recommended to always double-check the results for potentially erroneous outliers and ideally to get advice from experts who might be able to judge the realism of the results and can provide warnings about potentially problematic predictions.

3.8 Station distribution and density

In comparison to the rest of Europe the density of suitable air quality stations in Norway is very low. A considerable increase in mapping accuracy could be achieved through establishing additional air quality stations in various parts of the country. As can be seen in Figure 4a, the entire northern half of Norway is lacking suitable background stations measuring long time series of NO₂. Establishing suitable NO₂ background measurements in the Tromsø area alone would be very helpful. Additional measurements in the Trondheim and Kirkenes areas would

further reduce the uncertainty. With respect to O₃, it has already been mentioned previously that additional observations in Tromsø, Kirkenes, and possibly in the area of Bergen and Ålesund would have the greatest effect. As for PM₁₀, the southern half of the country is reasonably well represented in terms of observations, so the biggest gains could be achieved through additional measurements in Trondheim, Tromsø, and Kirkenes. Finally, as Figure 4d shows, only one station in Lillehammer provides suitably long time series of PM_{2.5}, so additional measurements of this variable are welcome almost anywhere, but would have the greatest effect in the northern half of the country (e.g. Tromsø) and in the western part of the country (e.g. Bergen).

4 Possible improvements

The methodology developed for this project and the associated results are primarily intended to provide an update to the previously used “Bakgrunnsatlas fra VLUFT” report which was developed in 1993. This goal has certainly been accomplished as the provided results can give estimates of background concentration at a much finer spatial and temporal resolution (see Figure A). However, to achieve this goal within the given time and budget constraints required the use of some techniques that might be somewhat simplifying. A variety of more advanced techniques could be applied in the future to improve the current results.

A modification with possibly significant impact is to perform the mapping of background concentration for the last several years instead of just for 2007/2008. This would have significant implications on the results in that the datasets could either be used individually if the user is interested in estimating concentration during one of those past previous years, or the maps for all available years could be averaged to result in a much representative “typical” reference year if the user is interested in current or future estimates.

For example, the mapping could be substantially improved by using more detailed auxiliary datasets. In particular the output from the EMEP model that was used has a quite coarse spatial resolution (50 km × 50 km). There is work currently in progress that can deliver similar gridded output of model reanalysis results at a much finer spatial resolution, e.g. the regional reanalysis results obtained within the MACC project (Rouil et al., 2011a,b). It is also conceivable that using satellite data as an additional auxiliary variable could be quite beneficial. For example, the mean annual tropospheric column of NO₂ obtained from instruments such as SCIAMACHY, GOME-2, and OMI appears to be a good source of information for the spatial distribution of NO₂, although observations gaps due to cloud cover and polar night could be problematic for the use in Norway.

In conjunction with more detailed auxiliary datasets it might also be useful to increase the spatial resolution of the mapping procedure, possibly even down to a grid cell size of 1 km × 1 km. While such a resolution is currently impractical at the European level due to the computational demands, it might be a realistic resolution for a single country such as Norway.

As mentioned previously it would also be useful to improve the methodology for estimating the representativity of the existing air quality stations in Norway. The currently used *nearest neighbor* approach is very simple and it would likely improve the results if more sophisticated methods were used for this purpose. Such methods could involve computing a station weight for each grid cell (for example based on the inverse of the square distance) and thus using the weighted average temporal pattern from several stations at a given grid cell. In contrast to these automated methods, another approach might be to use expert knowledge in manually identifying the local area for which each station can be considered as representative.

The mapping procedure for O₃ was simplified with respect to the more complex mapping algorithm operationally used by ETC/ACC. Improvements in O₃ mapping could be likely obtained by implementing some of the more sophisticated techniques used there, such as separate mapping for urban and rural areas and a combination of the two maps based on population density. It would further be valuable to perform a validation of the O₃ residual kriging results.

Finally, the value of the reported results could be improved by performing a comprehensive validation of the estimated background concentrations for each hour of the year. Doing so is challenging as it requires the use of one (or several) of the existing air quality station, which then in turn would have to be eliminated from the station dataset used for the mapping. Since the station density is already low over Norway, the loss of an additional station is likely to have a detrimental effect on the quality of the predictions. Nonetheless, such a task would be valuable as it would not only allow for estimating the accuracy of the results but could also provide some form of uncertainty estimate.

5 Summary

Knowledge of the approximate background concentration is valuable for a variety of applications, in particular for estimating air quality in conjunction with various sources and for planning purposes within the municipalities. In Norway, a major source of information on background concentrations has previously been the “Bakgrunnsatlas fra VLUFT”, which is now nearly 20 years old. An updated dataset with higher spatial and temporal resolution and utilizing today’s more advances data sources and technology is therefore desirable.

In order to address this problem a methodology was developed to provide estimates of background concentrations for NO₂, O₃, PM₁₀, and PM_{2.5} over Norway at both relatively fine spatial and temporal scales. The methodology involves two major components: Spatial patterns of annual mean background concentrations were obtained using geostatistical methods and mapped on a 10 km × 10 km grid. In part, and where available, these datasets were acquired from the European Topic Centre on Air and Climate Change (ETC/ACC) and then modified accordingly to be usable within the framework of this project, and in part they were computed from raw station and auxiliary data using a similar methodology.

The second major component of the methodology involves the construction of representative time series of annual and daily variability at all available stations in order to provide a temporal dimension. For this purpose, air quality stations in Norway were selected based on the length of their data archive and time series of relative anomalies from the long-term mean were computed for each station as well as each of the four species considered. These time series at each station are then assumed to be representative for the area surrounding the station such that the background concentration of neighboring grid cells can be determined at a given time and day of year. The representativity of the stations is computed using a simple *nearest neighbor* approach.

The result of the project is a dataset estimating the Norwegian background concentrations for NO₂, O₃, PM₁₀, and PM_{2.5} at a spatial resolution of 10 km × 10 km and for each single hour of an “average” year, while using the background concentration of the year 2008 as a reference (2007 for NO₂). Access to the dataset is provided through a very simple Excel spreadsheet, a NetCDF file, as well as an online application on the website www.luftkvalitet.info. All three methods provide the user with easy access to the estimated values of various species’ background concentration for a given location in Norway and a given time and day of year.

Compared to the previously used VLUFT dataset, the method presented here has clear advantages in that it provides a significantly higher information density in both the spatial as well as the temporal dimension (see Figure A). The method provides quantitatively reasonable estimates of background concentrations, although the uncertainty at the hourly level is quite high. The main source of uncertainty is the low number of suitable background stations located in Norway. A major advantage of the technique is further that it is automated and can be easily updated with new data.

6 Acknowledgements

We are grateful to Jan Horálek at the Czech Hydrometeorological Institute (CHMI) for providing several updated datasets of European air quality developed within the European Topic Centre on Air and Climate Change.

7 References

- Bovensmann, H., Burrows, J. P., Buchwitz, M., Frerick, J., Noël, S., Rozanov, V. V., Chance, K. V., Goede, A. P. H. (1999) SCIAMACHY: Mission Objectives and Measurement Modes. *J. Atmos. Sci.*, 56, 127–150.
- Cressie, N. A. C. (1993) *Statistics for spatial data*. New York, Wiley-Interscience.
- Denby, B., Gola, G., de Leeuw, F., de Smet, P., Horálek, J. (2011) Calculation of pseudo PM_{2.5} annual mean concentrations in Europe based on annual mean PM₁₀ concentrations and other supplementary data. Bilthoven, European Topic Centre on Air and Climate Change (ETC/ACC Technical paper, 2010/9).

EROS Data Center (1996) GTOPO30 (Global 30 Arc-Second Elevation Data Set).

URL:

http://eros.usgs.gov/#/Find_Data/Products_and_Data_Available/gtopo30_info

Fagerli, H., Gauss, M., Benedictow, A., Griesfeller, J., Jonson, J. E., Nyiri, A., Schulz, M., Simpson, D., Steensen, B. M., Tsyro, S., Valdebenito, A., Wind, P., Aas, W., Hjellbrekke, A.-G., Mareckova, K., Wankmueller, R., Iversen, T., Kirkevåg, A., Seland, O., Vieno, M. (2011) Transboundary acidification, eutrophication and ground level ozone in Europe in 2009. Oslo, Norwegian Meteorological Institute (EMEP Status Report 1/2011).

Fagerli, H., Simpson, D., Tsyro, S., Solberg, S., Aas, W. (2003) Transboundary acidification, eutrophication and ground level ozone in Europe. Part II - Unified EMEP model performance. Oslo, Norwegian Meteorological Institute (EMEP Status Report 1/2003).

Gesch, D. B., Verdin, K. L., Greenlee, S. K. (1999) New land surface digital elevation model covers the earth. *EOS Transactions*, 80, 67–70.

Goovaerts, P. (1997) *Geostatistics for natural resources evaluation*. New York, Oxford University Press.

Gottwald, M., Bovensmann, H., Lichtenberg, G., Noel, S., von Barga, A., Slijkhuis, S., Piters, A., Hoogeveen, R., von Savigny, C., Buchwitz, M., Kokhanovsky, A., Richter, A., Rozanov, A., Holzer-Popp, T., Bramstedt, K., Lambert, J.-C., Skupin, J., Wittrock, F., Schrijver, H., Burrows, J. (2006) *SCIAMACHY - Monitoring the Changing Earth's Atmosphere*. Wessling, DLR, Institute für Methodik der Fernerkundung (IMF).

Horálek, J., Denby, B., Smet, P. D., Leeuw, F. D., Kurfürst, P., Swart, R., van Noije, T. (2007) Spatial mapping of air quality for European scale assessment. European Topic Centre on Air and Climate Change. (ETC/ACC Technical paper, 2006/6).

Horálek, J., Smet, P. D., Leeuw, F. D., Conková, M., Denby, B., Kurfürst, P. (2010) Methodological improvements on interpolating European air quality maps. European Topic Centre on Air and Climate Change (ETC/ACC Technical paper, 2009/16).

Isaaks, E. H., Srivastava, R. M. (1989) *Applied geostatistics*. New York, Oxford University Press.

Levelt, P., van den Oord, G., Dobber, M., Malkki, A., Stammes, P., Lundell, J., Saari, H. (2006) The ozone monitoring instrument. *IEEE Trans. Geosci. Rem. Sens.*, 44, 1093–1101.

Munro, R., Eisinger, M., Anderson, C., Callies, J., Corpaccioli, E., Lang, R., Lefebvre, A., Livschitz, Y., Albiñana Perez, A. (2006) GOME-2 on MetOp. In: *Proceedings of the 2006 EUMETSAT Meteorological Satellite Conference*, Helsinki, Finland. **URL:**

http://www.eumetsat.int/Home/Main/AboutEUMETSAT/Publications/ConferenceandWorkshopProceedings/2006/groups/cps/documents/document/pdf_conf_p48_s4_01_munro_v.pdf.

Rouil, L., Massart, S., Beekman, M., Foret, G., Sofiev, M., Vira, J., Eskes, H., Meleux, F., Ung, A., Peuch, V.-H., Aldebenito, A., Gauss, M., Elbern, H., Friese, E., Strunk, A., Robertson, L., Schaap, M., Timmermans, R., Curier, L. (2011a) Assessment report: Air quality in Europe for 2007. INERIS (Technical Report D-R-EVA-3.1). URL: http://www.gmes-atmosphere.eu/documents/deliverables/r-eva/2007_Assessment%20Report.pdf.

Rouil, L., Massart, S., Beekman, M., Foret, G., Sofiev, M., Vira, J., Eskes, H., Meleux, F., Ung, A., Peuch, V.-H., Aldebenito, A., Gauss, M., Elbern, H., Friese, E., Strunk, A., Robertson, L., Schaap, M., Timmermans, R., Curier, L. (2011b) Evaluation report of the Air quality assessments in Europe for 2007. INERIS (Technical Report D-R-EVA-2.2). URL: http://www.gmes-atmosphere.eu/documents/deliverables/r-eva/2007_evaluation_%20Report_V1.pdf.

Simpson, D., Fagerli, H., Jonson, J., Tsyro, S., Wind, P. (2003) Transboundary acidification, eutrophication and ground level ozone in Europe. Part I: Unified EMEP model description. Oslo, Norwegian Meteorological Institute (Technical Report 1/2003).

Vestreng, V., Mareckova, K., Kakareka, S., Malchykhina, A., Kukharchyk, T. (2007) Inventory review 2007 - emission data reported to LRTAP Convention and NEC Directive - Stage 1 and 2 review. Oslo, Norwegian Meteorological Institute (Technical Report MSC-W 1/07).

Wackernagel, H. (2003) *Multivariate geostatistics: an introduction with applications*. Berlin, Springer.

Appendix A

Annual variability at all stations for all four species

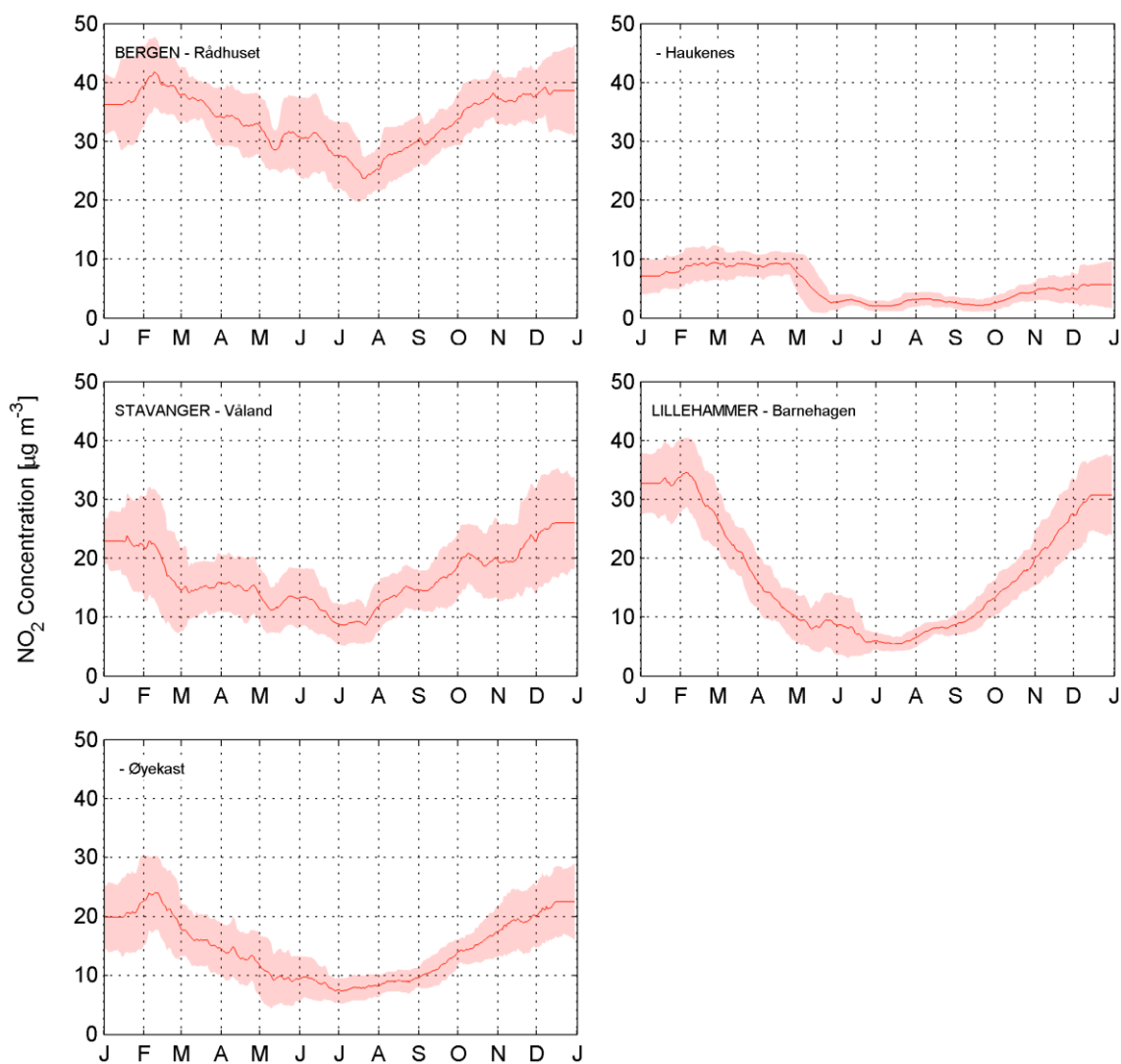
A.1 NO₂

Figure 15: Average seasonal variability of absolute observed NO₂ concentrations at each station with sufficiently long time series of data. The solid line shows the 1-month moving average, whereas the shaded area represents the 1-month moving standard deviation.

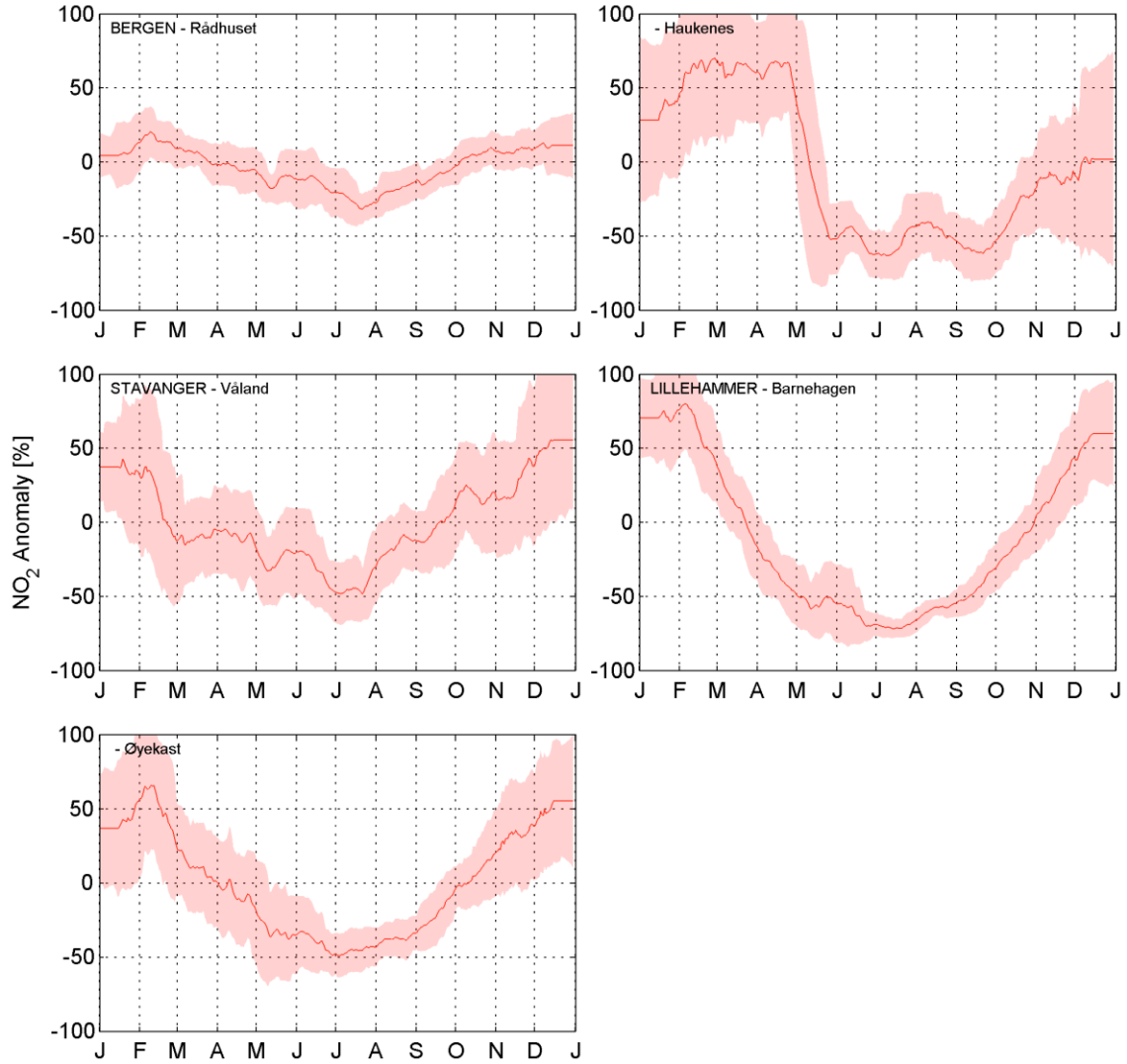


Figure 16: Average seasonal variability of relative NO₂ anomalies with respect to the long-term mean at each station with sufficiently long time series of data. The solid line shows the 1-month moving average, whereas the shaded area represents the 1-month moving standard deviation.

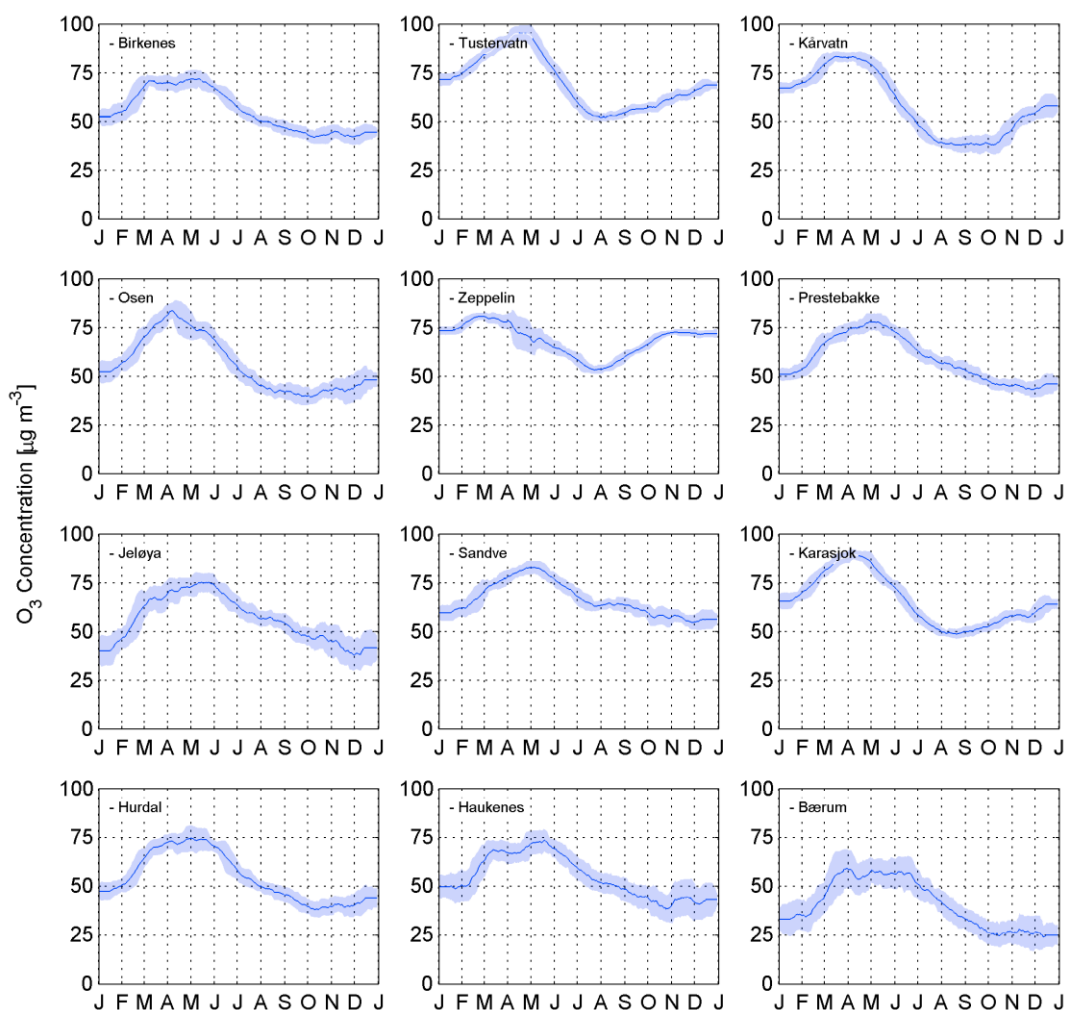
A.2 O₃

Figure 17: Average seasonal variability of absolute observed O₃ concentrations at each station with sufficiently long time series of data. The solid line shows the 1-month moving average, whereas the shaded area represents the 1-month moving standard deviation.

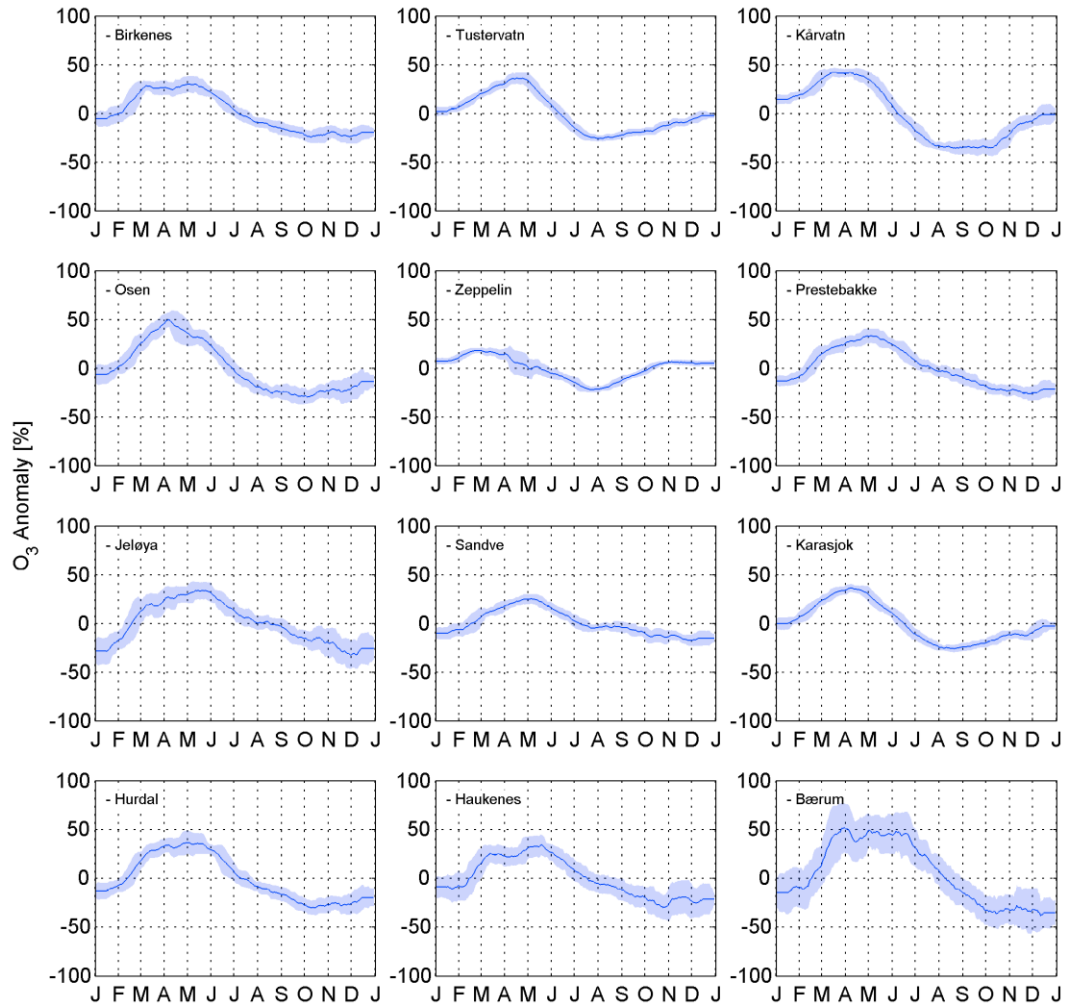


Figure 18: Average seasonal variability of relative O_3 anomalies with respect to the long-term mean at each station with sufficiently long time series of data. The solid line shows the 1-month moving average, whereas the shaded area represents the 1-month moving standard deviation.

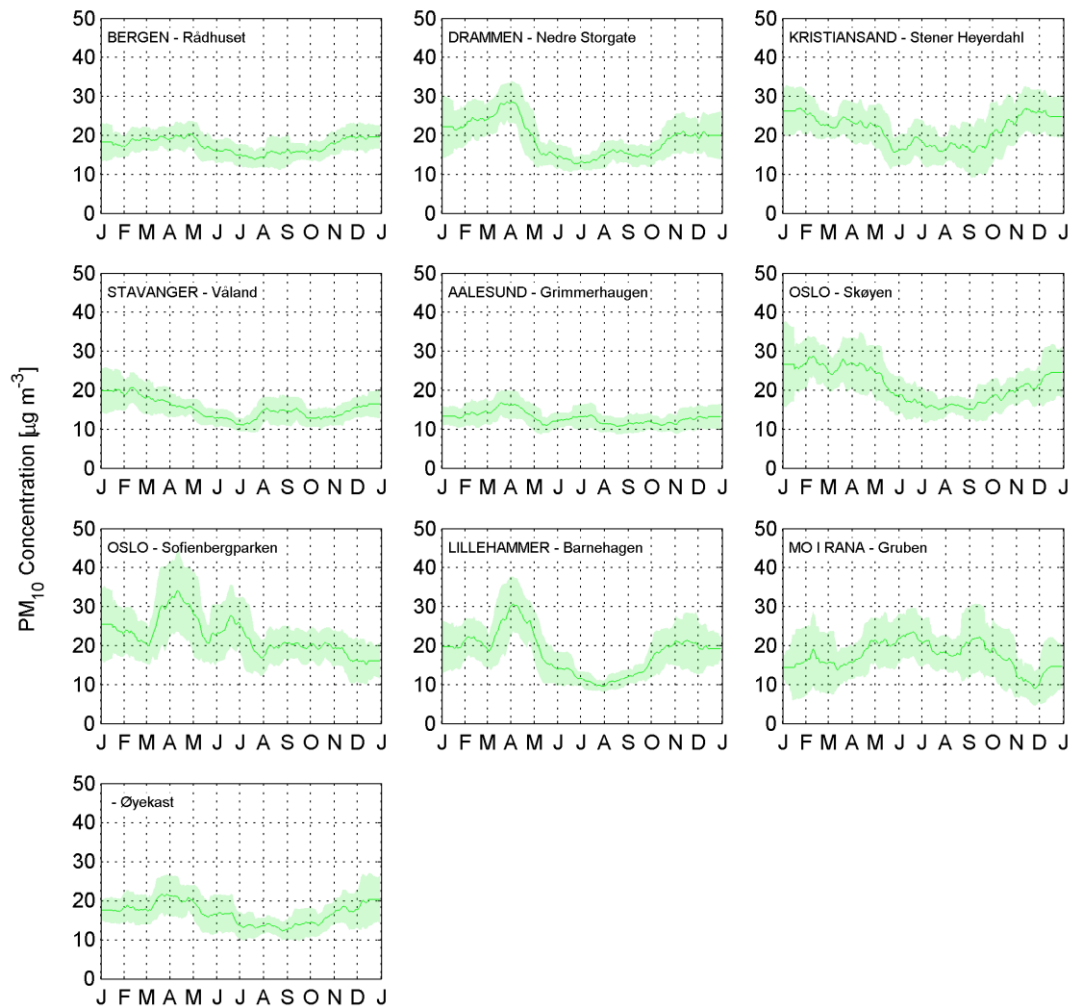
A.3 PM₁₀

Figure 19: Average seasonal variability of absolute observed PM₁₀ concentrations at each station with sufficiently long time series of data. The solid line shows the 1-month moving average, whereas the shaded area represents the 1-month moving standard deviation.

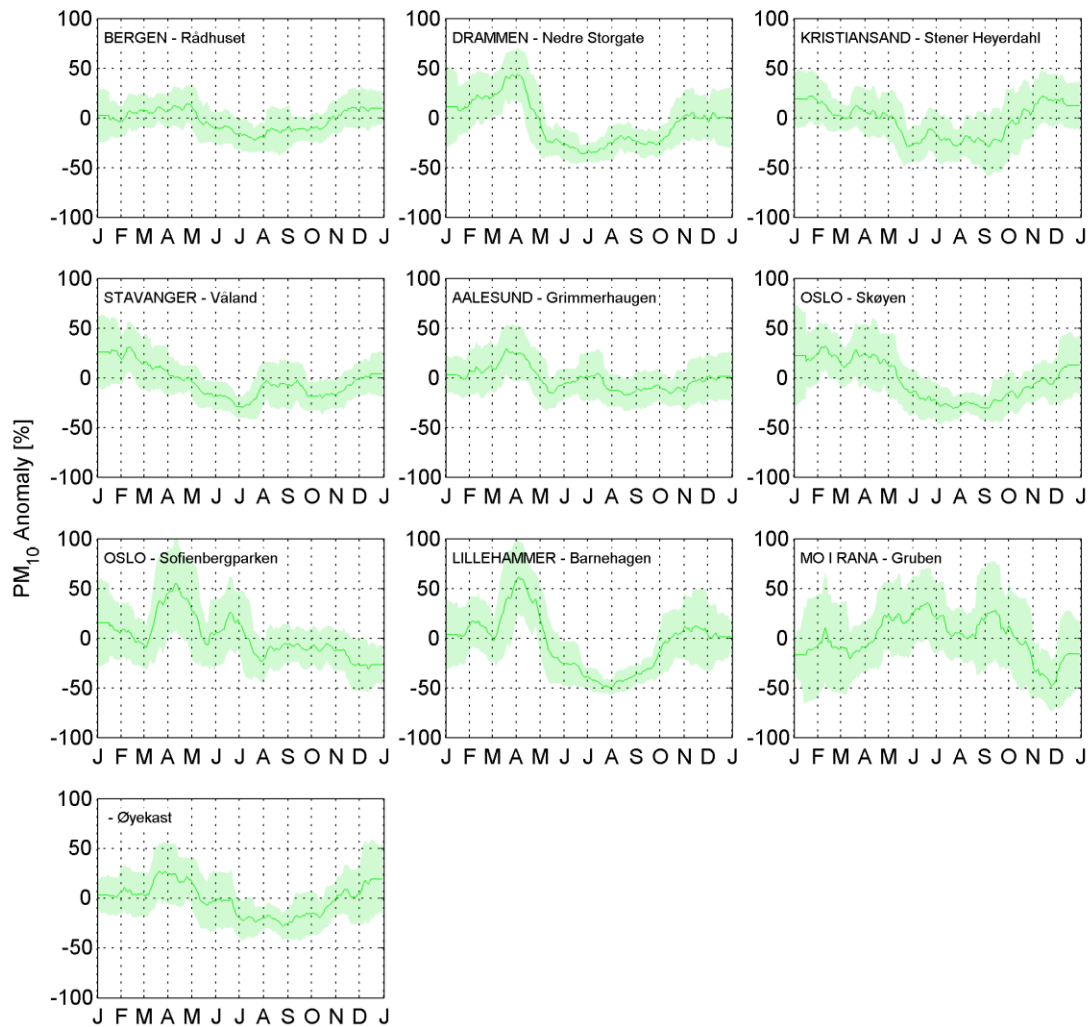


Figure 20: Average seasonal variability of relative PM_{10} anomalies with respect to the long-term mean at each station with sufficiently long time series of data. The solid line shows the 1-month moving average, whereas the shaded area represents the 1-month moving standard deviation.

A.4 PM_{2.5}

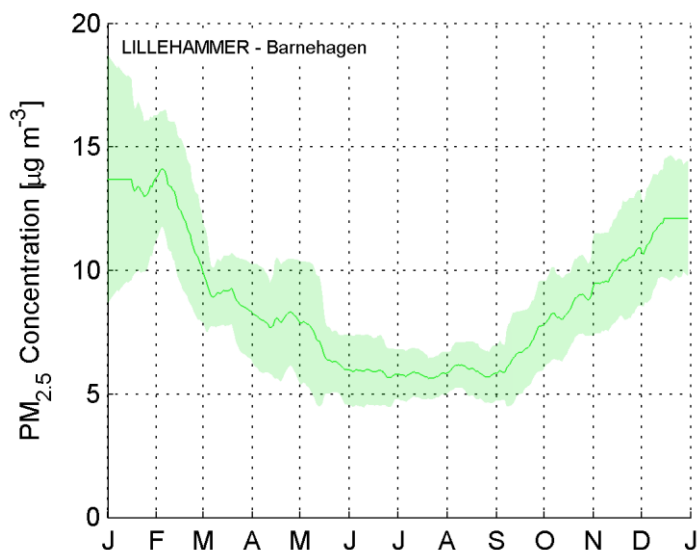


Figure 21: Average seasonal variability of absolute observed PM_{2.5} concentrations at the only station with sufficiently long time series of data. The solid line shows the 1-month moving average, whereas the shaded area represents the 1-month moving standard deviation.

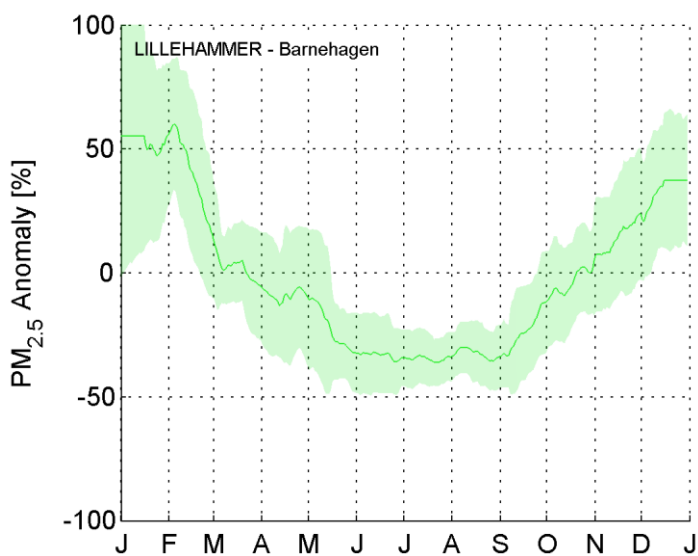


Figure 22: Average seasonal variability of relative PM_{2.5} anomalies with respect to the long-term mean at the only station with sufficiently long time series of data. The solid line shows the 1-month moving average, whereas the shaded area represents the 1-month moving standard deviation.

Appendix B

Daily variability at all stations for all four species

B.1 NO₂

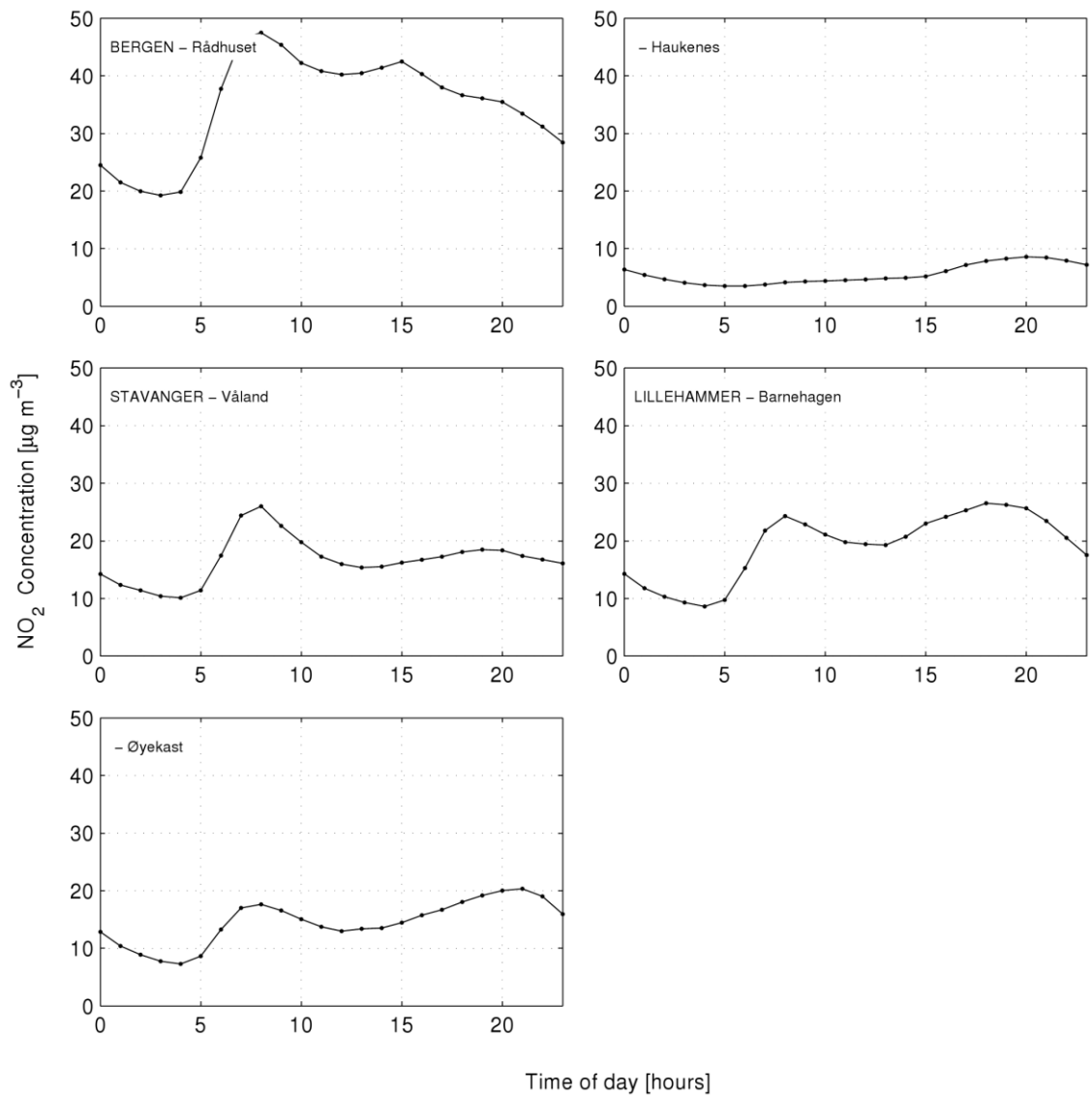


Figure 23: Average daily variability of absolute observed NO₂ concentrations at each station with sufficiently long time series of data.

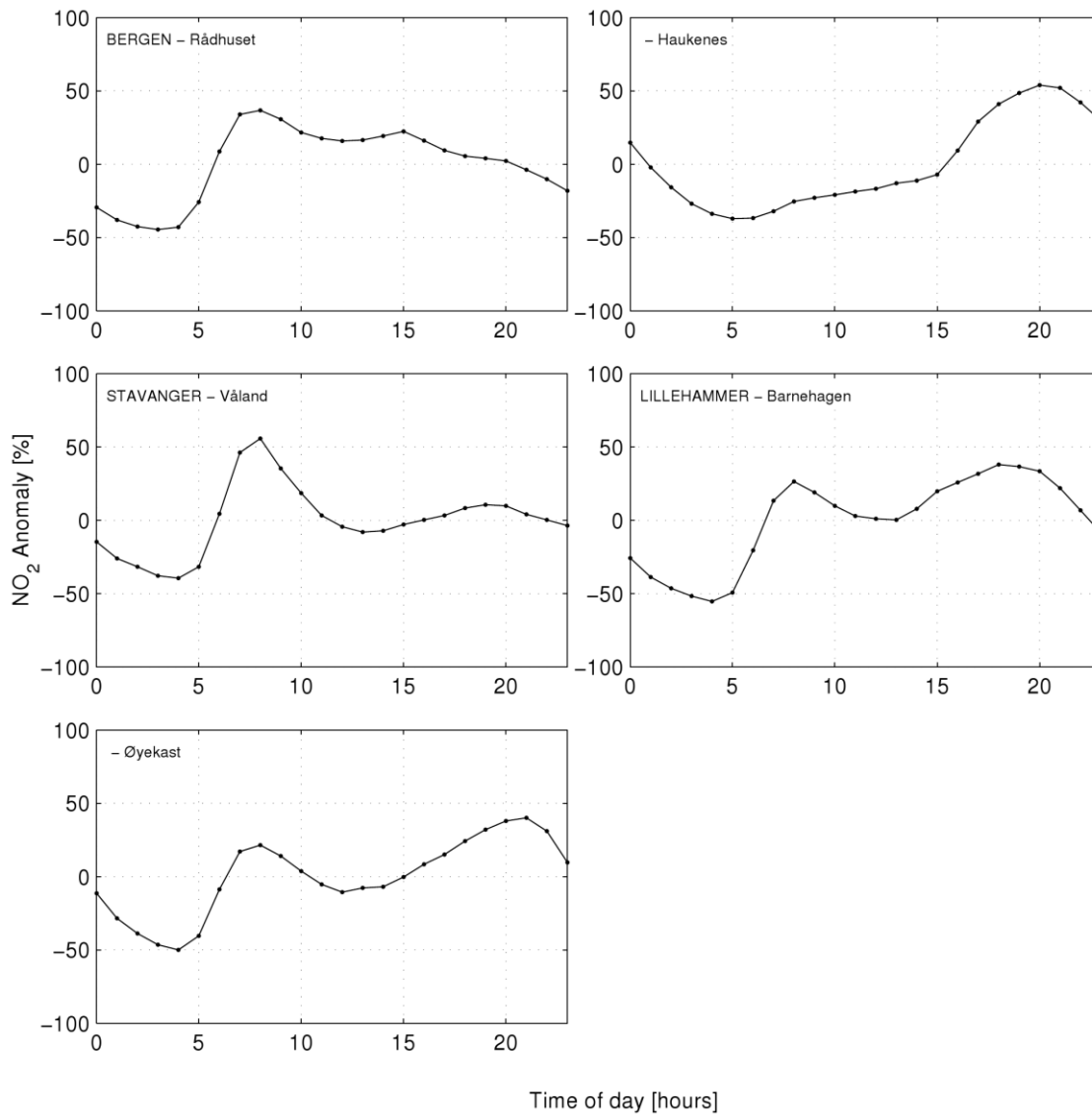


Figure 24: Average daily variability of relative NO₂ anomalies with respect to the long-term mean at each station with sufficiently long time series of data.

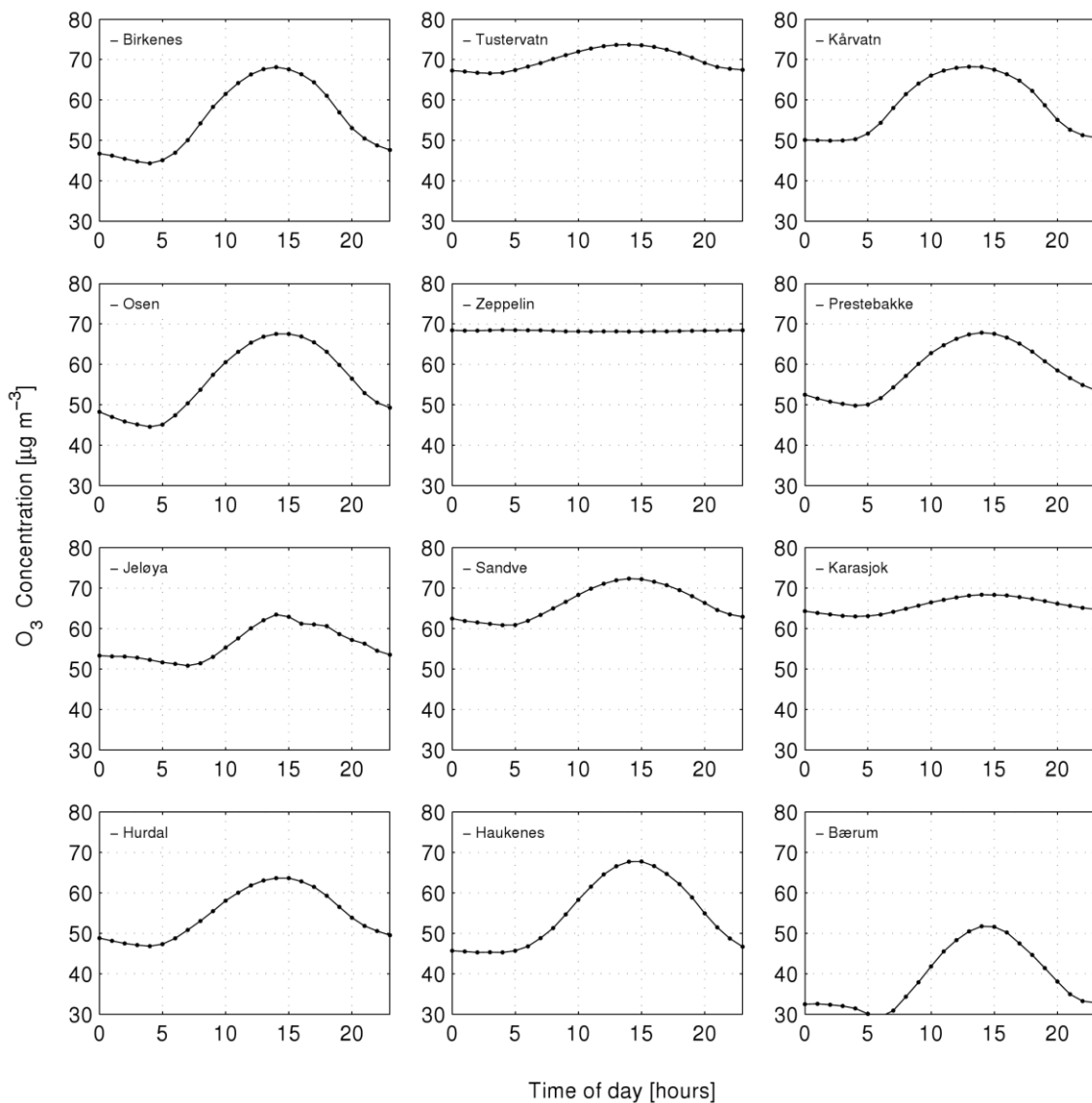
B.2 O₃

Figure 25: Average daily variability of absolute observed O₃ concentrations at each station with sufficiently long time series of data.

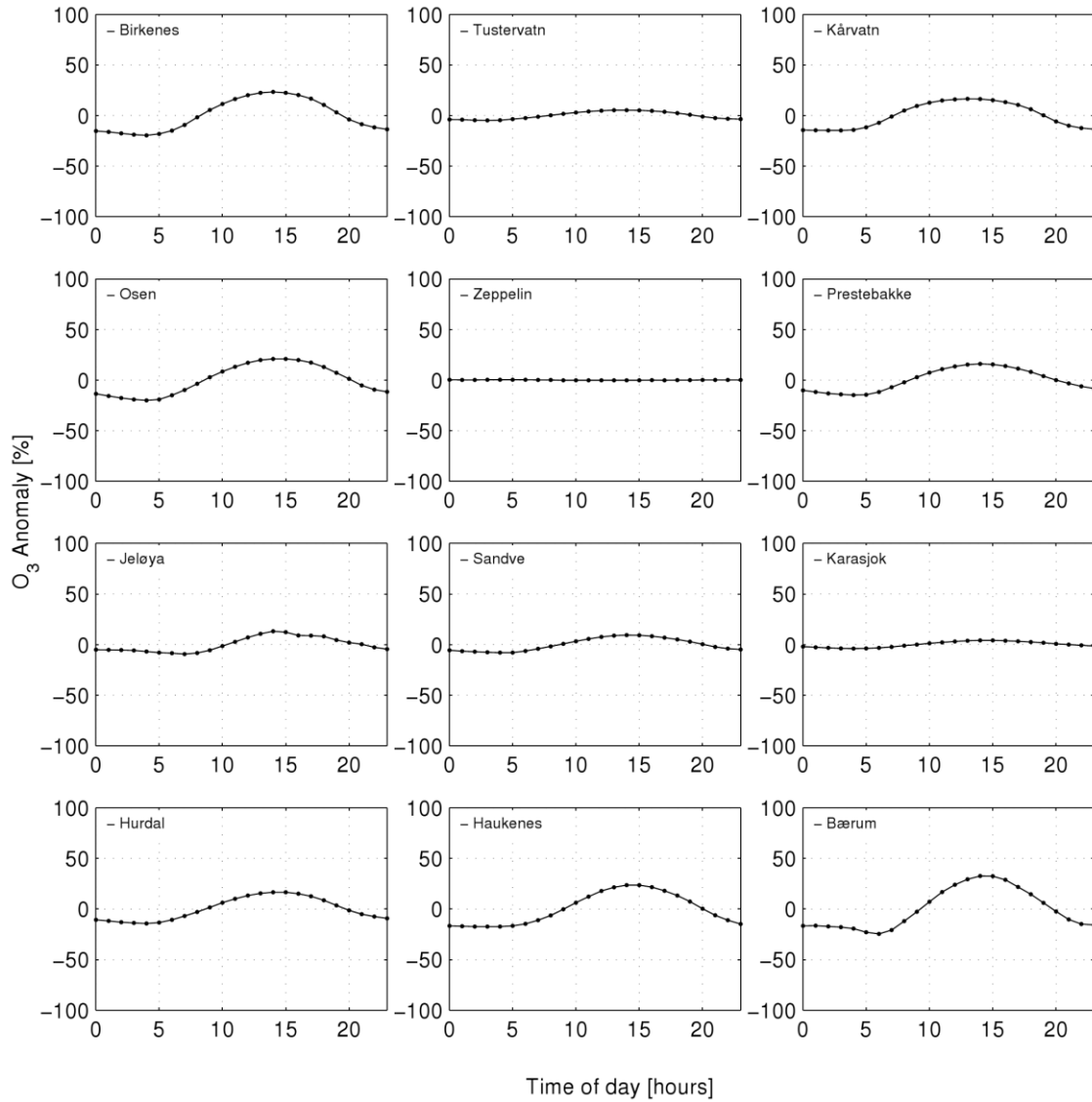


Figure 26: Average daily variability of relative O_3 anomalies with respect to the long-term mean at each station with sufficiently long time series of data.

B.3 PM₁₀

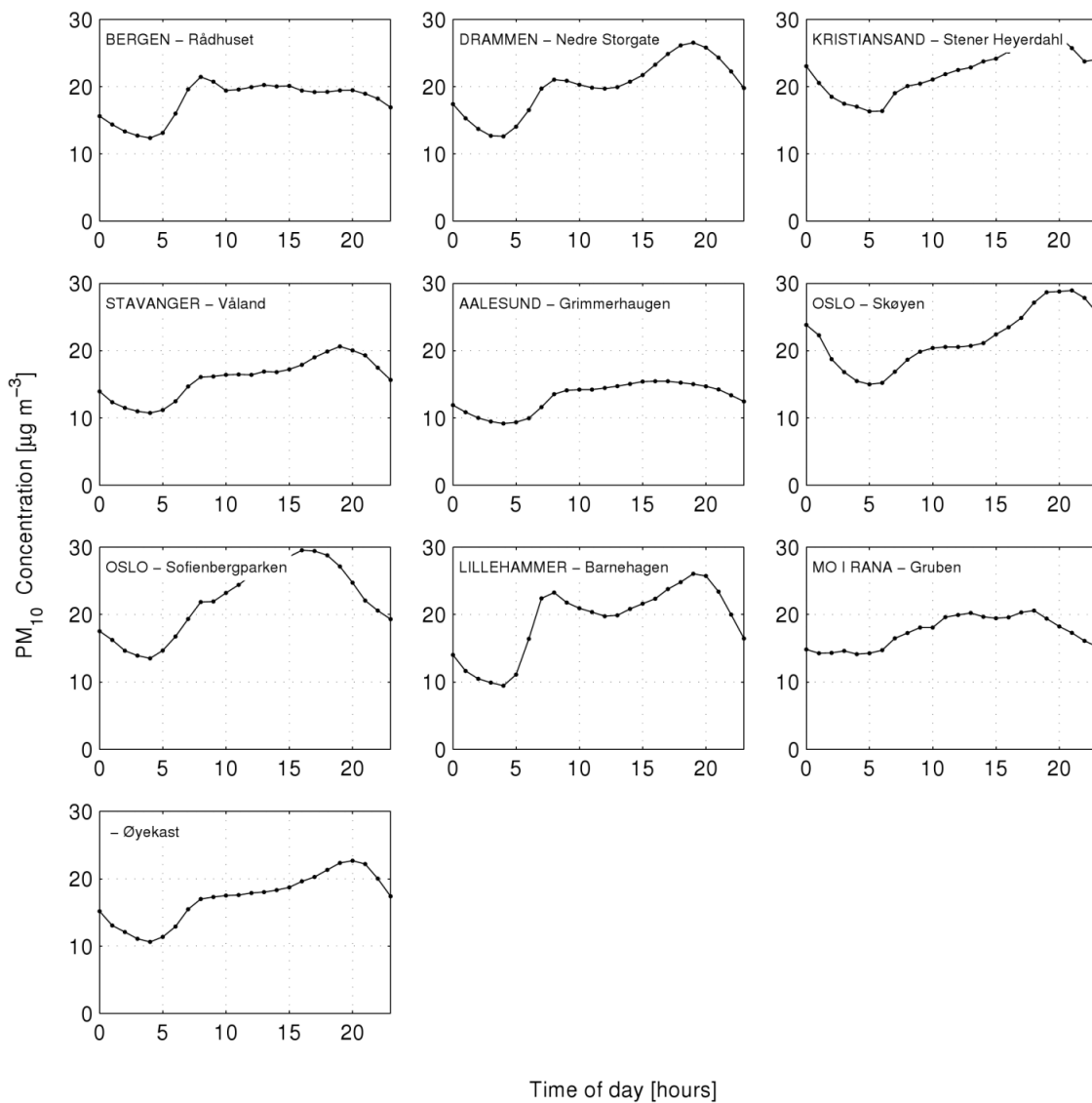


Figure 27: Average daily variability of absolute observed PM₁₀ concentrations at each station with sufficiently long time series of data.

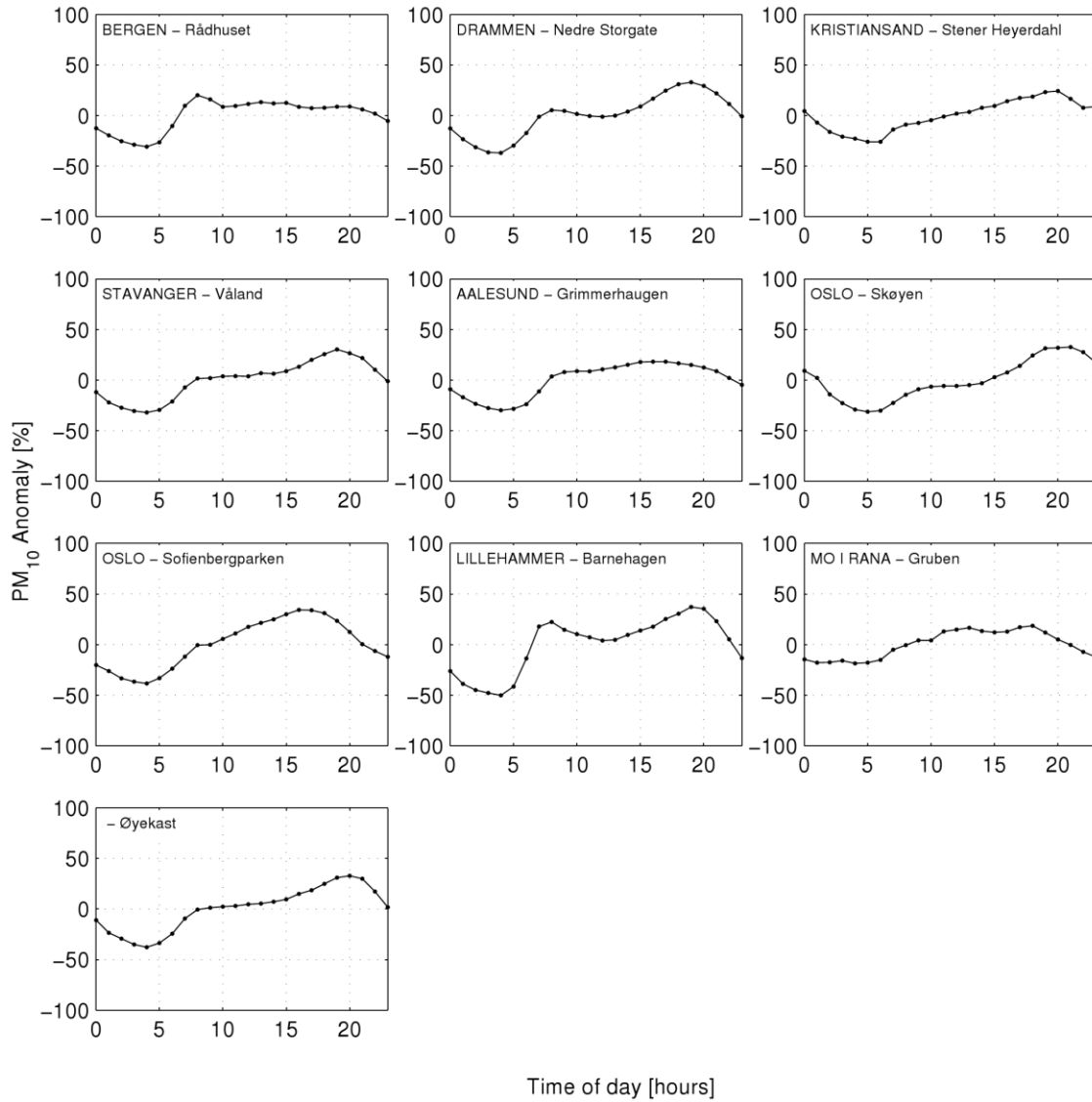


Figure 28: Average daily variability of relative PM_{10} anomalies with respect to the long-term mean at each station with sufficiently long time series of data.

B.4 PM_{2.5}

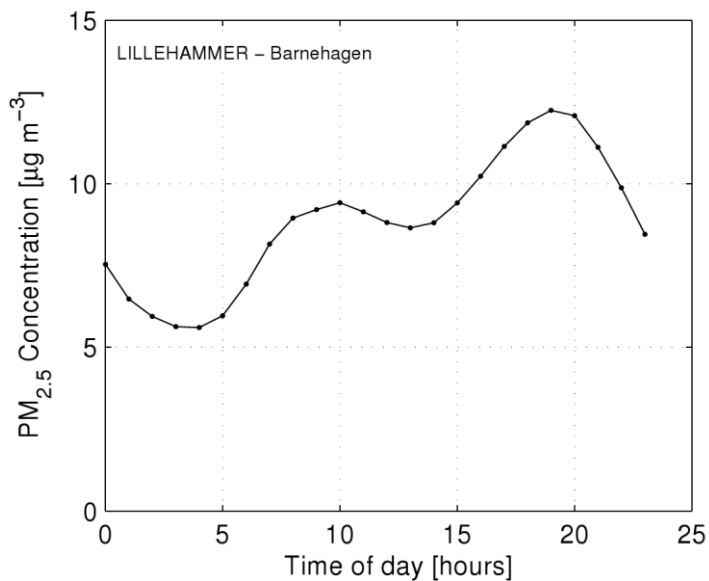


Figure 29: Average daily variability of absolute observed PM_{2.5} concentrations at the only station with sufficiently long time series of data.

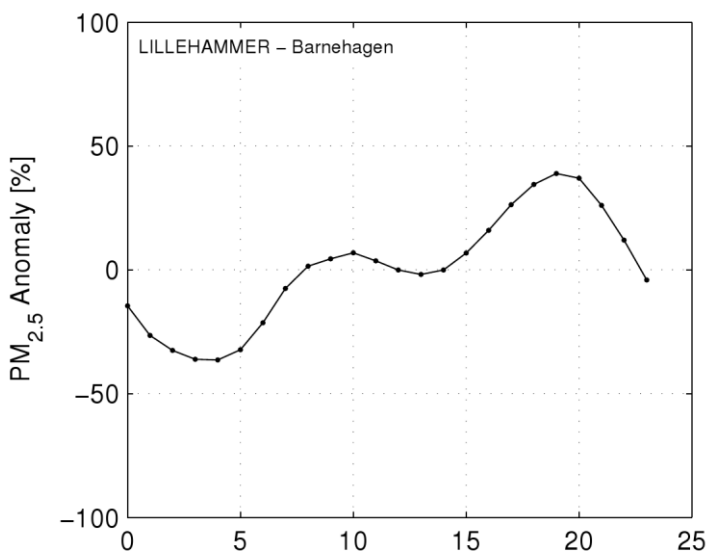


Figure 30: Average daily variability of relative PM_{2.5} anomalies with respect to the long-term mean at the only station with sufficiently long time series of data.

Appendix C

Matrix visualization of annual and daily variation at all stations

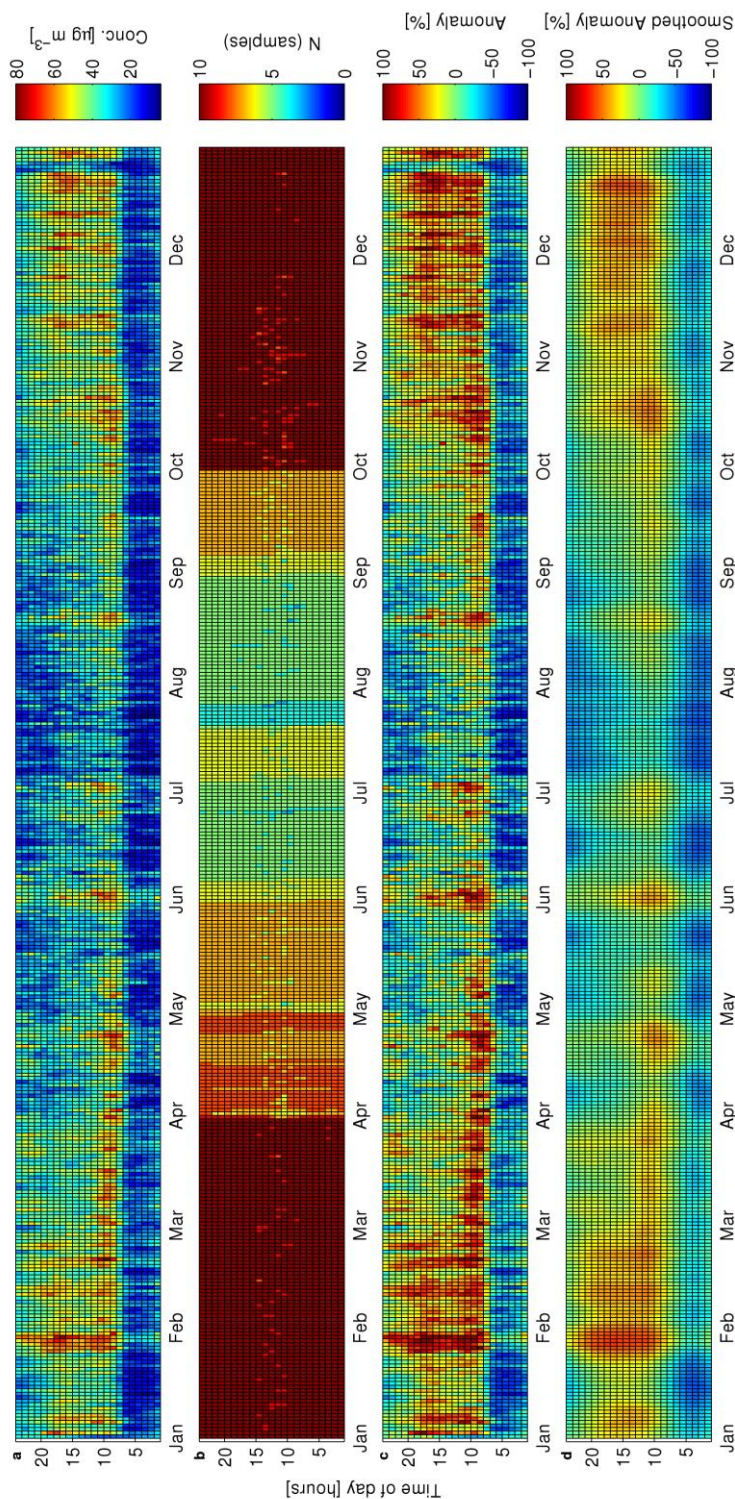
C.1 NO₂

Figure 31: NO₂ at station *NO0015A Rådhuset*: Annual matrices of hourly averages computed over entire available time series, shown as a) Observations, b) number of years with available data, c) the anomaly computed from the long-term mean, and d) the anomaly from the long-term mean smoothed using a low-pass filter.

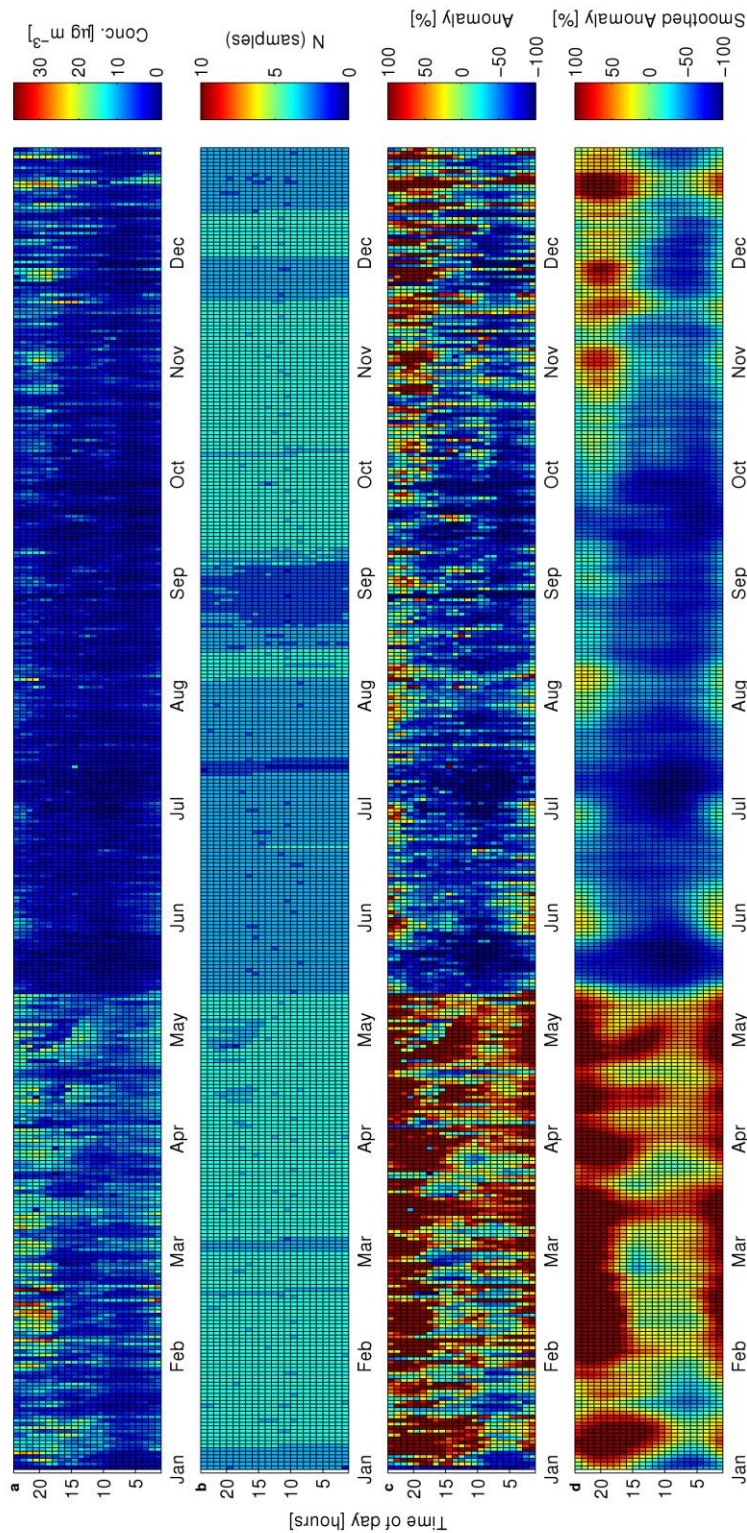


Figure 32: NO_2 at station *NO0062A Haukenes*: Annual matrices of hourly averages computed over entire available time series, shown as a) Observations, b) number of years with available data, c) the anomaly computed from the long-term mean, and d) the anomaly from the long-term mean smoothed using a low-pass filter.

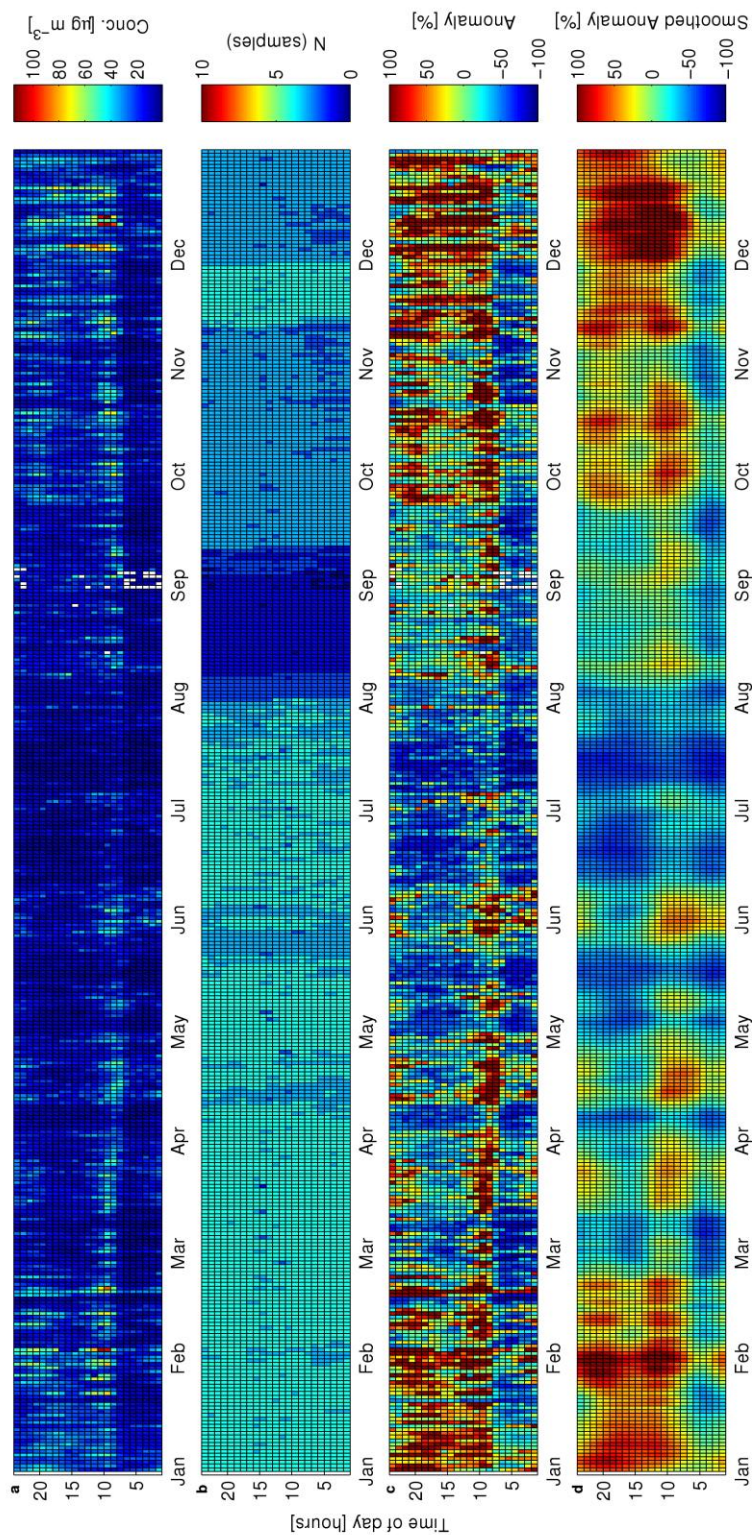


Figure 33: NO_2 at station *NO0065A Våland*: Annual matrices of hourly averages computed over entire available time series, shown as a) Observations, b) number of years with available data, c) the anomaly computed from the long-term mean, and d) the anomaly from the long-term mean smoothed using a low-pass filter.

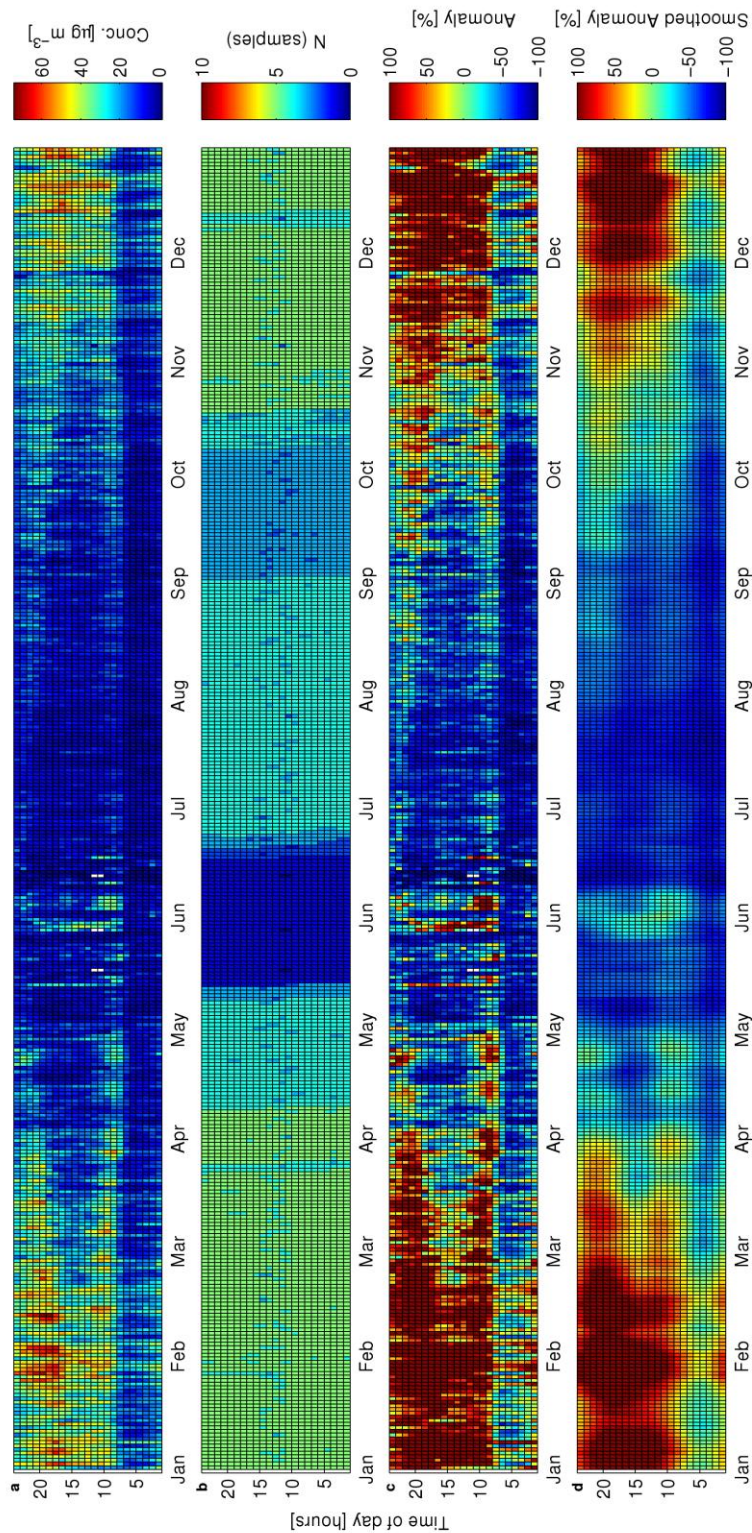


Figure 34: NO₂ at station *NO0075A Barnehegen*: Annual matrices of hourly averages computed over entire available time series, shown as a) Observations, b) number of years with available data, c) the anomaly computed from the long-term mean, and d) the anomaly from the long-term mean smoothed using a low-pass filter.

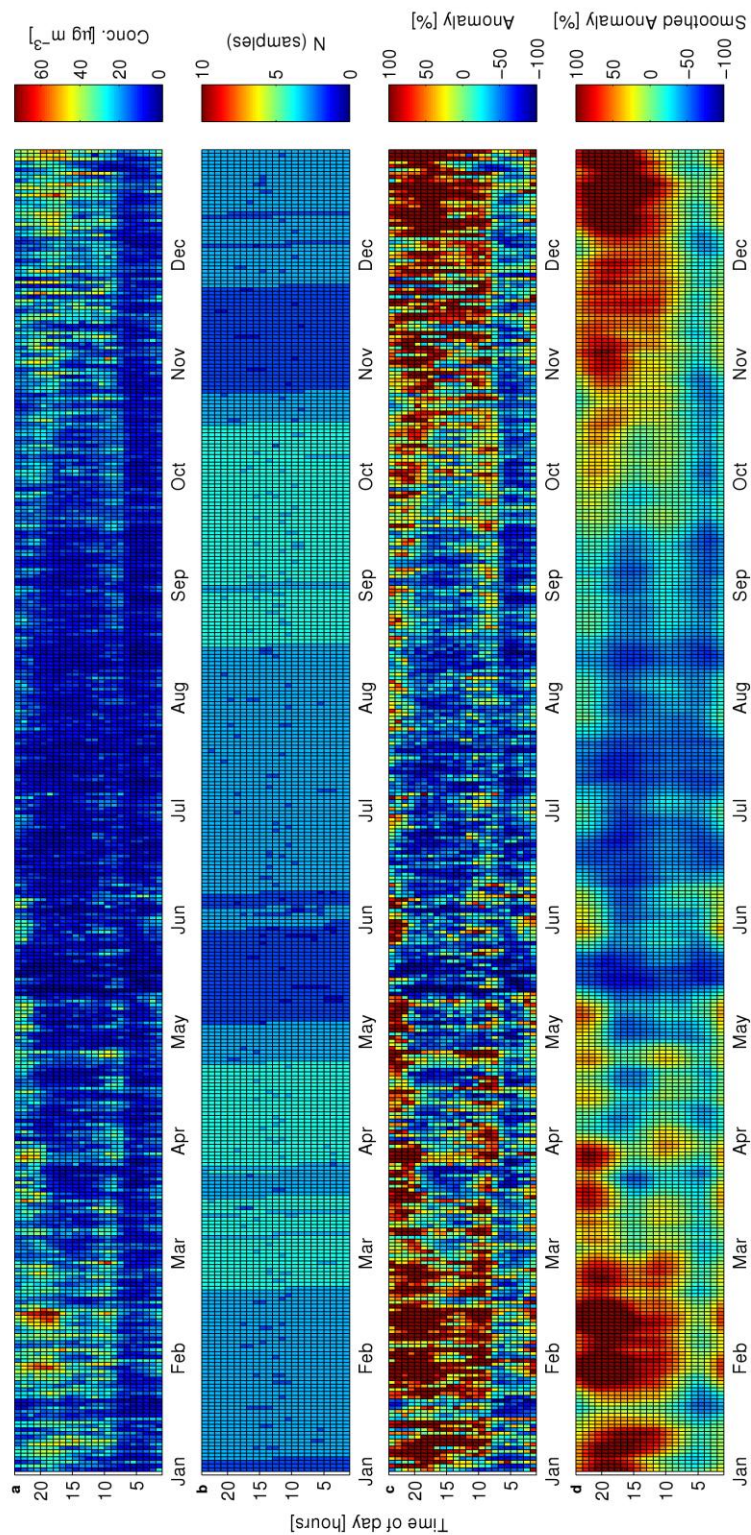


Figure 35: NO₂ at station NO0080A Øyekast: Annual matrices of hourly averages computed over entire available time series, shown as a) Observations, b) number of years with available data, c) the anomaly computed from the long-term mean, and d) the anomaly from the long-term mean smoothed using a low-pass filter.

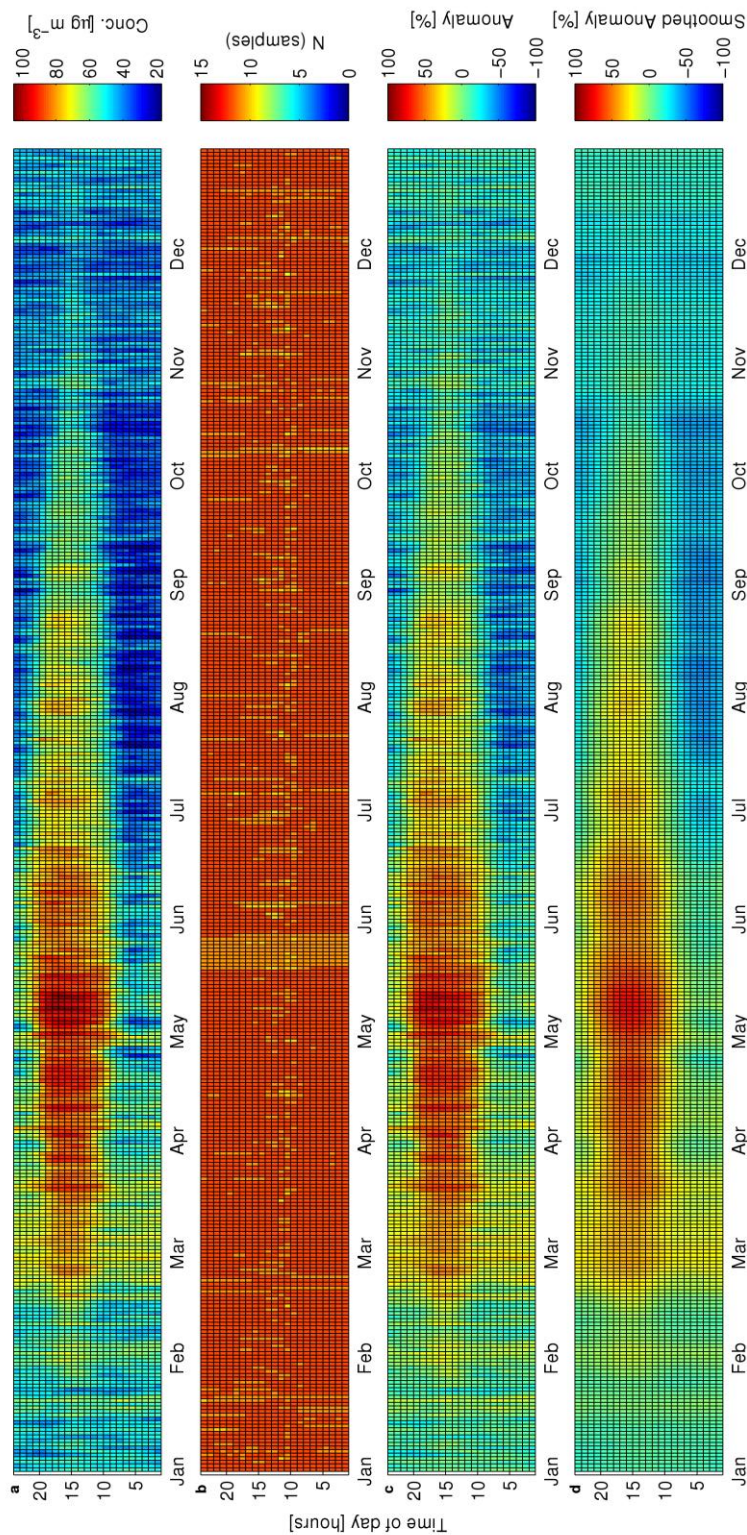
C.2 O₃

Figure 36: O₃ at station *NO0001R Birkenes*: Annual matrices of hourly averages computed over entire available time series, shown as a) Observations, b) number of years with available data, c) the anomaly computed from the long-term mean, and d) the anomaly from the long-term mean smoothed using a low-pass filter.

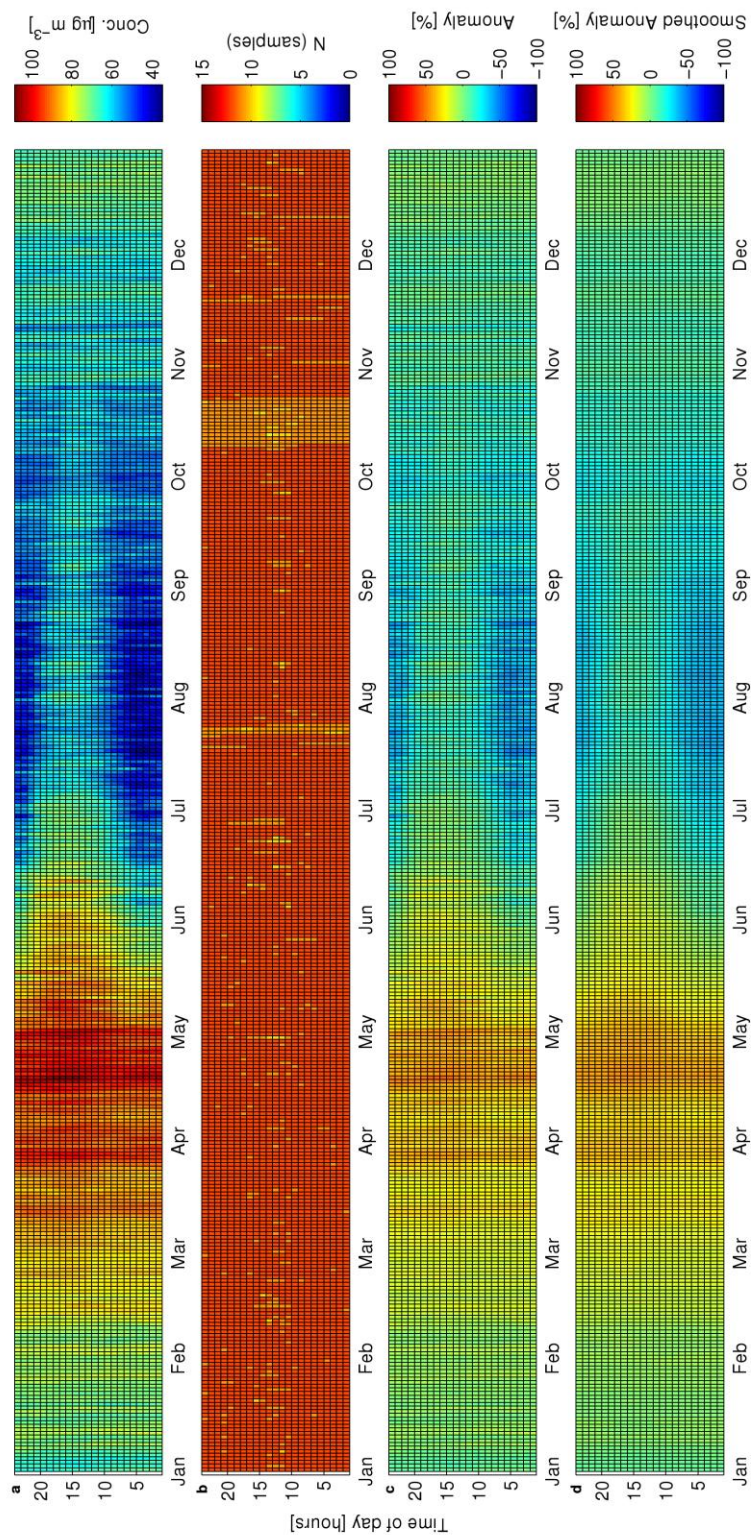


Figure 37: O_3 at station *NO0015R Tustervatn*: Annual matrices of hourly averages computed over entire available time series, shown as a) Observations, b) number of years with available data, c) the anomaly computed from the long-term mean, and d) the anomaly from the long-term mean smoothed using a low-pass filter.

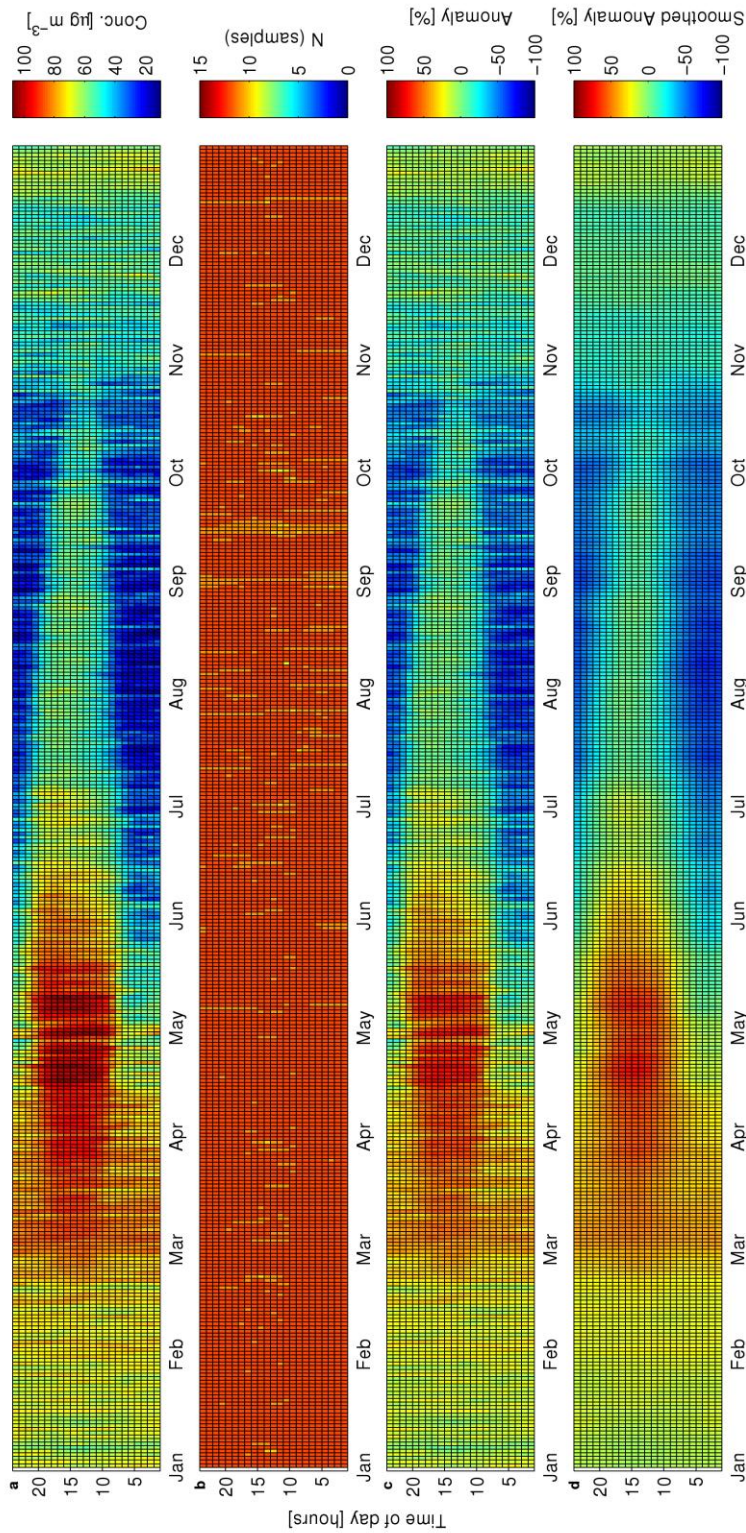


Figure 38: O₃ at station NO0039R Kårvatn: Annual matrices of hourly averages computed over entire available time series, shown as a) Observations, b) number of years with available data, c) the anomaly computed from the long-term mean, and d) the anomaly from the long-term mean smoothed using a low-pass filter.

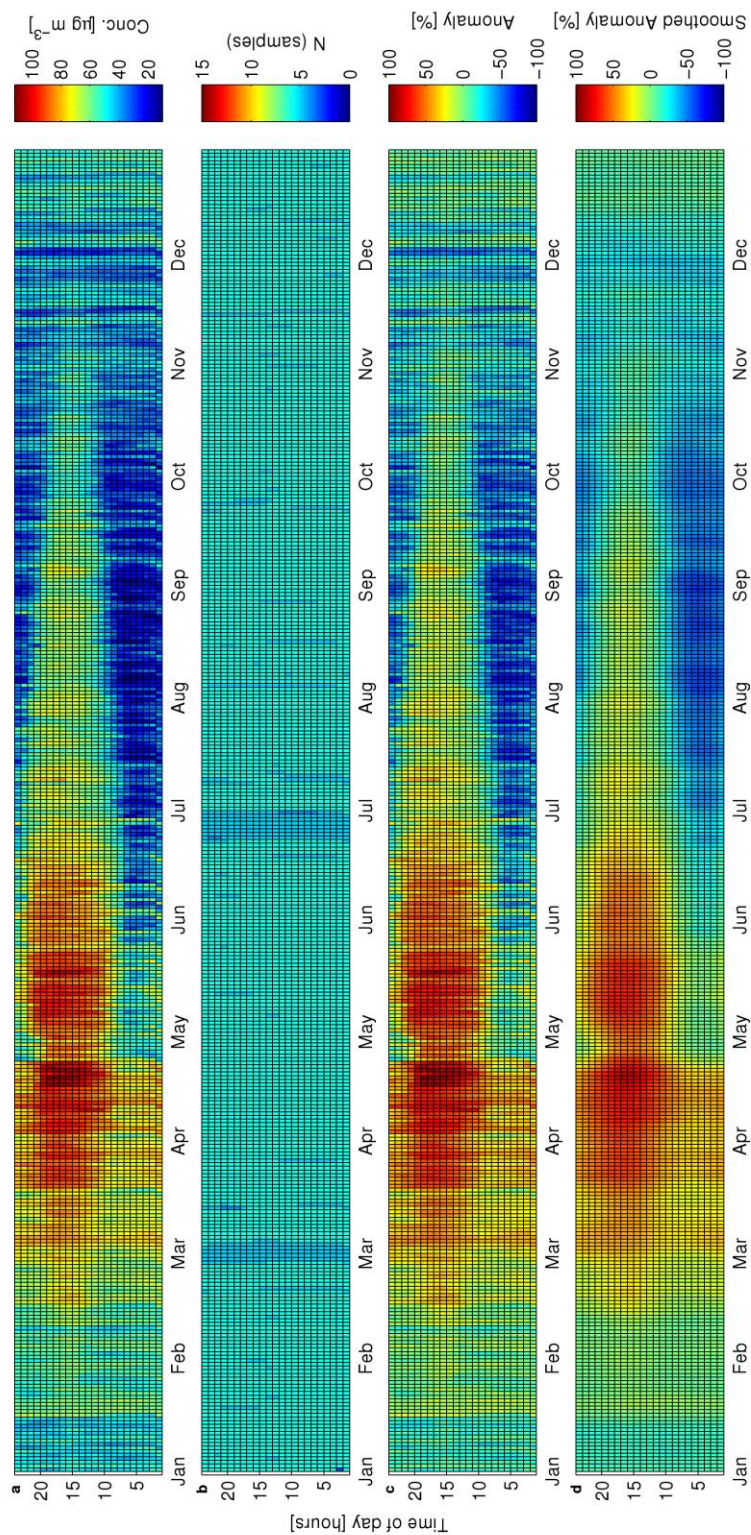


Figure 39: O₃ at station *NO0041R Osen*: Annual matrices of hourly averages computed over entire available time series, shown as a) Observations, b) number of years with available data, c) the anomaly computed from the long-term mean, and d) the anomaly from the long-term mean smoothed using a low-pass filter.

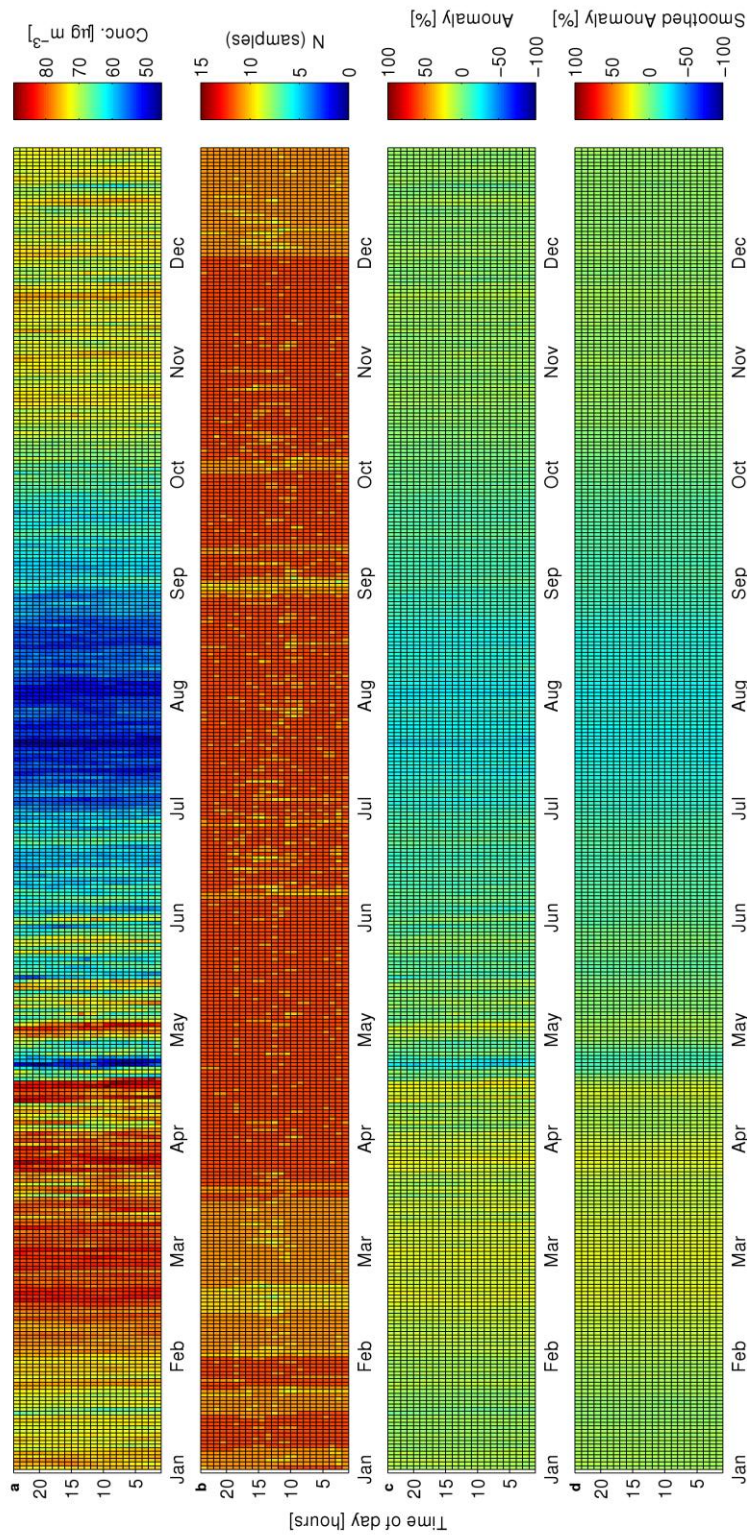


Figure 40: O₃ at station *NO0042R Zeppelin*: Annual matrices of hourly averages computed over entire available time series, shown as a) Observations, b) number of years with available data, c) the anomaly computed from the long-term mean, and d) the anomaly from the long-term mean smoothed using a low-pass filter.

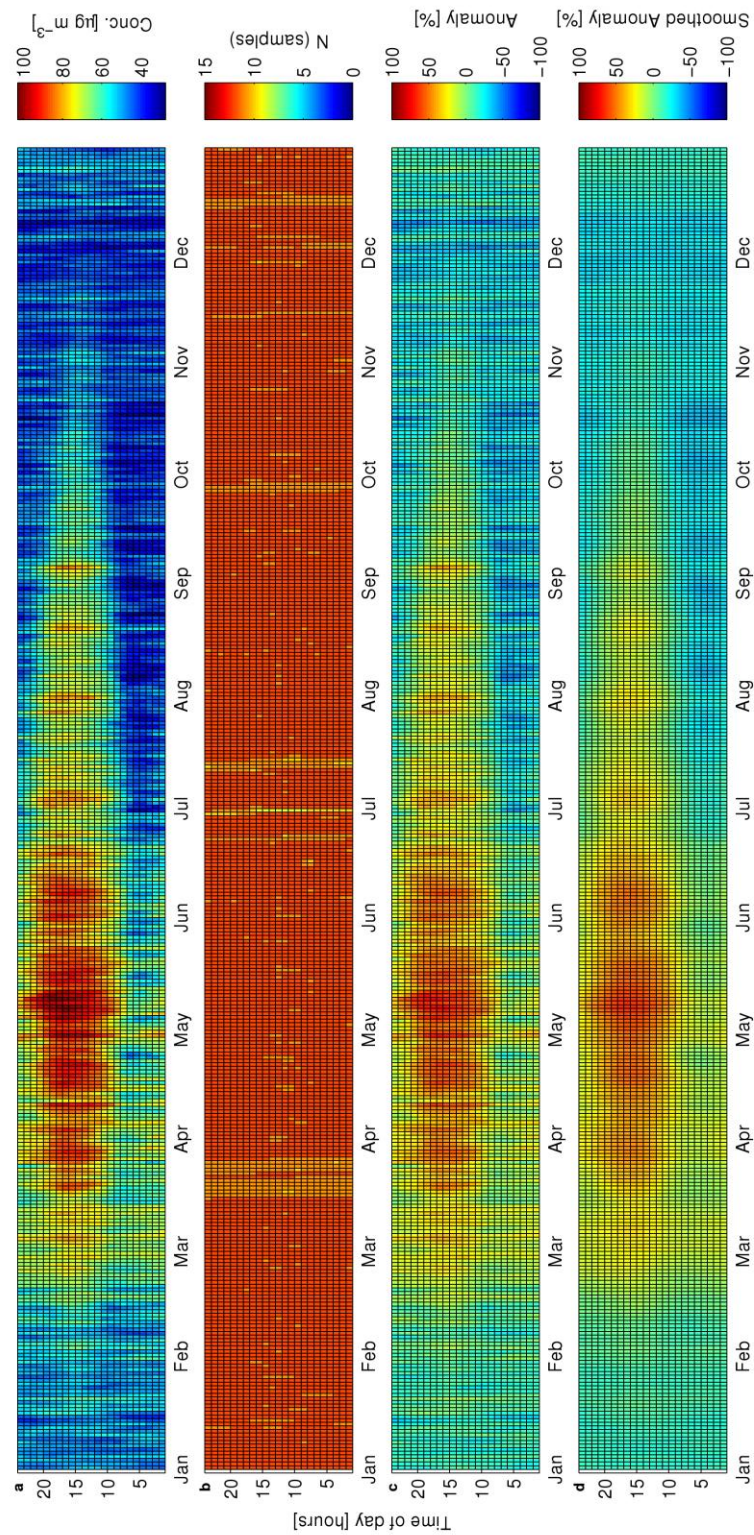


Figure 41: O₃ at station *NO0043R Prestebakke*: Annual matrices of hourly averages computed over entire available time series, shown as a) Observations, b) number of years with available data, c) the anomaly computed from the long-term mean, and d) the anomaly from the long-term mean smoothed using a low-pass filter.

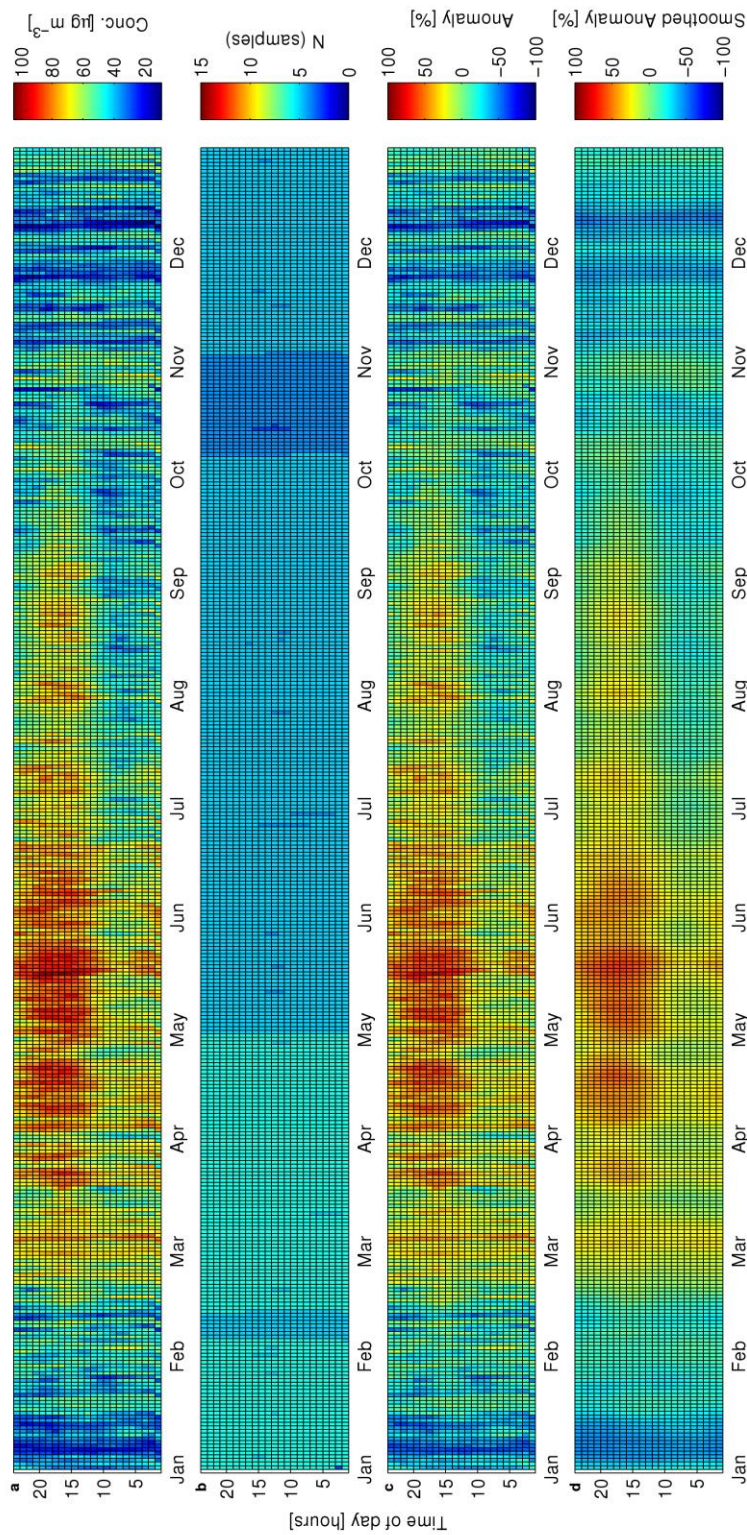


Figure 42: O_3 at station *NO0045R Jeløya*: Annual matrices of hourly averages computed over entire available time series, shown as a) Observations, b) number of years with available data, c) the anomaly computed from the long-term mean, and d) the anomaly from the long-term mean smoothed using a low-pass filter.

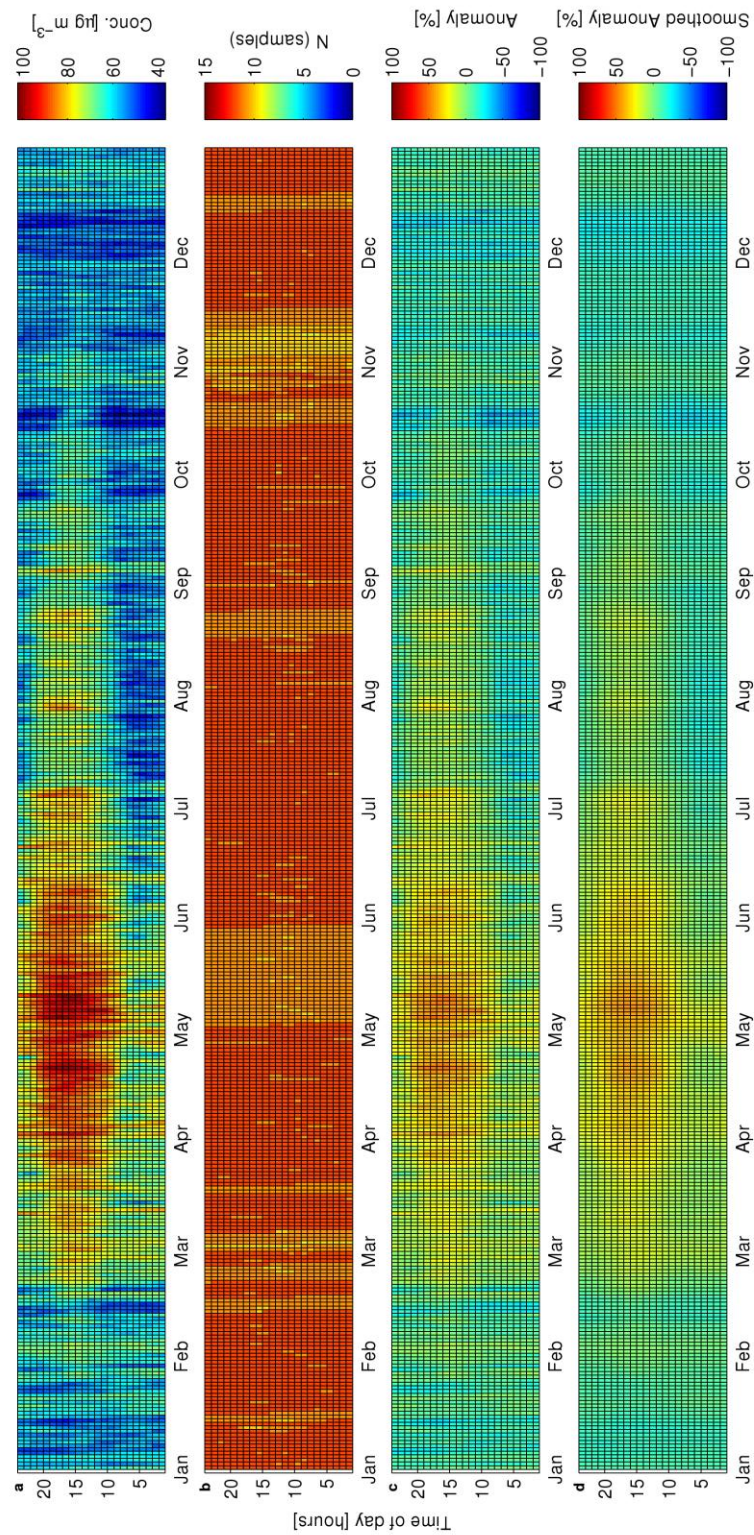


Figure 43: O_3 at station *NO052R Sandve*: Annual matrices of hourly averages computed over entire available time series, shown as a) Observations, b) number of years with available data, c) the anomaly computed from the long-term mean, and d) the anomaly from the long-term mean smoothed using a low-pass filter.

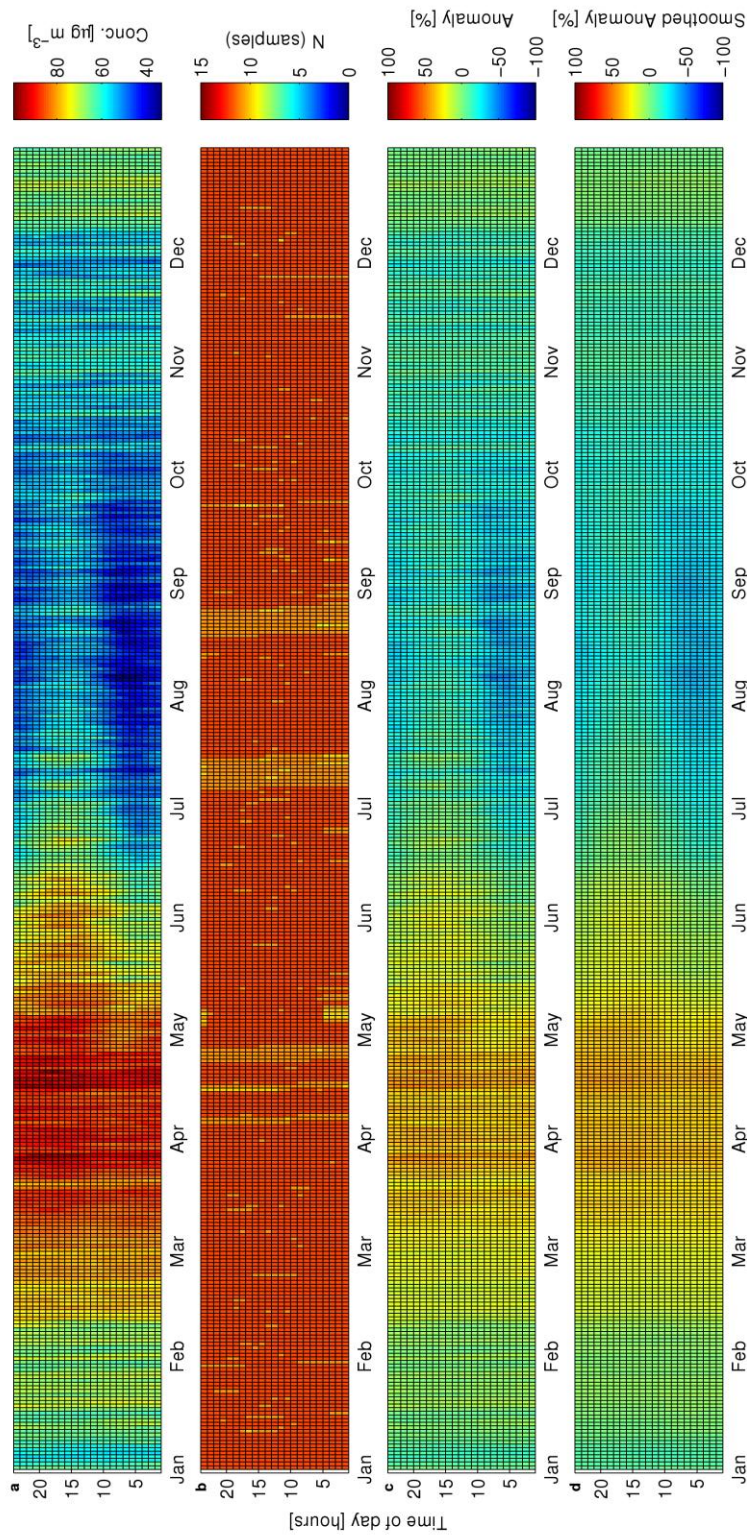


Figure 44: O₃ at station *NO0055R Karasjok*: Annual matrices of hourly averages computed over entire available time series, shown as a) Observations, b) number of years with available data, c) the anomaly computed from the long-term mean, and d) the anomaly from the long-term mean smoothed using a low-pass filter.

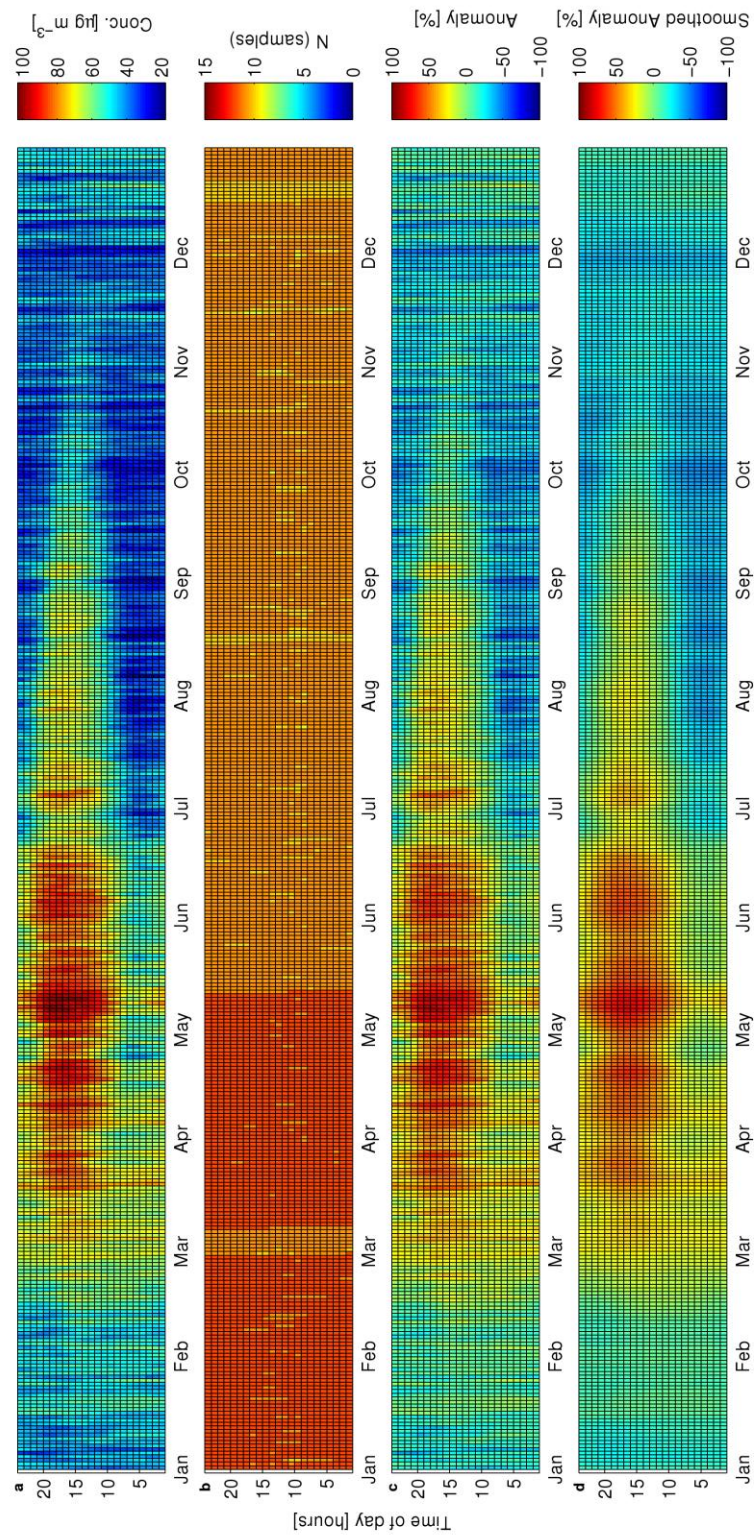


Figure 45: O_3 at station *NO056R Hurdal*: Annual matrices of hourly averages computed over entire available time series, shown as a) Observations, b) number of years with available data, c) the anomaly computed from the long-term mean, and d) the anomaly from the long-term mean smoothed using a low-pass filter.

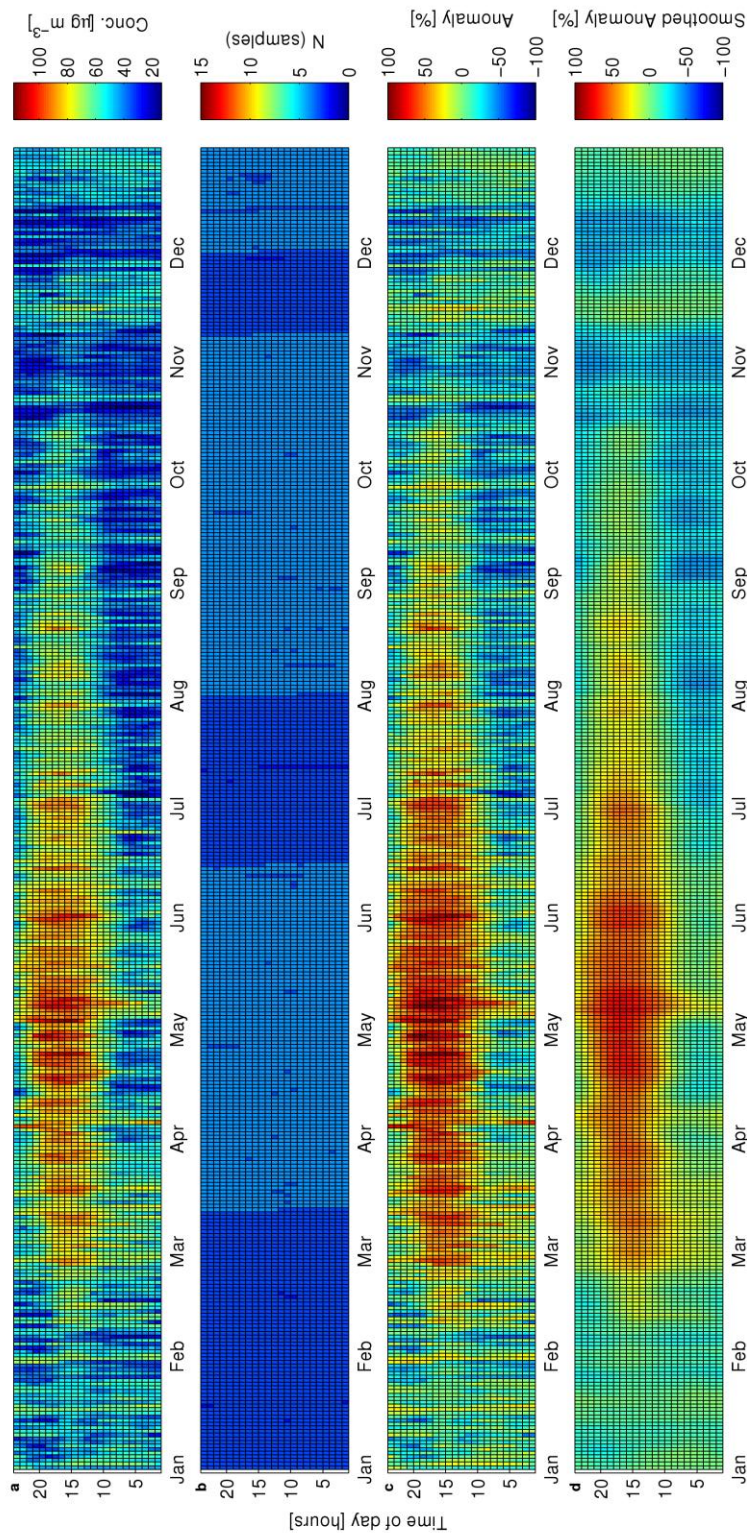


Figure 46: O₃ at station *NO0062A Haukenes*: Annual matrices of hourly averages computed over entire available time series, shown as a) Observations, b) number of years with available data, c) the anomaly computed from the long-term mean, and d) the anomaly from the long-term mean smoothed using a low-pass filter.

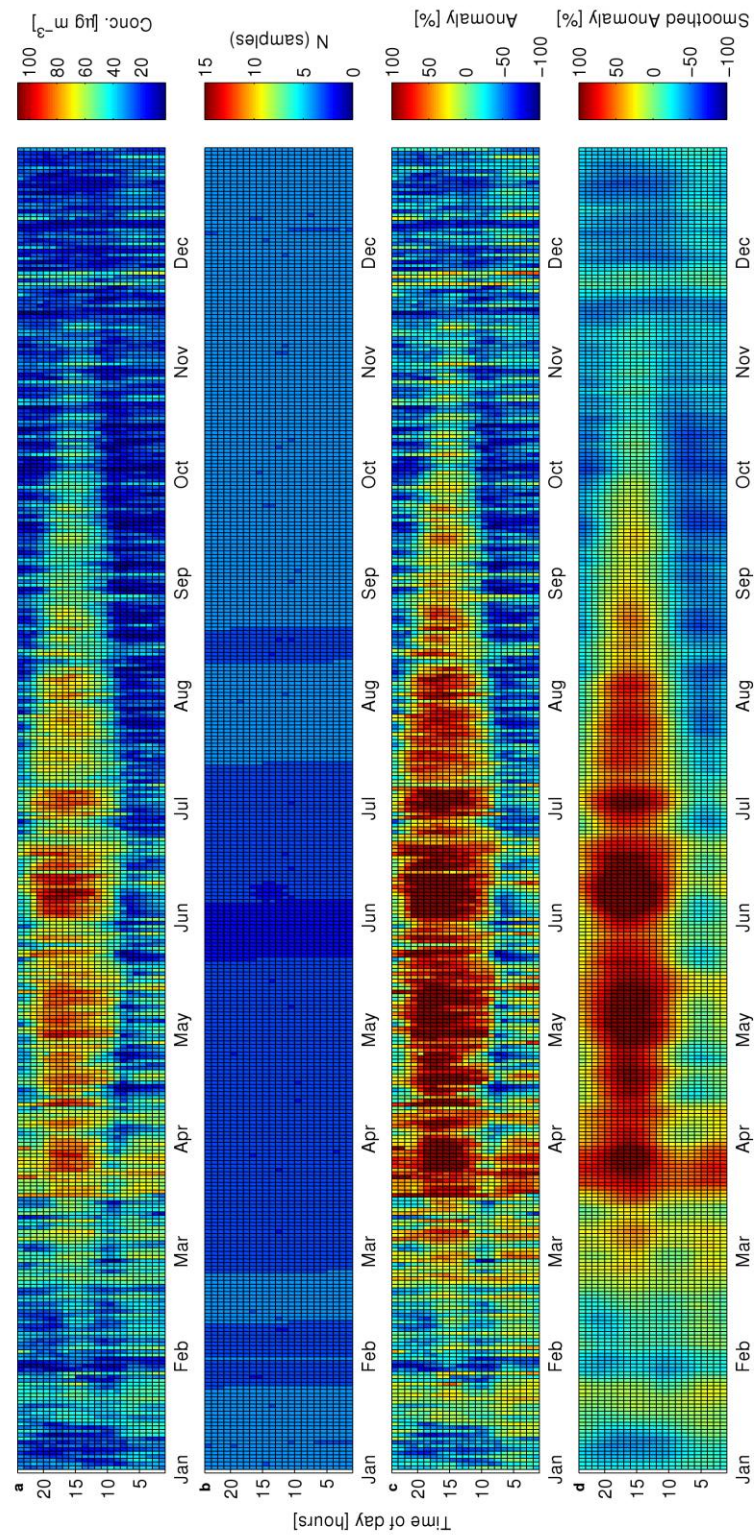


Figure 47: O₃ at station NO0081A Bærum: Annual matrices of hourly averages computed over entire available time series, shown as a) Observations, b) number of years with available data, c) the anomaly computed from the long-term mean, and d) the anomaly from the long-term mean smoothed using a low-pass filter.

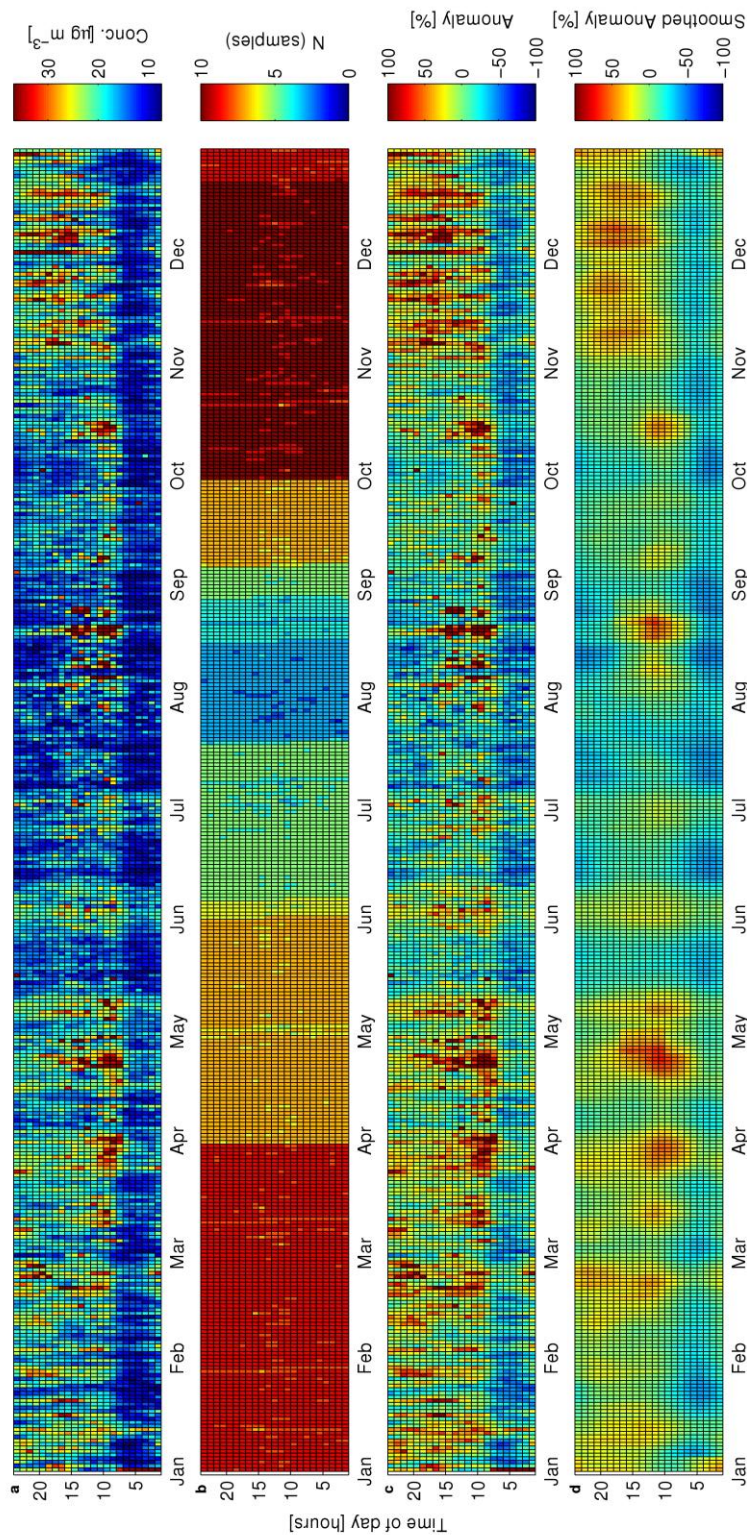
C.3 PM₁₀

Figure 48: PM₁₀ at station *NO0015A Rådhuset*: Annual matrices of hourly averages computed over entire available time series, shown as a) Observations, b) number of years with available data, c) the anomaly computed from the long-term mean, and d) the anomaly from the long-term mean smoothed using a low-pass filter.

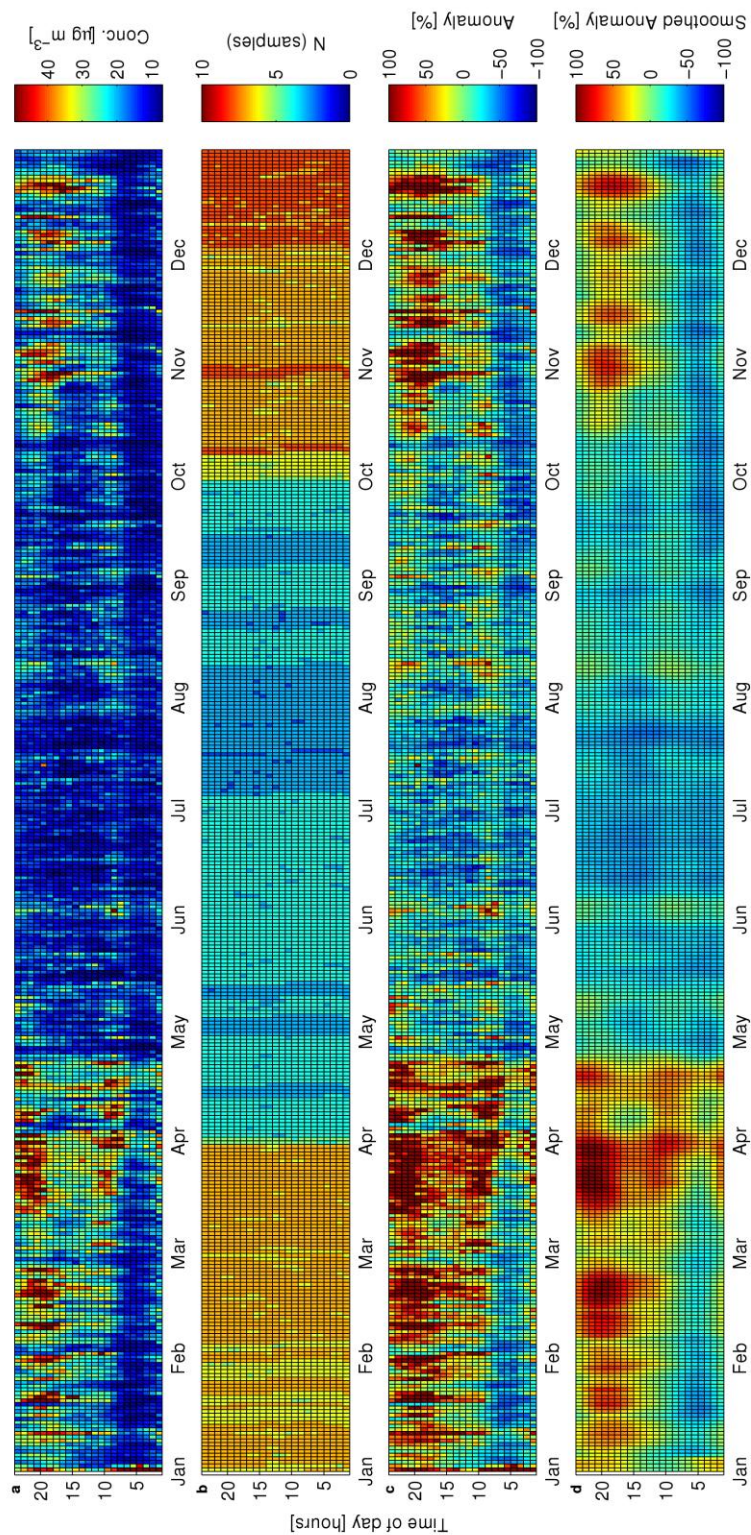


Figure 49: PM₁₀ at station *NO0016A Nedre Storgate*: Annual matrices of hourly averages computed over entire available time series, shown as a) Observations, b) number of years with available data, c) the anomaly computed from the long-term mean, and d) the anomaly from the long-term mean smoothed using a low-pass filter.

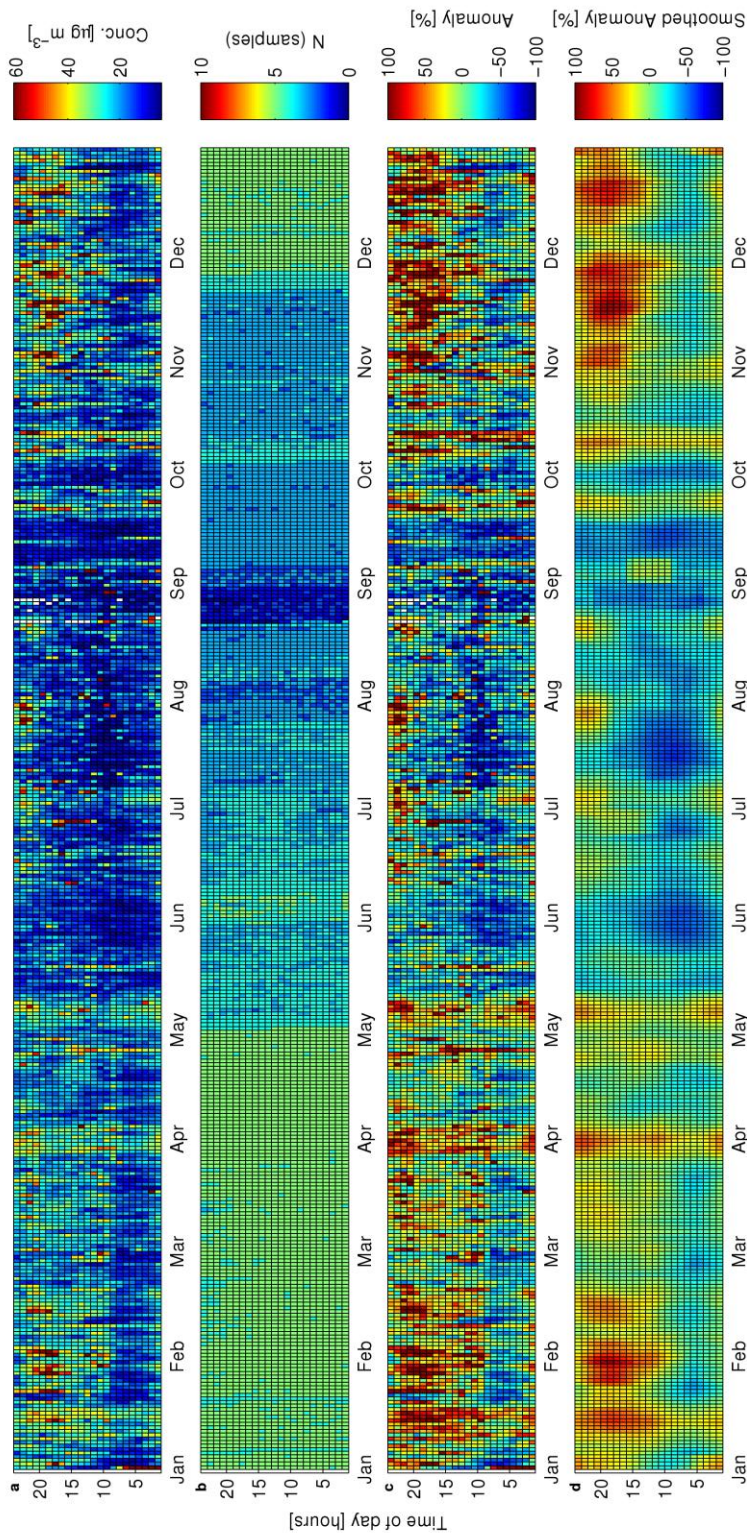


Figure 50: PM_{10} at station *NO0063A Stener Heyerdahl*: Annual matrices of hourly averages computed over entire available time series, shown as a) Observations, b) number of years with available data, c) the anomaly computed from the long-term mean, and d) the anomaly from the long-term mean smoothed using a low-pass filter.

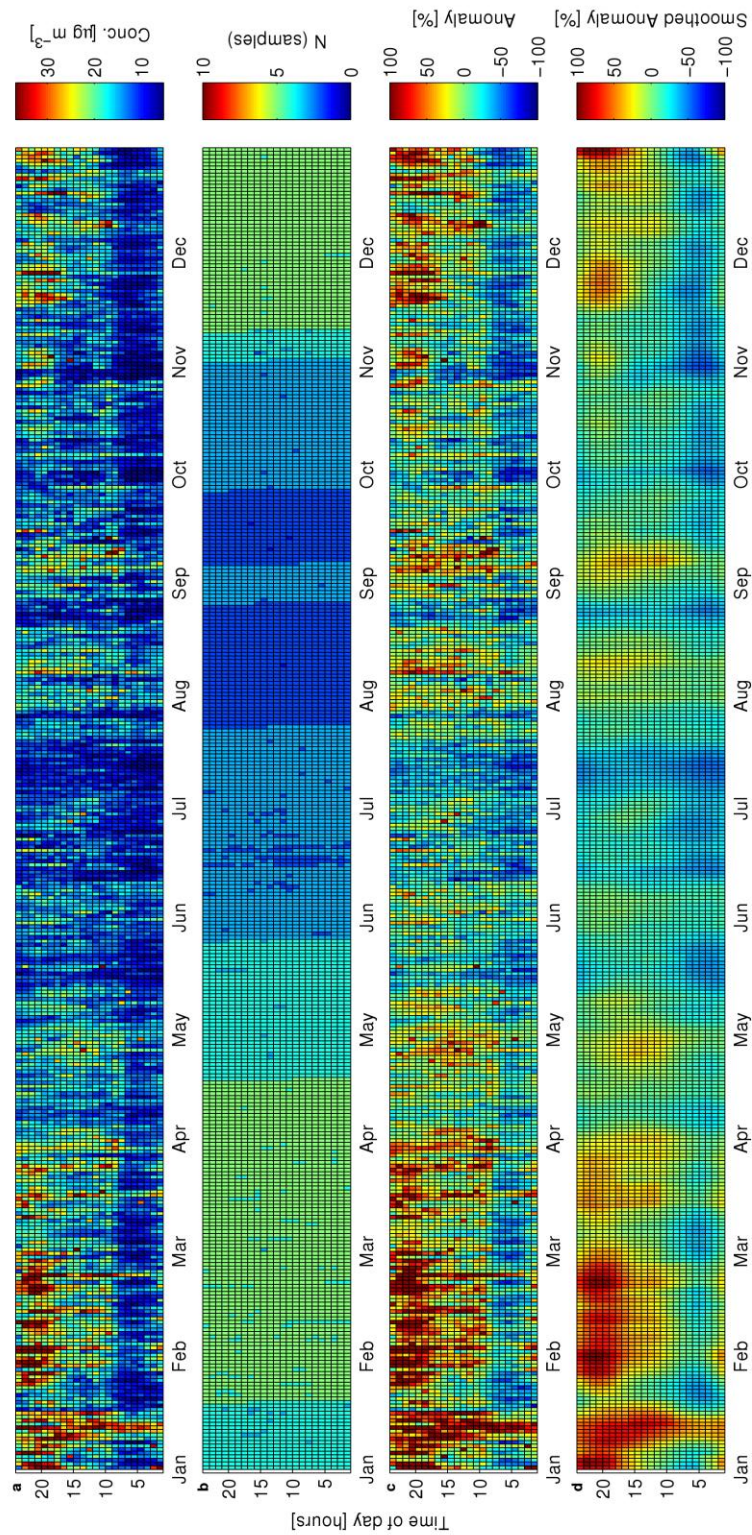


Figure 51: PM₁₀ at station *NO0065A Våland*: Annual matrices of hourly averages computed over entire available time series, shown as a) Observations, b) number of years with available data, c) the anomaly computed from the long-term mean, and d) the anomaly from the long-term mean smoothed using a low-pass filter.

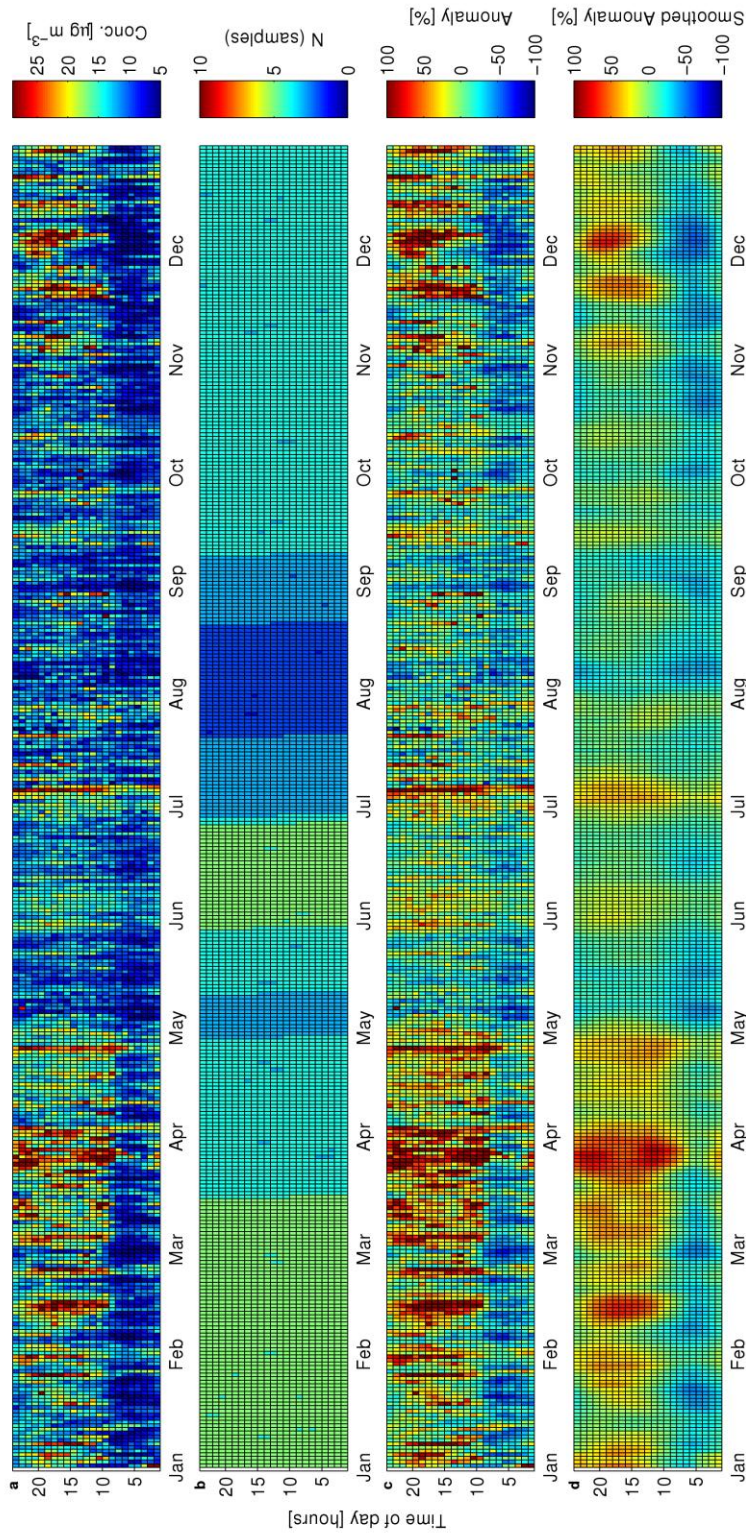


Figure 52: PM₁₀ at station NO0070A Grimmerhaugen: Annual matrices of hourly averages computed over entire available time series, shown as a) Observations, b) number of years with available data, c) the anomaly computed from the long-term mean, and d) the anomaly from the long-term mean smoothed using a low-pass filter.

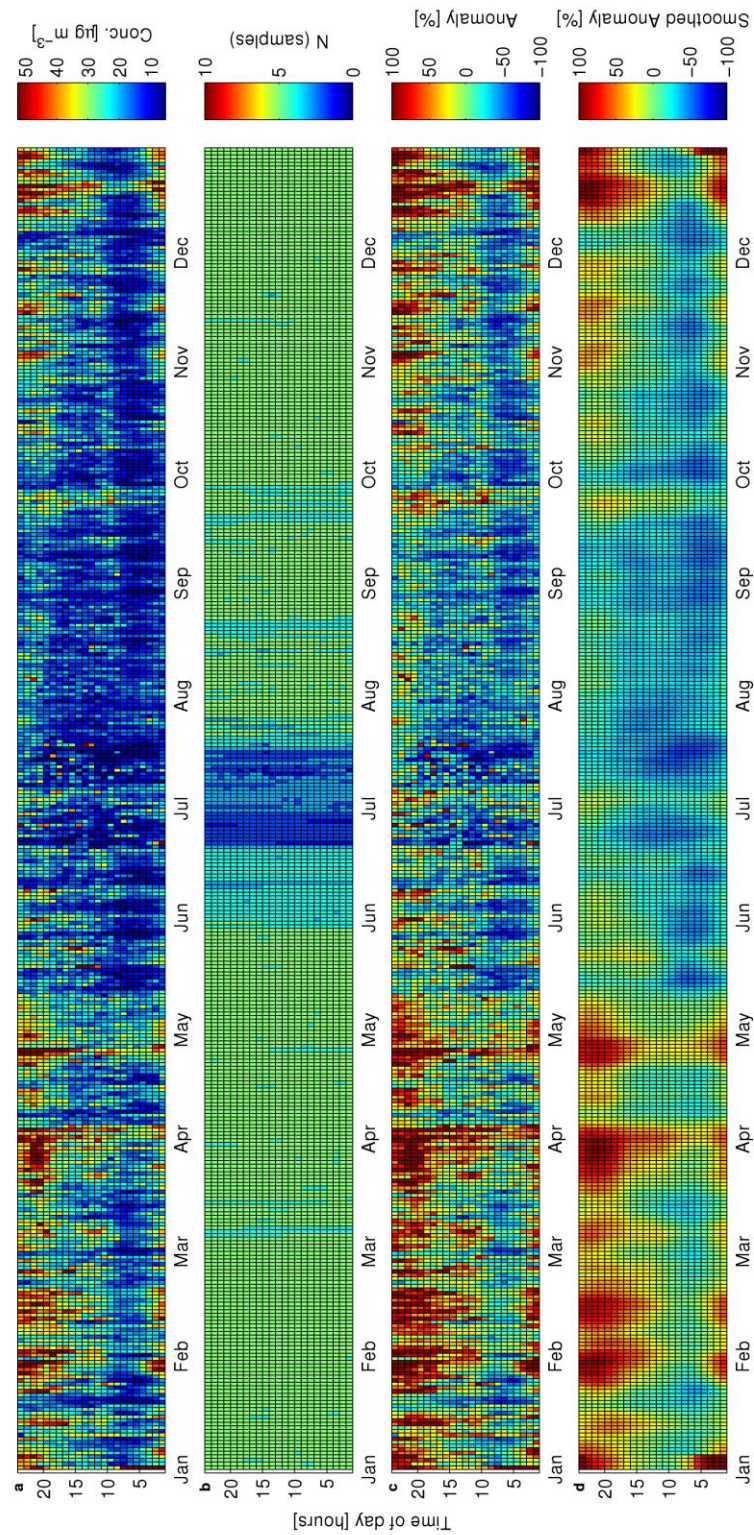


Figure 53: PM₁₀ at station *NO0072A Skøyen*: Annual matrices of hourly averages computed over entire available time series, shown as a) Observations, b) number of years with available data, c) the anomaly computed from the long-term mean, and d) the anomaly from the long-term mean smoothed using a low-pass filter.

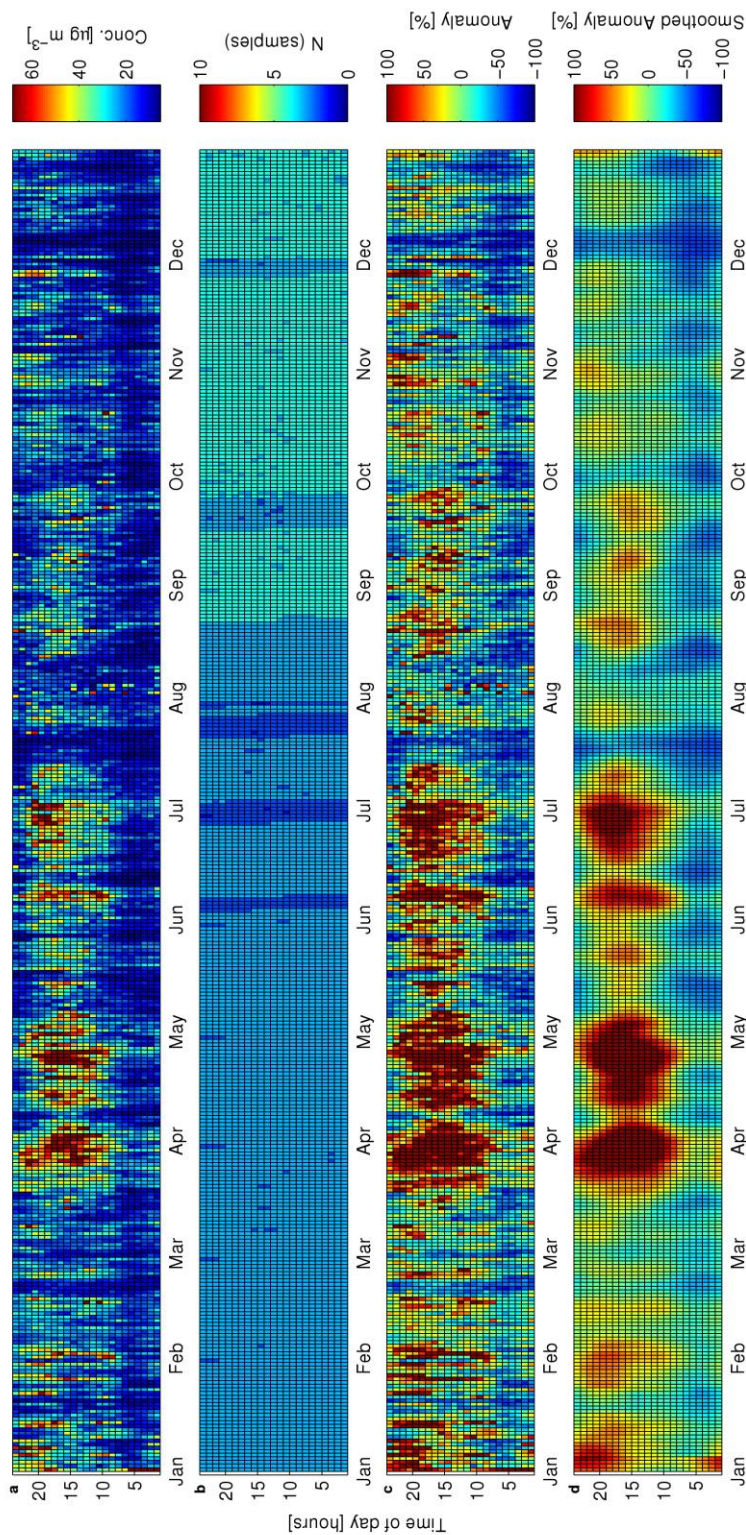


Figure 54: PM_{10} at station *NO0073A Sofienbergparken*: Annual matrices of hourly averages computed over entire available time series, shown as a) Observations, b) number of years with available data, c) the anomaly computed from the long-term mean, and d) the anomaly from the long-term mean smoothed using a low-pass filter.

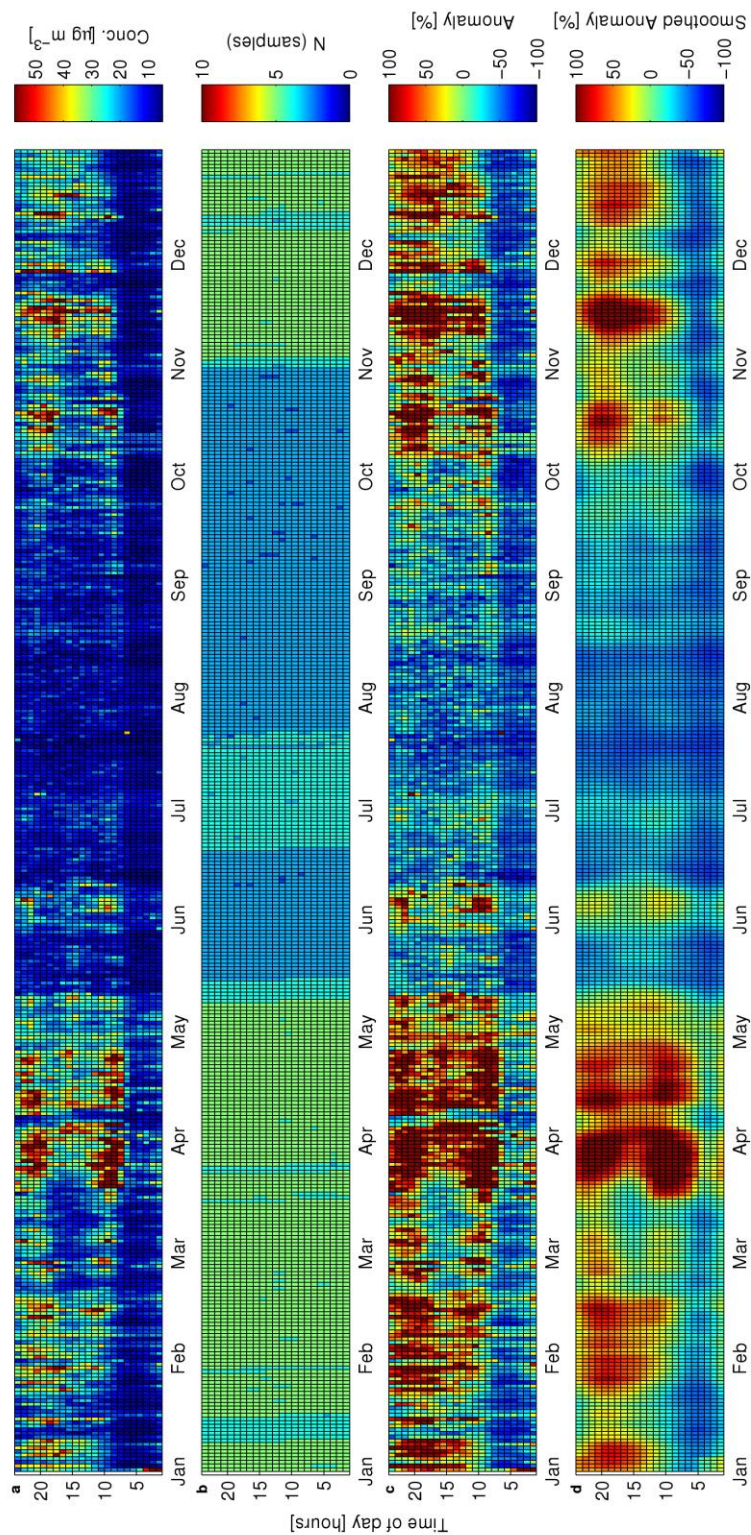


Figure 55: PM₁₀ at station *NO0075A Barnehamen*: Annual matrices of hourly averages computed over entire available time series, shown as a) Observations, b) number of years with available data, c) the anomaly computed from the long-term mean, and d) the anomaly from the long-term mean smoothed using a low-pass filter.

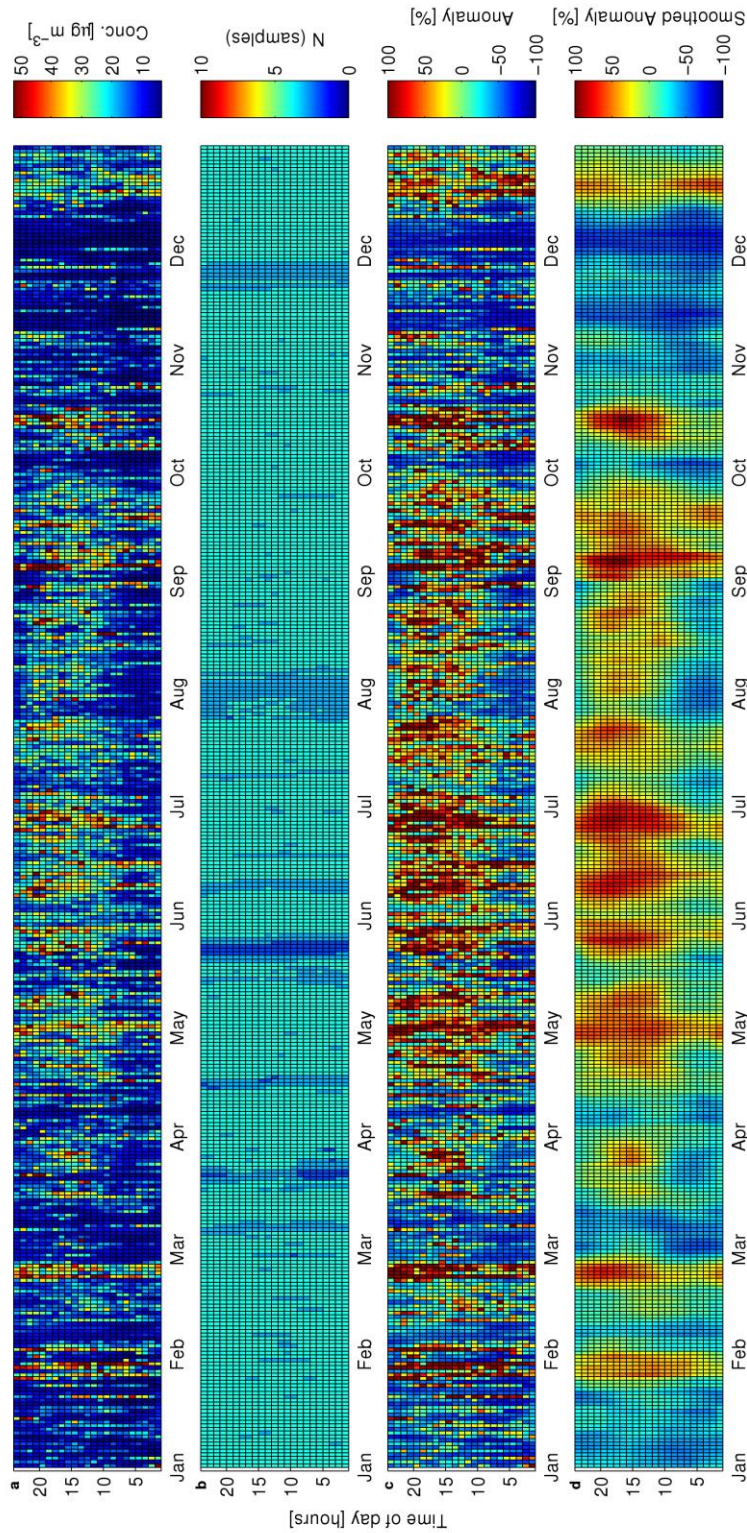


Figure 56: PM_{10} at station *NO0077A Gruben*: Annual matrices of hourly averages computed over entire available time series, shown as a) Observations, b) number of years with available data, c) the anomaly computed from the long-term mean, and d) the anomaly from the long-term mean smoothed using a low-pass filter.

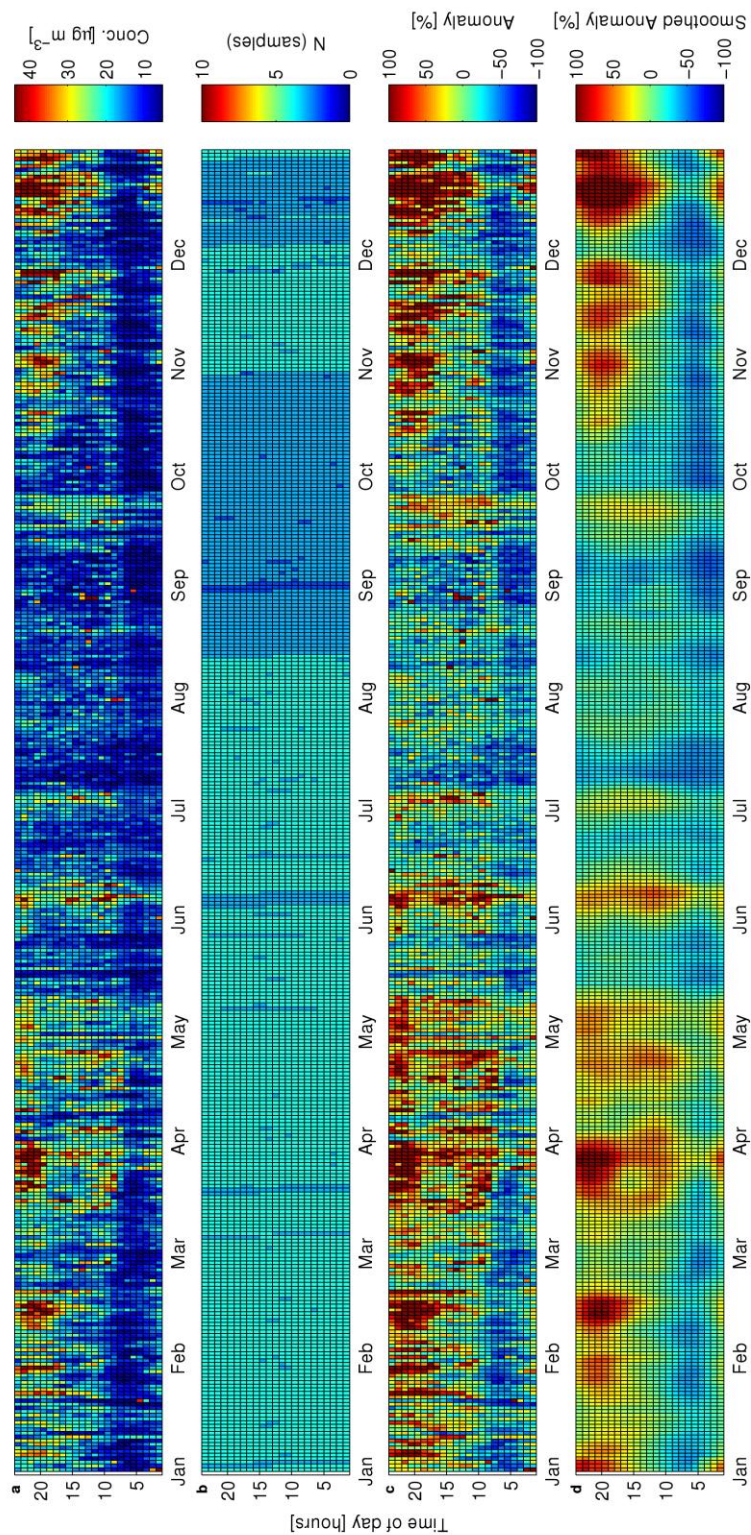


Figure 57: PM₁₀ at station NO0080A Øyekast: Annual matrices of hourly averages computed over entire available time series, shown as a) Observations, b) number of years with available data, c) the anomaly computed from the long-term mean, and d) the anomaly from the long-term mean smoothed using a low-pass filter.

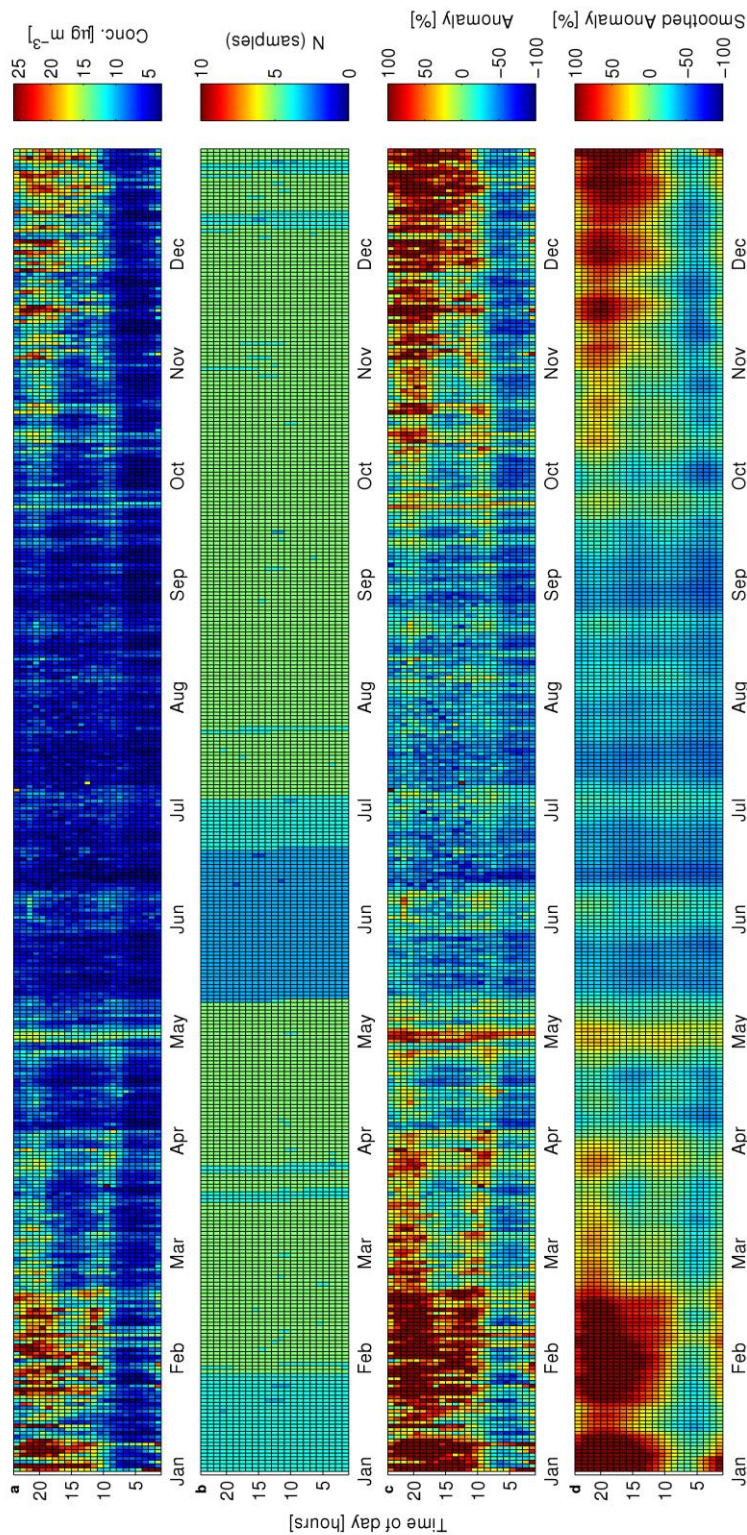
C.4 PM_{2.5}

Figure 58: PM_{2.5} at station *NO0075A Barnehamen*: Annual matrices of hourly averages computed over entire available time series, shown as a) Observations, b) number of years with available data, c) the anomaly computed from the long-term mean, and d) the anomaly from the long-term mean smoothed using a low-pass filter.



**Norwegian Institute
for Air Research**

NILU – Norwegian Institute for Air Research
P.O. Box 100, N-2027 Kjeller, Norway
*Associated with CIENS and the
Environmental Research Alliance of Norway*
ISO certified according to NS-EN ISO 9001/ISO 14001

REPORT SERIES SCIENTIFIC REPORT	REPORT NO. OR 68/2011	ISBN: 978-82-425-2470-6 (print) 978-82-425-2471-3 (electronic)	
		ISSN: 0807-7207	
		ISSN: 0807-7185	
DATE 15.2.2012	SIGN. 	NO. OF PAGES 88	PRICE NOK 150.-
TITLE Update of background concentrations over Norway		PROJECT LEADER Dag Tønnesen	
		NILU PROJECT NO. O-111098	
AUTHOR(S) Philipp Schneider, Dag Tønnesen and Bruce Denby		CLASSIFICATION * A	
		CONTRACT REF. Ingrid Myrtveit	
QUALITY CONTROLLER: Ingrid Sundvor			
REPORT PREPARED FOR Klima- og forurensningsdirektoratet Postboks 8100 Dep 0032 OSLO			
<p>ABSTRACT</p> <p>A methodology for creating a new dataset of estimated background concentrations of NO₂, O₃, PM₁₀, and PM_{2.5} that are representative of a typical year over Norway, was developed. The dataset has a spatial resolution of 10 km × 10 km and an hourly temporal resolution. The methodology is based on a spatial mapping component for obtaining information on annual mean background concentrations, and a temporal characterization component, which uses long-term time series of station data to describe the typical development of background concentrations throughout a day and a year. When combined, these two components allow estimates of typical background concentrations at any time of the year at any location in Norway. Whereas the previously used VLUFT method of 1993 only provided spatially constant data at the county level, the new method presented here provides spatially continuous data at a comparatively high spatial resolution. Furthermore, while the previous method only gave a range of constant values that were considered valid throughout the entire year, the new technique provides continuous time series for a typical year at hourly resolution at any location in Norway.</p>			
<p>NORWEGIAN TITLE</p> <p>En oppdatering av bakgrunnskonsentrasjoner i Norge</p>			
KEYWORDS Air quality		Environmental Monitoring	
ABSTRACT (in Norwegian)			

* Classification A *Unclassified (can be ordered from NILU)*
 B *Restricted distribution*
 C *Classified (not to be distributed)*

REFERENCE: O-111098
DATE: FEBRUARY 2012
ISBN: 978-82-425-2470-6 (print)
978-82-425-2471-3 (electronic)

NILU is an independent, nonprofit institution established in 1969. Through its research NILU increases the understanding of climate change, of the composition of the atmosphere, of air quality and of hazardous substances. Based on its research, NILU markets integrated services and products within analyzing, monitoring and consulting. NILU is concerned with increasing public awareness about climate change and environmental pollution.